

https://dspace.org/

Evaluation of performance influencing parameters on alkaline water electrolysis systems

Gillespie, Malcolm Ivor

2016
http://hdl.handle.net/10539/20024

Downloaded from a DSpace repository. https://dspace.org/

EVALUATION OF PERFORMANCE INFLUENCING PARAMETERS ON ALKALINE WATER ELECTROLYSIS SYSTEMS

Malcolm Ivor Gillespie

A dissertation submitted to the University of the Witwatersrand, Johannesburg, Faculty of Engineering and the Built Environment, in fulfillment of the requirements for the full time degree of Master of Science in Engineering (Chemical Engineering).

Johannesburg, 2015

DECLARATION

I declare that this dissertation is my own unaided work under the supervision of my supervisor Dr. S. Kauchali. It is in fulfillment toward the Degree of Masters of Science in Chemical Engineering to the University of the Witwatersrand, Johannesburg. This dissertation has not been submitted before for any degree or examination to any other University.

_____

(Signature of Candidate)

_____day of_____, _____

(day) *(month)* *(year)*

ABSTRACT

Alkaline Water Electrolysis (AWE) has shown to be an effective method of producing hydrogen from renewable sources of energy. However this process accounts for only 4-5% of the global hydrogen production. Challenges abound for water electrolysis technologies that presents the traditional methods as comparably favourable.

This research focuses on investigating the relevant performance influencing parameters for alkaline water electrolysers, their contribution to compromising or enhancing cell performance and the various interdependencies that exist between variables. Hydrox Holdings Ltd., in partnership with Demcotech Engineering, provided permission to analyse the performance of a membraneless alkaline water electrolysis pilot plant.

Using pure nickel for the anode and cathode electrodes yielded current densities of 51.9 $mA.cm^{-2}$ (at 1.8VDC, 82% HHV efficiency) and 242.9$mA.cm^{-2}$ (at 2 VDC, 73% HHV efficiency) at an electrode gap of 2.5mm, temperature of 70°C and a flow velocity of 0.075$m.s^{-1}$. At these same experimental conditions, employing Ir-RuO_2 on a Ti substrate for the anode and Pt on a Ti substrate for the hydrogen evolution reaction, current densities of 220 $mA.cm^{-2}$ (at 1.765VDC) and 474 $mA.cm^{-2}$ (at 2 VDC) was achieved.

Marini et al., (2012), notes that performance for conventional alkaline water electrolysers should be in the order of > 100 $mA.cm^{-2}$ when operating at a cell potential of 2 VDC. The performance of the membraneless technology has therefore exceeded this benchmark by more than 2 times with the use of basic nickel electrodes and being more than 4 times with the use of PGM catalytic materials, and hence could be described to very comparable as advanced methods of alkaline water electrolysis. The ability to obtain high current density thresholds implies that the membraneless technology has potential for a substantial reduction in scale and hence, in the total capital cost of the technology.

ACKNOWLEDGEMENTS

I wish to thank the following for their contributions to my work:

- My family, for their continued support and motivation.
- Demcotech Engineering, for funding and providing the opportunity for me to engage in the development of the membraneless technology.
- Hydrox Holdings, for the use of their propriety membraneless alkaline electrolysis technology, and for funding the development of this dissertation.
- Dr Shehzaad Kauchali, for his continual guidance, inspiration and insight into the alternative energy industry along with his continued support of this work.

CONTENTS

DECLARATION ii
ABSTRACT iii
ACKNOWLEDGEMENTS iv
LIST OF FIGURES ix
LIST OF TABLES xv
LIST OF SYMBOLS xvi
NOMENCLATURE xviii
GLOSSARY OF TERMS xix
1. INTRODUCTION 1
1.1. Background 2
1.2. Problem Statement and Research Motivation 5
1.3. Research Objectives 5
1.4. Source of Data and Methodology 6
1.5. Dissertation Structure 6
2. LITERATURE REVIEW 7
2.1. Introduction to Water Electrolysis Technology 7
2.2. Technology Advantages, Limitations and Outlook 8
2.3. Water Electrolysis Thermodynamics 9
2.4. Efficiency Determination of Electrolysers 13
2.5. Basis for Current Density 15
2.6. Types of Water Electrolysers 17
2.6.1. Alkaline Water Electrolysis 17
2.6.2. Proton Exchange Membrane Electrolysis 18
2.6.3. Solid Oxide Electrolysis 20
2.7. Performance Influencing Parameters 21

2.7.1. Electrolytic Concentration and Temperature 21
2.7.2. Pressure 25
2.7.3. Electrode Gap 25
2.7.4. Size and Alignment of Electrodes 27
2.7.5. Bubble Resistance 29
2.7.6. Separator Material 32
2.7.7. Electro-catalysts for Hydrogen and Oxygen Evolution Reactions 33
3. METHODOLOGY 38
3.1. Overview 38
3.2. Process Flow Diagram Description 40
3.3. Experimental Apparatus 42
3.3.1. Electrolyser 43
3.3.2. Gas/Liquid Separators 44
3.3.3. Electrolytic Sump 45
3.4. Reagents and Material Stability 46
3.5. Experimental Procedure 47
3.5.1. Initial Plant Commissioning and Safety Checklist 47
3.5.2. Test Parameters and schedule for Parameter Optimisation 49
3.5.3. Additional Test Parameters 53
3.5.4. Test Methodology 55
3.6. Analytical Procedure 57
4. RESULTS AND DISCUSSION 60
4.1. Optimisation of Electrolytic Concentration 60
4.1.1. Concentration Fluctuation and Monitoring 62
4.1.2. Concentration as a Function of Flow Velocity and Temperature 64
4.2. Effect of Electrolytic Temperature and Electrolytic Flow Velocity 68
4.3. Optimisation of Electrode Materials 71
4.4. Effect of the Variation in Electrode Gap and Electrolytic Flow Velocity 75
4.5. The Effect of Increasing the Effective Area for Reaction 79

4.6. Gas Purity Analysis 80
4.7. Medium Term Stability 81
4.8. Stack Efficiency, Specific Energy Consumption and Technology Comparison 82
5. CONCLUSIONS 86
5.1. Future Work 86
5.2. Conclusions to Research 86
REFERENCES 89
APPENDIX A - ACTIVITY COMPARISON OF MESH ELECTRODES VERSUS PLATE ELECTRODES 95
APPENDIX B - DESIGN CONSIDERATIONS OF THE APPARATUS COMPRISING THE HYDROX HOLDINGS LTD. ELECTROLYSER TECH RIG 100
B.1. Electrolyser Apparatus 100
B.2. Gas/Liquid Separation Apparatus 103
B.3. Electrolytic Storage Sump 108
B.4. Electrolytic Circulation Chemical Pump 112
B.5. Gravity Recycle Loop Piping 118
B.6. Flow Measurement 120
B.7. Temperature Measurement 121
B.8. Pressure Measurement 121
APPENDIX C – ELECTROLYTIC COCENTRATION PREPARATION 122
APPENDIX D - SAFETY AND COMMISIONING CHECKLISTS AS DETAILED FROM ISO 22734-1 124
D.1. Mechanical Equipment Checklist 124
D.2. Electrical and Ventilation Equipment Checklist 125
D.3. Operator Controls Checklist 126
D.4. Ion Transport Medium Checklist 127
D.5. Personnel Equipment Checklist 127
D.6. Test Method Equipment Checklist 128
D.7. Marking and Labeling Checklist 129

APPENDIX E - ..... EMPIRICAL RESULTS FOR THE OPTIMISATION OF THE HYDROX HOLDINGS LTD. AWE ELECTROLYSER TECHNOLOGY 131

E.1. Concentration Fluctuation and Monitoring 131

E.2. Concentration as a Function of Flow Velocity and Temperature 133

E.3. Effect of Increasing Temperature and Flow Velocity on Cell Performance 134

E.4. Optimisation of Electrode Materials to Maximise Cell Performance 135

E.5. Optimisation of the Electrode Gap 137

LIST OF FIGURES

Figure 1: A schematic illustration of a basic water electrolysis system (Zeng and Zhang. 2010) 3
Figure 2: Hydrox Holdings Ltd. membraneless alkaline electrolysis operating principle 4
Figure 3: Thermodynamics of water electrolysis at 1 atm (Jensen et al., 2008) 12
Figure 4: Schematic diagram of an alkaline water electrolysis cell taken from P. Millet and S. Grigoriev. 2013 17
Figure 5: Schematic diagram of a PEM electrolysis cell taken from Millet and Grigoriev (2013) 19
Figure 6: Schematic diagram of solid-oxide electrolysis cell taken from Millet and Grigoriev (2013) 20
Figure 7: Conductivity of static aqueous solutions of potassium hydroxide (Allebrod et al., 2011) 22
Figure 8: Temperature dependence of the electrical conductivity of aqueous solutions of KOH and NaOH (Wendt, 1990) 23
Figure 9: Polarisation curve for 10 cm^2 electrolyser making use of gas diffusion electrodes as a function of temperature (Mazloomi and Sulaiman, 2012) 24
Figure 10: Effect on cell performance for an experimental set-up utilising a separator (Nagai et al., 2003b) 26
Figure 11: Effect on cell performance for an experimental set-up utilising no separator (Nagai et al., 2003b) 26
Figure 12: Normal insulating wall and counter electrode width configuration, potential distribution and electric current lines respectively as dashed and continuous curves (de Maubeuge, 2011) 28
Figure 13: This parallel mask configuration, potential distribution and electric current lines respectively as dashed and continuous curves (de Maubeuge, 2011) 29
Figure 14: The void fraction formation in the electrolyte (Mazloomi and Sulaiman, 2012) 30
Figure 15: Microscope image of bubbles emanating from a hydrogen cathode (Nagai et al., 2003b) . 30
Figure 16: Volcano plot for the hydrogen evolution reaction (Yde et al., 2013) 34
Figure 17: Volcano plot for the oxygen evolution reaction (J. Lee et al., 2013) 35
Figure 18: Pourbaix diagrams at 80°C for Iron (above-left), Nickel (above-right) and cobalt (bottom), in a water system (Yde et al. 2013) 36
Figure 19: Electrode geometry and assembly procedure within the HH electrolyser apparatus 38
Figure 20: Process flow diagram of the Hydrox Holdings Ltd. membraneless test rig 40
Figure 21: Illustrations of (a) The electrolyser apparatus and product gas L/G separators (b) The process ancillaries showing the system sump, chemical pump and control panels 41

Figure 22: Membraneless alkaline electrolyser apparatus 43
Figure 23: (a) Hydrogen gas/liquid separator (b) Packing media contained within gas/liquid separators 44
Figure 24: (A) Electrolytic Sump (B) Circulation of electrolytic fluid within sump electrolytic sump apparatus 45
Figure 25: KOH crystal formation at high concentration and temperature resulting in rapid degradation of the chemical pump mechanical seal. 60
Figure 26: Change in mV for progressing experimental runs for the performance investigation for stainless steel 316 electrodes and 20 wt% potassium hydroxide 63
Figure 27: Change in pH for progressing experimental runs for the performance investigation for stainless steel 316 electrodes and 20 wt% potassium hydroxide 63
Figure 28: Polarisation curves of test rig as a function of potassium hydroxide (KOH) concentration at a temperature of 50°C and 70°C, an electrode gap of 3.5 mm and a flow velocity of 0.3 $m.s^{-1}$ for stainless steel 316 electrodes. 65
Figure 29: Polarisation curves of test rig as a function of potassium hydroxide (KOH) concentration at a temperature of 50°C and 70°C, an electrode gap of 3.5 mm and a flow velocity of 0.1 $m.s^{-1}$ for stainless steel 316 electrodes. 65
Figure 30: Polarisation curves of test rig as a function of potassium hydroxide (KOH) concentration at a flow velocity of 0.1$m.s^{-1}$ and 0.3 $m.s^{-1}$, an electrode gap of 3.5 mm and a temperature of 50°C for stainless steel 316 electrodes. 65
Figure 31: Polarisation curves of test rig as a function of potassium hydroxide (KOH) concentration at a flow velocity of 0.1$m.s^{-1}$ and 0.3 $m.s^{-1}$, an electrode gap of 3.5 mm and a temperature of 70°C for stainless steel 316 electrodes. 65
Figure 32: Polarisation curves of test rig as a function of potassium hydroxide (KOH) concentration at a flow velocity of 0.1$m.s^{-1}$ and 0.3 $m.s^{-1}$, an electrode gap of 3.5 mm and a temperature of 80°C for stainless steel 316 electrodes. 66
Figure 33: Left: - General silver sheen of the cathodic conductive head. Right: - Altered appearance to a bronze appearance of the anodic conductive head. 67
Figure 34: Left: - Clear electrolytic solution. Right: - Contaminated appearance of electrolytic solution 67
Figure 35: Current Density versus Average Velocity of electrolytic fluid as a function of electrolytic temperature at an electrolytic concentration of 30 wt%, a cell potential of 2 VDC and for stainless steel 316 electrodes. 69
Figure 36: Current Density versus Average Velocity of electrolytic fluid as a function of electrolytic temperature at an electrolytic concentration of 40 wt%, a cell potential of 2 VDC and for stainless steel 316 electrodes. 69

Figure 37: Current Density versus Average Velocity of electrolytic fluid as a function of electrolytic temperature at an electrolytic concentration of 30 wt%, a cell potential of 3 VDC and for stainless steel 316 electrodes. 69
Figure 38: Current Density versus Average Velocity of electrolytic fluid as a function of electrolytic temperature at an electrolytic concentration of 40 wt%, a cell potential of 3 VDC and for stainless steel 316 electrodes. 69
Figure 39: Polarisation curves of test rig as a function of cathodic and anodic material for a temperature of 70 °C, a flow velocity of 0.1 $m.s^{-1}$, an electrode gap of 3.5 mm and 30 wt% potassium hydroxide (SS: stainless steel). 71
Figure 40: Bench top experimental set-up configuration for the determination of a suitable stable conductive material 73
Figure 41: Left – Anodic electrode responsible for oxygen evolution, Right – Cathodic electrode responsible for hydrogen evolution 74
Figure 42: Nickel star shaped electrodes as observed after a beaker test at 2.5VDC for a testing duration exceeding 24 hours. 74
Figure 43: Pictures of (a) Evidence of void fracture taking place between an electrode pair for an electrode gap of 2.5mm, current density of 3000mA/cm^2 and below the recommended fluid velocity of 0.075$m.s^{-1}$ (b) the reduction of void fracture between an electrode pair for an electrode gap of 2.5mm, current density of 3000mA/cm^2 and above the recommended fluid velocity of >0.075$m.s^{-1}$ .. 75
Figure 44: Polarisation curves of a membraneless stack as a function of electrode gap for pure nickel electrodes at a temperature of 50 °C, 30wt% potassium hydroxide and a flow velocity of 0.15 $m.s^{-1}$. 76
Figure 45: Polarisation curves of a membraneless stack as a function of electrode gap for pure nickel electrodes at a temperature of 70 °C, 30wt% potassium hydroxide and a flow velocity of 0.075 $m.s^{-1}$. 77
Figure 46: Polarisation curves of a membraneless stack as a function of electrode gap for pure nickel electrodes at a temperature of 70 °C, 30wt% potassium hydroxide and a flow velocity of 0.15 $m.s^{-1}$. 77
Figure 47: Polarisation curves of the test rig stack as a function of electrode geometric area for pure nickel electrodes at a temperature of 70 °C, 30wt% potassium hydroxide and a flow velocity of 0.15 m.s-1 79
Figure 48: Stability curve for cell potential as a function of testing duration for pure nickel electrodes at a flow rate of 0.075$m.s^{-1}$, an electrode gap of 2.5mm, 60°C and 30 wt% potassium hydroxide 81
Figure 49: Optimal polarisation curves for (i) the minimum electrolytic flow velocity of 0.075 m.s-1 at an electrode gap of 2.5 mm (For PGM catalysts and Ni Catalysts), and (ii) the highest demonstrated flow velocity of 0.2 m.s-1 at an electrode gap of 0.8 mm (for Ni catalyst only), as a function of theoretical and actual HHV stack efficiency at 70 °C and 30 wt% KOH 84
Figure 50: Polarisation curves and specific energy consumption of main water electrolysis technologies: (1) industrial alkaline electrolysers (70 – 95 °C), (2) solid polymer electrolysers (90 –

110 °C), (3) high temperature solid oxide electrolysers (900 °C), (4) current polarisation region for the Hydrox Holdings AWE technology for the temperature range of 50-80°C 85
Figure A1: Prior Simplified Experimental Set-up 96
Figure A2: Experimental set-up with mechanical agitator for activity determination investigation 96
Figure A3: Agitation system in motion moving fluid over the porous mesh electrodes..... 96
Figure A4: Experimental system in correct configuration for activity determination investigation..... 97
Figure A5: Current density versus cell potential for various tested systems for the determination for activity rations between mesh and plate electrodes in static and dynamic systems..... 98
Figure B1: Momentum boundary conditions as defines for the sizing of the system chemical pump 114
Figure B2: Velocity-dependant pressure drop for three different weave types of filtration mesh (E. Glatt et al., 2009) 117
Figure E1: Change in mV for progressing experimental runs for the performance investigation for stainless steel 316 electrodes and 30 wt% potassium hydroxide. 131
Figure E2: Change in pH for progressing experimental runs for the performance investigation for stainless steel 316 electrodes and 30 wt% potassium hydroxide. 131
Figure E3: Change in mV for progressing experimental runs for the performance investigation for stainless steel 316 electrodes and 40 wt% potassium. Hydroxide. 132
Figure E4: Change in pH for progressing experimental runs for the performance investigation for stainless steel 316 electrodes and 40 wt% potassium hydroxide. 132
Figure E5: Change in mV for progressing experimental runs for the performance investigation for stainless steel 316 electrodes and 50 wt% potassium hydroxide. 132
Figure E6: Change in pH for progressing experimental runs for the performance investigation for stainless steel 316 electrodes and 50 wt% potassium hydroxide. 132
Figure E7: Polarisation curves of test rig as a function of potassium hydroxide (KOH) concentration at a temperature of 50°C and 70°C, an electrode gap of 3.5 mm and a flow velocity of 0.2m.s^{-1} and stainless steel 316 electrodes. 133
Figure E8: Polarisation curves of test rig as a function of potassium hydroxide (KOH) concentration at a temperature of 50°C and 70°C, an electrode gap of 3.5 mm and a flow velocity of 0.4 m.s^{-1} and stainless steel 316 electrodes. 133
Figure E9: Polarisation curves of test rig as a function of potassium hydroxide (KOH) concentration at a temperature of 50°C and 70°C, an electrode gap of 3.5 mm and a flow velocity of 0.6 m.s^{-1} and stainless steel 316 electrodes. 133
Figure E10: Polarisation curves of test rig as a function of potassium hydroxide (KOH) concentration at a temperature of 50°C and 70°C, an electrode gap of 3.5 mm and a flow velocity of 0.5 m.s^{-1} and stainless steel 316 electrodes. 133

Figure E11: Polarisation curves of test rig as a function of potassium hydroxide (KOH) concentration at a flow velocity of 0.1m.s^{-1} and 0.3m.s^{-1}, an electrode gap of 3.5 mm and a temperature of 40°C and stainless steel 316 electrodes. 134
Figure E12: Polarisation curves of test rig as a function of potassium hydroxide (KOH) concentration at a flow velocity of 0.1m.s^{-1} and 0.3m.s^{-1}, an electrode gap of 3.5 mm and a temperature of 60°C and stainless steel 316 electrodes. 134
Figure E13: Current Density versus Average Velocity of electrolytic fluid as a function of electrolytic temperature at an electrolytic concentration of 40 wt%, a cell potential of 2.5 VDC and for stainless steel 316 electrodes. 134
Figure E14: Current Density versus Average Velocity of electrolytic fluid as a function of electrolytic temperature at an electrolytic concentration of 30 wt%, a cell potential of 2.5 VDC and for stainless steel 316 electrodes. 134
Figure E15: Polarisation curves of test rig as a function of cathodic and anodic material for a temperature of 50 °C, a flow velocity of 0.075 m.s^{-1}, an electrode gap of 3.5 mm and 30 wt% potassium hydroxide (SS: stainless steel). 135
Figure E16: Polarisation curves of test rig as a function of cathodic and anodic material for a temperature of 50 °C, a flow velocity of 0.1 m.s^{-1}, an electrode gap of 3.5 mm and 30 wt% potassium hydroxide (SS: stainless steel). 135
Figure E17: Polarisation curves of test rig as a function of cathodic and anodic material for a temperature of 50 °C, a flow velocity of 0.15 m.s^{-1}, an electrode gap of 3.5 mm and 30 wt% potassium hydroxide (SS: stainless steel). 135
Figure E18: Polarisation curves of test rig as a function of cathodic and anodic material for a temperature of 60 °C, a flow velocity of 0.075 m.s^{-1}, an electrode gap of 3.5 mm and 30 wt% potassium hydroxide (SS: stainless steel). 136
Figure E19: Polarisation curves of test rig as a function of cathodic and anodic material for a temperature of 60 °C, a flow velocity of 0.1 m.s^{-1}, an electrode gap of 3.5 mm and 30 wt% potassium hydroxide (SS: stainless steel). 136
Figure E20: Polarisation curves of test rig as a function of cathodic and anodic material for a temperature of 60 °C, a flow velocity of 0.15 m.s^{-1}, an electrode gap of 3.5 mm and 30 wt% potassium hydroxide (SS: stainless steel). 136
Figure E21: Polarisation curves of test rig as a function of cathodic and anodic material for a temperature of 70 °C, a flow velocity of 0.075 m.s^{-1}, an electrode gap of 3.5 mm and 30 wt% potassium hydroxide (SS: stainless steel). 137
Figure E22: Polarisation curves of test rig as a function of cathodic and anodic material for a temperature of 70 °C, a flow velocity of 0.15 m.s^{-1}, an electrode gap of 3.5 mm and 30 wt% potassium hydroxide (SS: stainless steel). 137

Figure E23: Polarisation curves of a membraneless stack as a function of electrode gap for pure nickel electrodes at a temperature of 50 °C, 30wt% potassium hydroxide and a flow velocity of 0.075 $m.s^{-1}$. 137
Figure E24: Polarisation curves of a membraneless stack as a function of electrode gap for pure nickel electrodes at a temperature of 50 °C, 30wt% potassium hydroxide and a flow velocity of 0.1 $m.s^{-1}$. 137
Figure E25: Polarisation curves of a membraneless stack as a function of electrode gap for pure nickel electrodes at a temperature of 70 °C, 30wt% potassium hydroxide and a flow velocity of 0.1 $m.s^{-1}$. 138

LIST OF TABLES

Table 1: Electrolysis cells and their specialties (Jensen et al., (2008)) 2
Table 2: Material compatibility determined from material corrosion resistance tables for potassium hydroxide solutions 46
Table 3: Safety and commissioning main point checklist 47
Table 4: Constant and variable test parameters for electrolytic concentration optimisation 49
Table 5: Constant and variable test parameters for catalytic material optimisation 50
Table 6: Constant and variable test parameters for electrode gap optimisation 52
Table 7: Constant and variable test parameters for three dimensional electrode performance optimisation 53
Table 8: Constant and variable test parameters for gas purity analysis 54
Table 9: Constant and variable test parameters for medium term stability testing 54
Table 10: Confidence interval table (Peters, 2001) 58
Table 11: Points of deactivation and subsequent electrode replacement during the investigation of determining the optimised electrolytic concentration for stainless steel 316 electrodes 61
Table 12: Gas purity of hydrogen and oxygen as a function of electrolytic fluid velocity over the electrode face. 81
Table A1: Physical Parameters of mesh and plate electrodes for activity determination investigation 97
Table A2: Dynamic versus static ratios for various tested systems 99
Table B1: Voidage characteristics related to the diameter of the packing media taken from Sinnot (1999) 106
Table C1: Expressions for substitution when solving for potassium hydroxide mass for a particular concentration 122
Table D1: Mechanical equipment checklist 124
Table D2: Electrical and Ventilation Equipment Checklist 125
Table D3: Control systems and equipment checklist 126
Table D4: Ion transport medium equipment checklist 127
Table D5: Personnel equipment checklist 127
Table D6: Test method equipment checklist 128
Table D7: Marking and Labeling Checklist 129

LIST OF SYMBOLS

Area (m^2)	A
Carbon Dioxide	CO_2
Standard equilibrium Potential (V)	E^0
Standard equilibrium potential for the cathodic electrode (V)	$E^0_{Cathode}$
Standard equilibrium potential for the anodic electrode (V)	E^0_{Anode}
Electrical Energy Consumed by Electrodes (W)	E
Faradays Constant ($C.mol^{-1}$)	F
Standard Gibbs Free Energy ($kJ.mol^{-1}$)	$\Delta G°$
Standard Enthalpy ($kJ.mol^{-1}$)	$\Delta H°$
Hydrogen Ion	H^+
Hydrogen Gas	H_2
Water	H_2O
Current (A)	I
Current Density ($mA.cm^{-2}$)	i
Iridium	Ir
Hydroxyl Ion	OH^-
Length (m)	l
Volumetric Flow Rate of Hydrogen (m^3/s)	N_{H2}

Nickel Metal	Ni
Moles	n
Efficiency	η
Oxygen Ion	O^{2-}
Oxygen Gas	O_2
Resistivity (Ω.m)	ρ
Partial Pressure of Hydrogen (Pa)	ρ_{H2}
Partial Pressure of Oxygen (Pa)	ρ_{O2}
Partial Pressure of Water (Pa)	ρ_{H2O}
Platinum	Pt
Additional Energy Required for a Spontaneous Reaction (W)	Q_{cell}
Energy lost to Surroundings as Heat (W)	Q_{H20}
Universal Gas Constant (J/mol.K)	R
Resistance (Ω)	R_Ω
Ruthenium	Ru
Thermo Neutral Voltage (VDC)	$u°_{tn}$
Standard Entropy ($J.mol^{-1}.K^{-1}$)	$\Delta S°$
Temperature (K)	T
Time (s)	t

NOMENCLATURE

AWE	Alkaline Water Electrolysis
CG	Gas Chromatography
HH	Hydrox Holdings Ltd.
HHV	Higher Heating Value of Hydrogen
MEA	Membrane Electrode Assembly
NREL	National Renewable Energy Laboratory
PEM	Proton Exchange Membrane
SOE	Solid Oxide Electrolysis
MMO	Metal Metal Oxide

GLOSSARY OF TERMS

Reactive Surface Area	Refers to the total surface area of a particular geometry that is undergoing reaction at a specific point in time
Alkali	A substance that creates a bitter taste and a slippery feel when dissolved in water. An alkali has a pH greater than seven and is characterised in solution by the release of the hydroxide molecule. Alkalis may include the soluble hydroxide, carbonate, and bicarbonate salts of calcium, magnesium, potassium and sodium.
Anode	The electrode that has a positive potential relative to the cathode. In an electrochemical cell this is the electrode where oxidation occurs.
Cathode	The electrode that has a lower or negative potential relative to the anode. In an electrochemical cell this is the electrode where reduction occurs in an electrochemical cell.
Cell Voltage / Cell Potential	The electrical potential difference between two electrodes or two poles of an electrochemical cell. In the case of a three-electrode cell, it is the potential difference between the working electrode and the counter electrode.
Current Density	In electrical engineering, current density is defined as the total flow of charge or current divided by the total cross sectional area of the conductor. The current density defined within this experimental investigation will be noted as the total current provided to an

	electrode divided by the available cross sectional area exposed to electrolytic fluid flow.
Efficiency	Efficiency in the context of this research is referred to as the higher heating value efficiency. The higher heating value refers to the quantity of energy released once hydrogen and oxygen has combusted and the products are returned to room temperature. The heating value divided by the total work input (Electrical, Heating and pumping energy); will be the efficiency of the system
Electro-catalysis	The phenomenon of increasing the rate of an electrode reaction by changing the electrode material. The rate of electrode reactions can be strongly dependant on the composition and morphological structure of the electrode surface.
Electrocatalyst	The electro-chemically active component that results in the phenomenon of electro-catalysis.
Electro-chemical Deposition	The electro-deposition process is defined as deposition of a metallic component in which electric current is carried between electrodes within an electrolyte and an unknown metallic or metallic oxide substance which is deposited at reducing electrode.
Electrode Gap	The electrode gap refers to the actual distance between the anode and cathode electrode face.
Electrolysis	A method by which chemical reactions are carried out by the passage of electric current through a solution of an electrolyte or through a molten salt.
Electrolyte	A chemical compound (salt, acid, or base) that dissociates into electrically charged ions when dissolved

	in a solvent. The resulting electrolyte (or electrolytic solution) is an ionic conductor of electricity.
Electroplating	The process that produces a thin, metallic coating on the surface of another metal. The metallic substrate to be deposited is termed the cathode with reference to an electrolytic cell configuration and is the site where the cations (positive ions) will be reduced to form a metal coating on the substrate surface.
Electro-catalytic	A catalyst that participates in electrochemical reactions
Fluid Velocity	The average velocity of fluid passing through each exposed electrode surface.
Geometric Surface Area	Refers to the total surface area of a particular geometric structure that is exposed to the solution when submerged
Hydrogen Evolution Reaction	An electrode reaction in which hydrogen gas is produced at the cathode of an electrolytic cell by the reduction of hydrogen ions or the reduction of water molecules of an aqueous solution.
Oxygen Evolution Reaction	An electrode reaction in which oxygen gas is produced at the anode of the electrolytic cell by the oxidation of water or hydroxide ions of an aqueous solution.
Ion	An electrically charged chemical particle (atom, molecule, or molecule fragment).
Overpotential	The difference in the electrode potential of an electrode between its equilibrium potential and its operating potential when a current is flowing. The overpotential represents the extra energy needed to force the electrode reaction to proceed at a desired rate. Consequently, the operating potential of an anode is always more positive

	than its equilibrium potential, while the operating potential of a cathode is always more negative than its equilibrium potential.
pH	A measure of the degree of the acidity or the alkalinity of a solution as measured on a scale of 0 to 14.
Polarisation	The change in the potential of an electrode from its equilibrium potential upon the application of an electrical current.
Pole Pair	A pole pair constitutes the pairing of an anode and a cathode electrode involved in an electro-chemical reaction.

1. INTRODUCTION

Hydrogen is typically produced as a by-product from processes such as natural gas reforming, gasification of coal or biomass as well as the gasification of heavy oils (Eunnyeong et al., 2012). Global demand of hydrogen in 2006 was 50 million metric tons (Zeng and Zhang, 2010). It is suggested by the National Renewable Energy Laboratory (NREL) that this demand is likely to increase as the production of hydrogen becomes more cost effective. Generation of hydrogen from non-renewable materials gives rise to additional harmful products such as carbon monoxide. The production or presence of carbonaceous products that fuel gas may have will have negative impact on the function of hydrogen fuel cells (Wang et al., 2014). It is foreseeable in the future, production of hydrogen gas through current methods will become unsustainable.

The key component preventing the commencement of a hydrogen economy is the capital and operating costs associated with the production of hydrogen gas. Electricity cost has a significant impact in the end cost factors of hydrogen produced by water electrolysis methods (Ivy, 2004). However it is noted by Ivy (2004) that the capital cost of electrolysis systems is far more significant than the operating costs. It is therefore imperative to identify areas that can be optimised in order to reduce the CAPEX and OPEX costs associated with hydrogen production from water electrolysis methods.

By examining the key contributors of hydrogen production performance, a detailed image can be drawn to the degree of optimisation possibilities, not only on energy consumption of hydrogen generation systems, but also to highlight the areas contributing to the excessive CAPEX and OPEX costs. Also, comparisons can be drawn between the operating benchmarks and those found by experimental methods using the HH alkaline electrolysis pilot plant.

1.1. Background

Water electrolysis is one of the simplest methods of producing hydrogen. The method produces no harmful by-products and the only required reactant is water. Alkaline Water Electrolysis (AWE) in particular, is regarded as the most simple and mature water electrolysis technology, having been demonstrated on the Mega-watt scale by companies such as Norsk-Hydro, Stuart and Teledyne (Ivy, 2004). This technology uses readily available electrode materials such as stainless steel and nickel (Kjartansdottir et al., 2013). Solid Oxide Electrolysis (SOE) and Proton exchange electrolysis (PEM) methods use capital intensive PGM materials for construction of electrodes due to the presence of an acidic operating medium (Marini et al., 2012). The basic reaction mechanism for any water electrolysis system is similar to the difference resulting in the charge carrier of choice. The individual half reactions consequently differ in formulation; however the overall reaction is fundamentally the same. The following table represents the fundamental differences of current water electrolysis systems taken from Jensen et al., (2008):

Table 1: Electrolysis cells and their specialties (Jensen et al. (2008))

Type	*Alkaline*	*Acid*	*Polymer electrolyte*	*Solid oxide*
Charge carrier	OH^-	H^+	H^+	O^{2-}
Reactant	Water	Water	Water	Water, CO_2
Electrolyte	Sodium or Potassium hydroxide	Sulphuric or Phosphoric acid	Polymer	Ceramic
Electrodes	Nickel	Graphite with Pt, polymer	Graphite with Pt, polymer	Nickel, ceramics
Temperature	80 °C	150°C	80°C	850°C

In order to dissociate water into its components (hydrogen and oxygen gas), energy is required, which in the case of an electrolyser, is a combination of electrical and heat energy. The overall reaction ((Equation (1)) for water electrolysis is as follows (Zeng and Zhang, 2010):

$$H_2O_{(l)} + Energy \xrightarrow{yields} H_{2\,(g)} + {}^1\!/_2\, O_{2\,(g)} \ldots\ldots\ldots (1)$$

The energy term in Equation 1 (above) is represented by the higher heating value of hydrogen having a value of 283.3kJ.mol^{-1} or 39kWh/kg H_2. The higher heating value of fuel is defined as the amount of heat released by the specified quantity (initially at 25°C) once it is combusted and the products have returned to the initial temperature of 25°C (Zeng and Zhang, 2010). The basic components of a water electrolysis system can be plainly illustrated by an electrolysis cell schematic below (Zeng and Zhang, 2010):

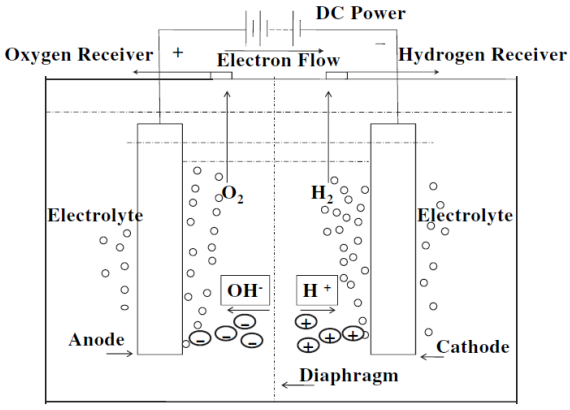

Figure 1: A schematic illustration of a basic water electrolysis system (Zeng and Zhang. 2010)

A basic water electrolysis cell consists of 2 electrodes in an ionic conductive solution referred to as the 'electrolyte' as represented in Figure 1 (above). The solution facilitates the transfer of charge between the cathode (negative electrode) and the anode (positive electrode).The cathodic and anodic electrode is the site for the reduction and oxidation half reaction respectively. A semi-permeable diaphragm/membrane allows for the flow of ions; however it restricts the movement of product gases into the corresponding compartment. This device facilitates the separation of the oxygen and hydrogen gas. As the process is non-spontaneous, an external driving force must be provided for the reaction to become spontaneous. A direct current external electrical power source drives electrons in an external circuit from the anode to the cathode. The rate at which these electrons flow or the charge flows (current), defines the theoretical production rate of hydrogen and oxygen gas. The potential will therefore define the magnitude of the current based on the magnitude of resistances or overpotentials of a particular experimental or electrolyser set-up.

These resistance contributors are comprised of a number of mass transfer and material resistances that will be examined in this paper.

The Hydrox Holdings Ltd. membraneless technology (South African Patent Number 21/02/2015/00696 – with further pending patents) used for determining the performance influencing parameter trends for this research demonstrates a number of similarities with conventional alkaline water electrolysis methods. This technology makes use of similar electrode materials and has similar performance trends with changing electrolytic solution concentration, temperature and flow rates. In contrast to existing technologies, this technology relies on the magnitude of flow and manipulation of the flow in order to create gas separation between porous electrodes. This has the fundamental benefit of eliminating the ohmic drop contribution of the conventional ion permeable membrane positioned between the electrodes. The trade off of this technology is that a constant flow of electrolytic solution is required at a minimum recommended flow velocity in order to maintain the separation of bi-phase mixtures of product gas and electrolytic solution which produces additional parasitic load required from the electrolytic solution circulation pump.

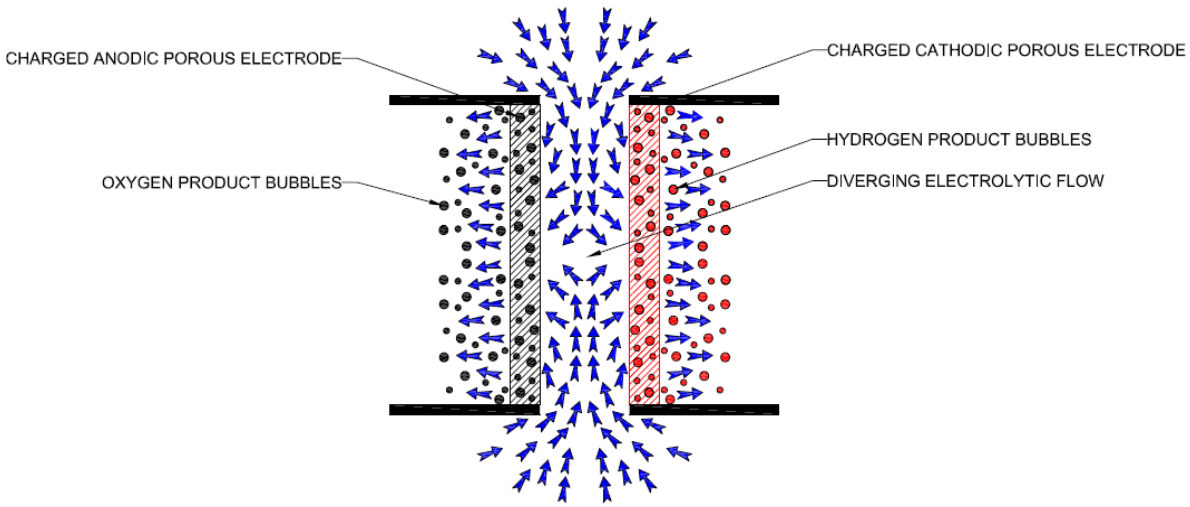

Figure 2: Hydrox Holdings Ltd. membraneless alkaline electrolysis operating principle

The above diagram shows the basic operating principle of the membraneless technology, being independent of any separation membrane/diaphragm, and using only the diverging flow of electrolyte to create separation of the produced product gases. The above configuration would represent a single electrode pair, of which scale up of production is achieved by incorporating a number of electrode pairs in the same pressurising chamber as will be illustrated in Section 3.3 – Experimental Apparatus.

1.2. Problem Statement and Research Motivation

As a promising method of producing hydrogen by renewable methods, water electrolysis has become a key research field for a number of institutions globally. The goal is to enormously reduce the inefficiencies and losses associated with electrolysers in order to produce hydrogen cost effectively. With renewable sources of power such as wind and solar energy, the pursuit of converting and storing energy in a clean energy carrier, such as hydrogen, is becoming increasingly attractive. A popular area of research looks at the efficiency optimisation of water electrolysis. The efficiency of a water electrolyser is closely related to a number of parameters and many attempts have been made to reduce the operating potential[1] of an electrolysis stack and maximise the current density[2] (Mazloomi and Sulaiman, 2012). Suggestions can therefore be given for attaining higher stack efficiencies[3]. It is therefore this papers intention to research and analyse these factors from observations and experimental results, thereby classifying their importance and influence on water electrolysis performance. Focus will be given in particular to AWE technologies given that the HH pilot plant shares the most similarities with conventional AWE technologies.

1.3. Research Objectives

The objectives of this are to:

- Identify the parameters that influence alkaline water electrolysis
- Test the effects of the identified parameters on AWE using the existing pilot plant
- Establish and evaluate trends for performance parameters and draw comparisons with industry practice
- Establish the advantages and disadvantages of current alkaline water electrolysis technologies and areas that need to be focused to allow the technology to become more economically lucrative.

[1] The operating potential of an electrolysis stack provides an indication of the stack electrical efficiency and is applied to overcome a number of resistances.

[2] The current density provides a theoretical measure of the amount of hydrogen produced per square unit area of an electrode.

[3] Stack efficiency is the HHV efficiency directly relating only to the electrolyser, and discounting any additional parasitic load such as power demand of the electrolytic circulation pump.

1.4. Source of Data and Methodology

The raw data obtained for interpretation in this research dissertation was done by using the HH alkaline electrolyser pilot plant and various calibrated equipment pieces (Boeco PT-380 mV/pH meter, TDK 2.4kW programmable power supply, HHD-50 Precision Meters' electromagnetic flow meter and the Agilent 6890 gas chromatograph). Experimental investigations and methodologies pertaining to these investigations were specifically formulated for the purpose of investigating the relevant performance influencing parameters. The literature review is focused on reporting findings from various sources in order to build on a hypothesis for expected results and observations. Additionally, research will be performed into the physical and operational differences of various water electrolysis technologies in order to distinguish unexpected deviations of parameters as to what can be potentially discovered during experimental investigations. In this manner, areas of excessive capital and operational cost can be revealed based on the complexity of design, preparation of materials and durability of materials.

1.5. Dissertation Structure

This dissertation is structured into five chapters which represents a 'logic flow' to the resolution of the problem statement.

Chapter 1 serves to introduce the research problem and the purpose of the research. Chapter 2 provides a detailed literary review that will compare and discuss the various technologies available to perform water electrolysis along with a detailed look at the performance influencing parameters. Chapter 3 details the experimental methodologies and equipment involved in generation and collection of experimental raw data. Chapter 4 will serve to present the results obtained from the investigation methodologies along with a discussion of results. Chapter 5 will draw on conclusions based on the interpretation of experimental findings, while also presenting recommendations for future work.

2. LITERATURE REVIEW

2.1. Introduction to Water Electrolysis Technology

Alkaline water electrolysis is regarded as the most simple and mature technology making use of cost effective and readily available electrode materials such as stainless steel and nickel (Kjartansdottir et al., 2013). Solid oxide and PEM technologies make use of expensive PGM materials for the construction of electrodes, which adds to the additional capital and operating costs of the system (Marini et al., 2012). These systems are costly as the majority of the total cost is made up of the electrodes and membranes. The electrode stack has an average design life of 5 to 7 years (Ivy, 2004), depending on the electrode durability, resulting in the membrane and electrodes requiring regular replacement at least twice in the 10 year design life, thus adding to the main disadvantages of PEM technology (Marini et al., 2012). Although PEM electrolysers have the largest potential to reduce the scale of water electrolysis technology, operating durability remains a challenge. Alkaline electrolysers have been recorded to last between 10 to 15 years (Ivy, 2004), with a number of plants operating as long as 40 years. Alkaline technology exhibits high flexibility when operating at low production rates and demonstrates ease of scaling; the large scale of the technology however incurs large capital costs (Marini et al., 2012). A substantial reduction in capital and operating expenditure is therefore required through simplified design, and a reduction in maintenance and capital costs, and a removal of different resistance components by the proposed methods. This will be the focus of this paper.

As the production cost is a limiting factor stagnating the growth of the hydrogen economy, the goal is to significantly reduce the cost to produce hydrogen on an industrial scale as well as reducing the cost associated with smaller household/neighborhood scale units. The US Department of Energy's current hydrogen production cost target is $3 per gasoline gallon equivalent (gge) (Ivy, 2004). This benchmark target is however subject to the changing electricity price and is representative of large forecourt electrolysis plants only (~1000 kg H_2 /day) and cannot therefore be compared to plants of lesser scale that have dedicated

applications. The NREL provides cost benchmarks for plants with various hydrogen production capabilities. It is stated that a hydrogen selling price of \$19.01/kg H_2 is relevant for small neighborhood scale units with approximate hydrogen production mass flow rates of ~20 kg H_2/day (Ivy. 2004). In the event that the combined capital and operating expenditure becomes less than this amount, for a typical 10 year operating lifespan, the technology would be financially viable. The cost of using hydrogen as energy storage medium needs to prove more cost effective to current energy storage methods for the technology to become popular as an energy storage medium.

2.2. Technology Advantages, Limitations and Outlook

Water electrolysis technologies provide a unique solution to the storage of energy and as a potential competitor to battery technologies. This hydrogen generation technology has a number of advantages as an alternative method of energy storage; however a number of limitations are still present stemming the rapid commercialisation of water electrolysis technologies:

Advantages

- Water electrolysis technology has a lower pollution footprint in comparison to battery technologies.
- Higher energy storage densities are possible with equipment of lower mass and occupational volume.
- The emissions from water electrolysis is only hydrogen and oxygen, and subsequently in the process of combusting the hydrogen, water is formed and can possibly be recycled back for subsequent water electrolysis yet again.
- Water electrolysis technology is capable of operation at high temperature and pressure to obtain high levels of energy conversion efficiency.
- Water electrolysis technology is capable of generating hydrogen gas as pressure without the need of additional compression equipment.
- A wide range of scaled-up production of hydrogen is possible from a residential scale (1-10 kg H_2) large forecourt scales (> 1000 kg H_2).

Limitations

- Current electrolysis technologies utilising a membrane in order to separate the produced hydrogen and oxygen gas, still encounter severe limitations with regard to the membrane operating temperature and pressure limitations. Therefore a drastic improvement into the operating lifetime of this component is required. The HH technology serves to curb this requirement by eliminating it at the requirement of a higher parasitic load from the circulation pump.
- Current methods employed in the production of hydrogen still remain economically attractive in comparison to electrolysis technologies, however as non-renewable fuels diminish and greater restrictions are imposed on emissions, the feasibility of a hydrogen water electrolysis economy is becoming more viable.
- Current electrode materials need to become more cost effective and more robust during operation in order to resist long term electro-catalytic poisoning.
- The scale of predominantly, the alkaline water electrolysers needs to be reduced by increasing the operating current density to be comparable with proton exchange membrane technologies.
- Water electrolysis technologies need to become more flexible in operation using renewable fluctuating energy sources such as solar power, as the means of supplying the electrodes with energy.
- Water electrolysis technologies need to become more flexible in terms of the water quality used to generate the hydrogen and oxygen. The production of ultra pure distilled water used as a feed stock for proton exchange technologies can be a cost intensive procedure.

2.3. Water Electrolysis Thermodynamics

The water electrolysis reaction as shown in Equation 1 (above) is similar to any REDOX reaction in terms of consisting of a reduction half reaction and an oxidation half reaction. The water electrolysis reaction (Equation 1) can be seen re-written below in a form that illustrates the energy required in order for the reaction to occur (Berry, 2004):

$$H_2O_l + 286\ kJ.mol^{-1} \xrightarrow{yields} H_{2_g} + {}^1/_2\, O_{2_g} \ldots\ldots\ldots (2)$$

The minimum energy required therefore to produce 1 mol of hydrogen is 286 kJ.mol^{-1}. This energy represents a combination of heat and electrical energy for an electrolyser. Due to inefficiencies[4], dependant on the electrolysis system configuration, an amount of energy greater than the specified minimum amount of energy is therefore required for the reaction to take place. It is therefore the goal of electrolyser designers to reduce these inefficiencies as much as possible in order to produce hydrogen cost effectively.

In order for any REDOX reaction to occur, a "barrier" of potential must first be overcome in order to make the reaction feasible. The potential is commonly referred to as the equilibrium potential (E^0). The equilibrium potential is defined as the equilibrium potential difference between the relevant anodic and cathodic reactions respectively and is described by the following equation (Mueller-Langer et al., 2007):

$$E^0 = E^0_{anode} - E^0_{cathode} \ldots\ldots\ldots (3)$$

Where, E^0_{anode} (V) is the standard reduction potential for the anodic reaction and $E^0_{cathode}$ (V) is the standard reduction potential for the cathodic reaction.

An alternate method of determining the equilibrium standard potential, other than using a table of standard potentials for reduction, is to use the Nernst equation of water electrolysis (Muzhong et al., 2011):

$$E^0 = 1.23 - 0.9X10^{-3}(T - 298) + \frac{RT}{4F}\ln\left(\frac{p^2_{H_2}.p_{O_2}}{p_{H_2O}}\right) \ldots\ldots\ldots (4)$$

Where, T(K) is temperature, R (m^3.Pa.K^{-1}.mol^{-1}) is the ideal gas constant, F is Faraday's constant amounting to 96 485 C.mol^{-1}, $p_{H2,}$ p_{O2} and p_{H2O} is the partial pressures (Pa) ofhydrogen, oxygen and water vapour respectively.

[4] Inefficiencies or energy losses typically refer to the various resistances of a system preventing free passage of charge.

It can be noted that when Equation (4) is solved for a temperature of 25°C, the expression will determine the equilibrium potential (Muzhong et al., 2011). This water dissociation potential is however, influenced by the temperature and the catalytic activity of the electrodes (Muzhong et al., 2011). By performing the reaction, for example, on platinum electrodes instead of nickel electrodes will yield a variance in the required dissociation/standard potential will be yielded.

The equilibrium potential of a water electrolysis reaction can be related to the Gibbs free energy by the following expression (Zeng and Zhang, 2010):

$$\Delta G^0 = nFE^0 \dots\dots\dots (5)$$

Where, n is the number of electrons involved in the reaction as shown in equation 1 (above), F is Faraday's constant amounting to 96 485 C.mol^{-1} and E^0(V) is the standard equilibrium potential for the water electrolysis reaction.

By substituting values for the above variables, it can be deduced that the equilibrium potential for the water electrolysis reaction amounts to 1.23V at a temperature of 25°C (Dieguez et al., 2008). Operating at this low potential will not produce a reaction without an energy contribution from heat. Therefore, an input of heat is required before this reaction could take place. Operating at a potential referred to as the thermo-neutral voltage which will require no additional heat or electrical energy. Operating above this voltage will therefore, result in the generation of heat from the system emitted to the surroundings. The total enthalpy of the system is related to the thermo-neutral potential by the following expression:

$$\Delta H^0 = nFU^0_{tn} \dots\dots\dots (6)$$

Where, n is the number of electrons involved in the water electrolysis reaction, F is Faraday's constant amounting to 96 485 C.mol^{-1} and U^0_{tn}(V) is the thermo-neutral voltage.

By substituting values in the variables for Equation (6) as similarly done for Equation (5) (above), it is deduced that the thermo-neutral voltage for a water electrolysis system at 25°C is 1.48V. The difference in potential from the equilibrium potential and the thermo-neutral voltage therefore generates sufficient heat energy in order to account for the minimum required energy as shown in Equation (2) (above), in order for the water electrolysis reaction to become spontaneous.

The following expression relates the total enthalpy of a system (Equation (6)) to the total heat and Gibbs free energy (Equation 5) (Dieguez et al., 2008):

$$\Delta H^0 = T\Delta S^0 + \Delta G^0 \dots\dots\dots (7)$$

Where, T(K) is temperature, S^0 (J.mol^{-1}.K^{-1}) is the standard molar entropy of the system and ΔG^0 (kJ.mol^{-1}) is the standard Gibbs free energy of the system.

The $T\Delta S^0$ term in Equation (7) represents the additional energy that is added to the system in the form of heat. It is noted upon closer inspection of Equation (7), that at a constant energy demand ΔH^0, the energy can be either accounted for by either increasing the Gibbs free energy term, or by increasing the Entropy term. The following figure taken from Jensen et al., (2008), demonstrates the thermodynamic contributions of the heat demand and electrical demand that constitutes the total energy demand for the water electrolysis reaction:

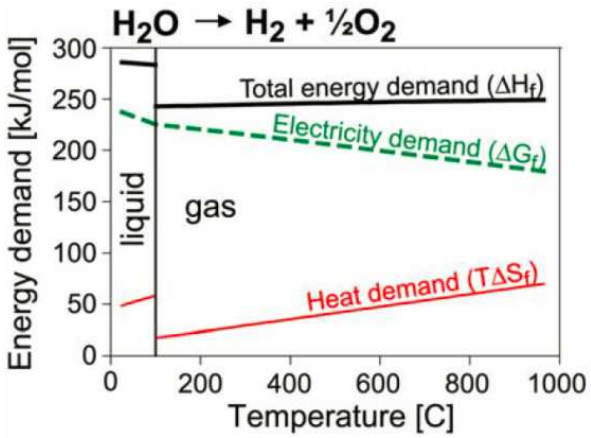

Figure 3: Thermodynamics of water electrolysis at 1 atm (Jensen et al., 2008)

This therefore describes how SOE electrolysers are able to obtain adequate current densities at low voltages (below the equilibrium voltage at 25°C) and at high temperatures exceeding 100°C.

Ultimately it is desirable to reduce the required "overpotential" by targeting key causes of potential loss. The following equation identifies all the components of energy loss (Zeng and Zhang, 2010):

$$E_{lossTOTAL} = E_{Loss_{Circuit}} + E_{Loss_{anode}} + E_{Loss_{O_2,Bubble}} + E_{Loss_{Ion}} + E_{Loss_{membrane}} + E_{Loss_{cathode}} + E_{Loss_{H_2,Bubble}} \ldots\ldots\ldots (8)$$

Where, $E_{Loss,Circuit}$ is the overpotential due to resistance in the external conductor, $E_{Loss,Anode}$ is the overpotential due to resistance in the anodic reaction, $E_{Loss,O2,Bubble}$ is the overpotential due to resistance associated with bubble generation on the anodic electrode, $E_{Loss,Ion}$ is the overpotential due to resistance in the electrolytic solution, $E_{Loss,Membrane}$ is the overpotential due to resistance associated with the membrane separator, $E_{Loss,Cathode}$ is the overpotential due to the cathodic reaction, and $E_{Loss,H2,Bubble}$ is the overpotential due to resistance associated with bubble generation on the cathodic electrode.

Equations (7) and (8) therefore broadly define the method required to increase the efficiency of an electrolyser. The first method would reduce the energy needed to decompose water into hydrogen and oxygen by thermodynamic means. This can be achieved by either increasing the temperature or the pressure. The second method of increasing efficiency would entail reducing the resistance contributions of the dominant causes of resistances represented by Equation (8) (above) which will be examined in greater detail within the following sections.

2.4. Efficiency Determination of Electrolysers

Within literature, there are a number of expressions available for determining the efficiencies of water electrolysis systems. The following expression, taken from Zhang et al., (2010), is believed to be accurate when considering the overall reaction efficiency of water electrolysis systems:

$$\eta_{overall} = \frac{\dot{N}_{H_2,out} HHV}{E + Q_{cell} + Q_{H_2O}} \ldots\ldots\ldots (9)$$

Where, $N_{H_{2,out}HHV}$ (Nm^3/hr) is the total volumetric flow rate of hydrogen, *HHV* is the higher heating value of hydrogen which amounts to 39kWh/kg H_2 or 3.54kWh/Nm^3 H_2, *E* (kWh) is the total electrical energy introduced into the system, having taken the power supply electrical efficiency into account, Q_{cell} (kWh) is the total amount of heat energy introduced into the electrolyser in order to make the reaction spontaneous, and Q_{H2O} (kWh) is the total amount of additional heat energy introduced into the system to make up for the heat losses from the system.

Equation (9) is used when determining the overall efficiency of a water electrolysis system noting all parasitic loads as part of the total energy consumption. In the case of experimental analysis, the electrical demand of the electrolysis cell will be the primary focus. As a result, an efficiency referred to as the 'stack efficiency' will be used to quantify cell performance. Therefore Equation (9) is adapted as follows:

$$\eta_{stack} = \frac{\dot{N}_{H_2,out}HHV}{E} \dots\dots\dots (10)$$

As a result, only the electrical energy demand by the power supply will be accounted for. Due to the nature of the experimental set-up and the sheer size of the heat loss surfaces, it would be improbable to define accurately the total heat introduced into the system and the total heat lost from the system as it is subject to ambient temperature fluctuation.

The molar flow rate of hydrogen is often measured experimentally; however it is possible to determine the flow of hydrogen by theoretical methods (Zhang et al., 2010). According to Faraday's law, the rate of an electrochemical reaction depends on the electrical current (Zhao et al., 2008):

$$\frac{dN}{dt} = \frac{I}{nF} \dots\dots\dots (11)$$

Where, *n* is the number of electrons involved in the consumption of 1 mol of water and *I* (A) is the electrical current and *F* is Faraday's constant amounting to 96 485 $C.mol^{-1}$.

2.5. Basis for Current Density

Current density is an important performance indicator and is often used in the construction of polarisation curves which is the plot of current density versus cell potential. Knowing the basis of current density for all data is essential for comparison between alternate sources and technologies. Current density is calculated by the following equation:

$$i = \frac{I}{A} \dots\dots\dots (12)$$

Where, I (mA) is the current and A (cm^2) is the electrode surface area.

There is no fixed benchmark relating current to the electrode surface area, as a number of methods and definitions are employed in determining the electrode surface area for input into Equation (12) above.

Current density has been found to be calculated on the basis of the geometric surface area, effective surface area, real or active surface area, and the cross sectional surface area. The most common correlation found, relates to the geometric area of the electrode as used by Ganley (2009) and Zeng and Zhang (2010). The geometric area, defined by Zeng and Zhang (2014), is the projected area of an electrode surface on a plane.

Geometrically calculated current densities however, fail to take into account the surface nature of catalytic substrates which often serve to increase the surface area of electrodes to an even greater extent. Zeng and Xhang (2014) define the effective surface area as the total 'wettable' area available for electron transfer. The determination of real surface area of electrodes however, is greatly dependant on the method employed and the experimental conditions (Jarzabek and Borkowska, 1997). Many methods are available for the determination of the effective electrode area, for example; X-ray diffraction (XRD), High resolution electron microscopy (HRTEM) and CO-stripping voltammetry. As noted by Schulenburg (2010), a possible error exists of ~23-30% between these methods.

Electrodes that have undergone surface modifications such as mechanical roughening may possess a greater effective surface area compared to the geometric surface area. As a result, it is expected that electrode activity may increase with regard to geometric surface area when comparing a smooth surface to a mechanically roughened surface. When examining the

electrode activity with reference to the effective electrode area, the electrode activity can be seen to increase proportionally with the electrode effective area and the subsequent increase in active sites (Zeng and Zhang, 2014).

The real or active area can be described as the actual area involved in the electrochemical reaction and is typically less than the geometric and effective areas. It is dictated by the presence of catalytic poisoning or the breakdown of the catalytic surface, the number of active sites present characterised by the crevices and cracks on the catalytic surfaces, the heterogeneous composition of the catalyst and the applied potential (Zeng and Zhang, 2014). In the case of the HH electrolyser technology, bubble retention on the electrode surface dependant on the solution velocity, temperature and concentration will influence the real or active area (Mazloomi and Sulaiman, 2012). Traditionally the active area is determined by performing a numerical integration of the hydrogen adsorption current, O_2 reduction or double layer capacitance methods (Sogaard et al., 2001). However conditions are not always perfect for the accurate determination of the active area (Fragkou et al., 2012).

The HH electrolyser electrodes can be described as porous electrodes and depend on the flow of electrolytic solution to govern its design principle. Determining the geometric or real surface area of these electrodes proves difficult as their structure is often irregular, and the current density distribution is not always uniform (Doherty et al., 1996). The high specific electrode surface area of porous electrodes makes an electrolyser compact both in volume and weight and capable of operating at low voltages (Ragunathan et al., 1981). Therefore the point of optimisation regarding the HH electroyser functioning with porous electrodes will be referenced to the cross section of the electrodes since performance should be optimised per unit cross sectional area of the electrode, in order to minimise the required electrolytic flow per unit area with the benefit for reducing the pump parasitic load contribution.

Further justification of using current density references to the cross sectional area for the HH electrodes was demonstrated by undertaking a simple investigation that involved the comparison of geometric current densities for standard plate electrodes and for mesh electrodes with the same geometric dimensions. It was found that a static solid plate system demonstrated better material activity than a dynamic mesh electrode system, therefore concluding that the resultant cross sectional area current density performance of the mesh electrodes is less effective than standard plate electrodes. Using current densities in reference to the geometric area will therefore not be a true indication of the HH-electrolyser

performance as the values reported would be too low for an accurate comparison to existing electrolysis technologies. A summary of this investigation can be found in *Appendix A*.

2.6. Types of Water Electrolysers

The type and production output range of available water electrolysis technologies vary greatly. AWE represents a very mature technology that is used as the current standard for large scale water electrolysis (Jensen et al., 2008). PEM electrolysers demonstrate greater energy efficiency, higher production rates and a more compact design when compared to AWE electrolysers, however PEM electroysers have emerged into the market only recently and are yet to be demonstrated on a large scale production basis. Solid oxide electrolysers have the capability of operating at temperatures exceeding 600°C, therefore establishing superior stack efficiencies when compared to PEM and AWE systems. Nevertheless, they remain largely in the research phase of development (Jensen et al., 2008).

2.6.1. Alkaline Water Electrolysis

The basic features of AWE electrolysers are shown in the illustration below taken from Millet and Grigoriev (2013):

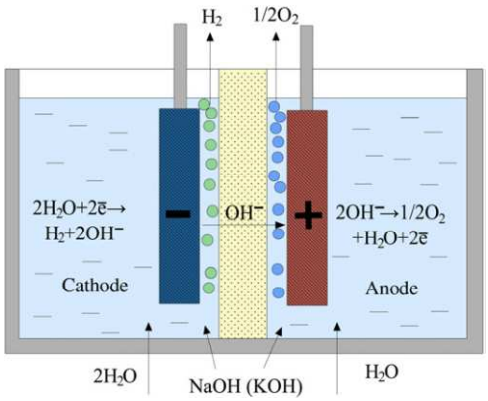

Figure 4: Schematic diagram of an alkaline water electrolysis cell taken from Millet and Grigoriev (2013)

Two metallic electrodes are immersed in a liquid electrolyte usually chosen to be either sodium hydroxide or potassium hydroxide. The anode and cathode electrode materials are generally comprised of nickel electro-plated carbon steel and carbon steel respectively. The ionic carrier is the hydroxyl ion (OH^-) generated from the decomposed alkaline solute. In the absence of leakages and evaporation, no solute is consumed during the alkaline reaction. The membrane is selectively permeable only to the hydroxyl ion in solution and maintains oxygen and hydrogen gas separation. The electrolytic operating concentration and temperature range for AWE is in the range of 20-30% by weight and 70-100°C respectively (Jensen et al., 2008). Operating current densities are generally in the region of 100-500 $mA.cm^{-2}$, resulting in the requirement of larger volume electrolysis units to produce appreciable amounts of hydrogen. AWE electrolysers have been shown to be capable of a maximum current density of 800 $mA.cm^2$ as a result of the non-PGM based materials used for the electrode assembly (Millet and Grigoriev, 2013) As a result, heat loss is generally high due to the large contact surfaces (Jensen et al., 2008). The net reaction as represented in Equation (1) (above), is shown split into its components as follows (Millet and Grigoriev, 2013):

$$4H_2O + 4e^- \xrightarrow{yields} 2H_2 + 4OH^- \ (E^0 = -0.828\,V, SHE) \ldots\ldots\ldots (13)$$

$$4OH^- \xrightarrow{yields} O_2 + 2H_2O + 4e^- \ (E^0 == 0.401\,V, SHE) \ldots\ldots\ldots (14)$$

Once again, only water is supplied to the process as represented in the above Equations (13) and (14), in order to maintain the electrolytic concentration within the desired operating range.

2.6.2. Proton Exchange Membrane Electrolysis

The basic features of PEM electrolysis are shown in the illustration below taken from Millet and Grigoriev (2013):

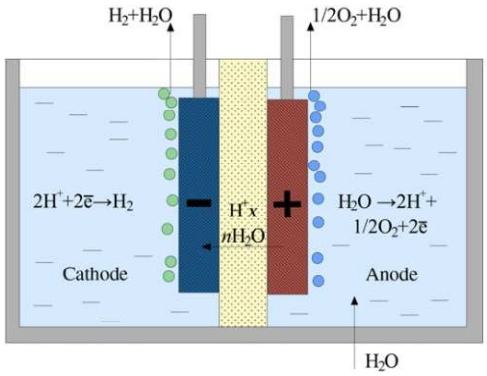

Figure 5: Schematic diagram of a PEM electrolysis cell taken from Millet and Grigoriev (2013)

PEM electrolysers make use of majority PGM based anodic and cathodic materials, and a charge is conducted between the electrodes using a proton conducting polymer type material. The material can be thought of as a solid electrolyte, as protons remain within the membrane material. As a result, the membrane has acidic properties and therefore noble metal based catalysts prove most stable to catalyse the half reactions. The technology can be thought of as a 'safer' method of water electrolysis as the fluid component of the technology is simply distilled water (Millet and Grigoriev, 2013). The resistances of the proton exchange membrane are resultantly higher than that of the liquid electrolyte. The net reaction as represented in Equation (1) (above) is split into its components as follows (Millet and Grigoriev, 2013):

$$2H_2O \xrightarrow{yields} \frac{1}{2}O_2 + 2e^- + 2H^+ \ (E^0 = 1.229\ V, SHE) \ldots\ldots\ldots (15)$$

$$2H^+ + 2e^- \xrightarrow{yields} H_2 \ (E^0 = 0\ V, SHE) \ldots\ldots\ldots (16)$$

PEM electrolysers are capable of exceeding 1000 mA.cm^{-2} at voltages as low as 1.65 V at temperatures between 60°C to 80°C (Jensen et al., 2008) and are alsocapable of significant current densities exceeding 10 000 mA.cm^2 which has been successfully demonstrated. These cells are capable of such high current densities due to the advanced PGM materials used in the membrane electrode assembly (MEA) (Millet and Grigoriev 2013). Consequently these systems are more efficient and occupy smaller volumes when compared to alkaline systems. However they are considerably more costly.

2.6.3. Solid Oxide Electrolysis

The basic features of SOE electrolysers are shown in the illustration below taken from Millet and Grigoriev (2013):

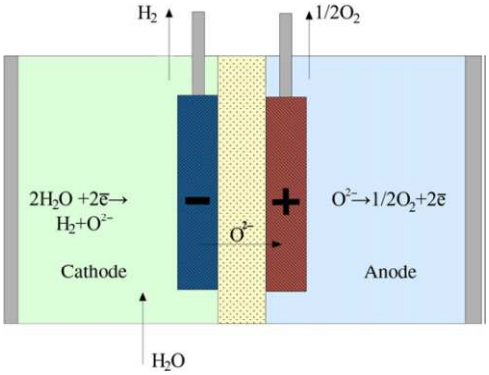

Figure 6: Schematic diagram of solid-oxide electrolysis cell taken from Millet and Grigoriev (2013)

The electrolytic material of choice for solid oxide electrolysers is an oxide conducting ceramic material such as zirconia and operate at unusually high temperatures between 800°C and 1000°C allowing them to have excellent stack efficiencies (Millet and Grigoriev, 2013). Solid oxide cells are capable of reaching current densities of 3500mA.cm^{-2} at cell potentials as low as 1.48V (Jensen et al., 2008). Resistivity of the ceramic medium is higher than those for AWE and PEM technologies. These resistances are however outweighed by the operating temperature. The net reaction as represented in Equation (1) is split into its components as follows (Millet and Grigoriev, 2013):

$$2H_2O + 2e^- \xrightarrow{yields} H_2 + O^{2-} \dots\dots\dots (17)$$

$$O^{2-} \xrightarrow{yields} \frac{1}{2}O_2 + 2e^- \dots\dots\dots (18)$$

The thermodynamic potential for the cathodic and anodic reactions respectively as shown above are not listed as their values are strongly dependant on the solvent used.

2.7. Performance Influencing Parameters

There are a number of factors that determine the rate of reaction for the water electrolysis reaction. An increase in current density would naturally create a noticeable increase in the ohmic voltage drop between the electrodes. This will result in the formation of unwanted electrical power losses and hence, lower process efficiencies. Therefore, it is desired, as far as possible, to reduce the ohmic voltage drop and maximise the resulting current density by modification of a number of performance influencing parameters. Major causes of overpotential contributors are introduced and discussed in the following sections of this paper. Optimal recommended parameters were identified and have been used as benchmarks around which experimental investigations have been based.

2.7.1. Electrolytic Concentration and Temperature

The purpose of a strong acid or base is to dissociate completely within the solution releasing a large number of ions that effectively alter the nonconductive nature of pure water (Mazloomi and Sulaiman. 2012). Two main electrolytic solutions are used for the process of alkaline electrolysis, namely potassium hydroxide and sodium hydroxide (Jensen et al., 2008). These electrolytes have the distinct advantage that are commonly found in metals such as nickel and carbon steel and can be used as the electrode materials of choice, along with the same materials as the construction materials used for the wetted parts of the electrolyser, without the need for the use of specialised expensive materials (Jensen et al., 2008). The conductivity of an electrolyte ultimately determines the degree to which polarisation will be reduced for the electrolytic process. It is therefore important to know the conductivity of the electrolyte at a given temperature and concentration. The material resistivity of the electrolytic solution will have important repercussions for the reduction in the electrical resistance contribution of the electrolyte as represented in Equation (8). The following equation makes reference to the relationship of resistivity and the resulting resistance of the solution (Mazloomi and Sulaiman, 2012):

$$R = \frac{\rho l}{A} \dots\dots\dots (19)$$

Where, ρ (Ω.m) is the material resistivity, l (m) is the length between the electrode faces and A (m^2) is the effective area of the electrode surface.

It is therefore obvious that the resistivity or conversely, the conductivity of an electrolyte needs to be optimised for the least resistance and the most conductance.

An investigation performed by Allebrod et al. (2012), involved the conductivity determination of potassium hydroxide solution at various temperatures and concentrations. The following figure taken from Allebrod et al. (2012) shows the dependence of conductivity on concentration and temperature:

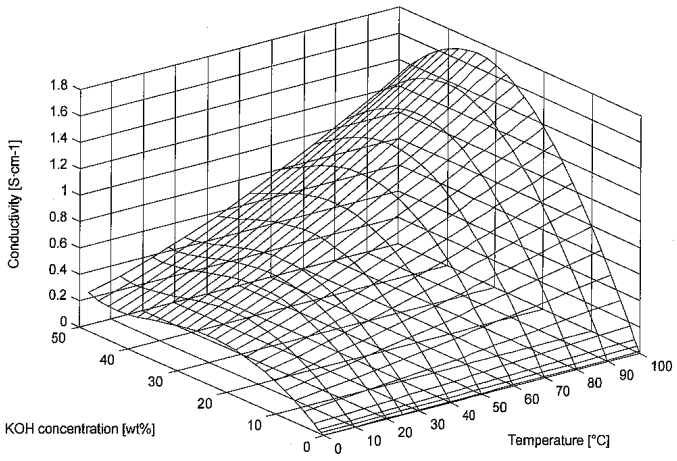

Figure 7: Conductivity of static aqueous solutions of potassium hydroxide (Allebrod et al., 2012)

Figure 7 notes that the concentration and temperature range investigated by Allebrod et al., (2012), is 0-50 % potassium hydroxide by mass and 0-100°C respectively. It is noted that the conductivity increases as a function of increasing temperature and the correlation seems linear in profile. The concentration portrays a different relationship in that an optimal concentration exists for potassium hydroxide for increasing temperatures. It is reported by Allebrod et al., (2012), that conductivity is maximised at 25°C and at a concentration of 35 % by mass. Data, however reported separately not shown in Figure 7, noted a maximum conductivity at 200°C and 45 wt%. Wendt (1990) shows that a maximum conductivity exists as a function of temperature and illustrates the maximum conductivity for potassium hydroxide and sodium hydroxide:

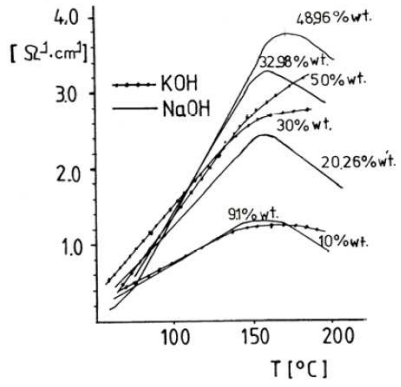

Figure 8: Temperature dependence of the electrical conductivity of aqueous solutions of KOH and NaOH (Wendt, 1990)

Figure 8 (above) shows that a maximum conductivity exists at 48.96% by mass NaOH at approximately 150°C and for 50% by mass KOH at above 200°C. Because of the high vapour pressures involved at operating electrolysers at these high temperatures, pressurised operation would be required to prevent the solution from vaporising (Jensen et al., 2008).

Consequently, the rise in operating temperature benefits[5] the systems electrical efficiency as a larger quantity of the enthalpy represented in Equation (2), is provided by the entropy term represented in Equation (7). Therefore the Gibbs contribution is reduced, and larger current densities can be achieved at lower voltages. Although temperature has benefits in improving the overall efficiency of electrolysers, it also serves to increase the size of gas bubbles forming on the metal surface along with reducing the bubble rise velocity, and as a consequence, the void fraction would increase between tightly spaced electrodes which could negatively impede efficiency (Nagai et al., 2003a). The phenomenon of void fracture will be discussed in detail in sections to follow. Conducting water electrolysis at higher temperature is seen to produce higher electrical efficiencies; however additional issues to be considered regarding the physical, mechanical and life time stability of the electrolysers need to be considered by designers of these units (Mazloomi and Sulaiman, 2012). A polarisation curve of a 10 cm^2 electrolyser making use of gas diffusion electrodes has been taken from Marini et al., (2012) to illustrate the improvement in performance with increasing temperature:

[5] Not exceeding temperature and concentration conditions where a sudden reduction in benefit is noted.

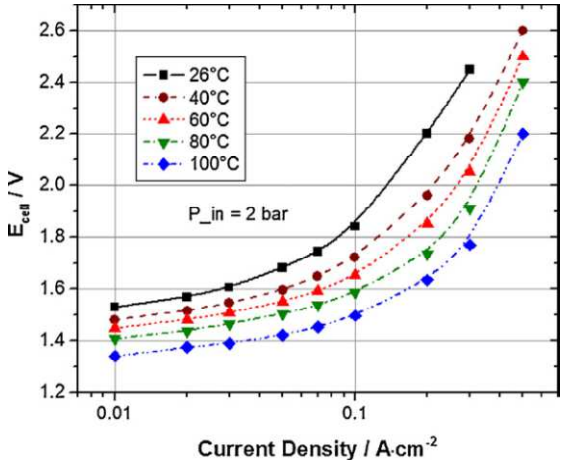

Figure 9: Polarisation curve for 10 cm^2 electrolyser making use of gas diffusion electrodes as a function of temperature (Mazloomi and Sulaiman, 2012)

Figure 9 (above) notes the improvement of overvoltage at a constant current density with increasing temperature. The stack efficiency therefore improves, but importantly the total enthalpy required for the water electrolysis reaction represented in Equation (2) never alters as a result of changing catalysts and temperatures. The contributing factors however alter in proportion; therefore the additional energy is introduced as heat. With the absence of a present heat source, this additional energy would have to be introduced by electrical energy which would not necessarily benefit the overall energy efficiency of the system (Mazloomi and Sulaiman, 2012).

Impurities within the electrolytic solution itself are important criteria to consider, as they may have the potential to reduce the system efficiency by creating numerous unwanted side reactions. Additionally, contaminations could block or poison (electro-chemical deposition) electrode/membrane surfaces which could further lead to mass and electron transfer complications that could lead to an increase in ohmic resistances with time (Mazloomi and Sulaiman, 2012). The degree of purity differs for the available electrolyser technologies. PEM and SOE electrolysers typically require ultrapure water with a specific conductance lower than 0.05 µS/cm (ASTM, D1193-91). AWE electrolysers are less sensitive to impurities within the electrolyte and do not require ultrapure water as a feed as these systems have been demonstrated using rain water (Millet and Grigoriev, 2013).

2.7.2. Pressure

Pressurised operation has a number of advantages for an alkaline water electrolysis system. Pressurisation by means of a liquid pump consumes substantially less energy in contrast to compression performed by means of a hydrogen compressor (Mazloomi and Sulaiman, 2012). An additional benefit of this would be a substantial saving in capital costs due to the non-requirement of a gas compression circuit (Monsouri et al., 2011). Pressurising the electrolytic solution has a shrinking effect on the produced gas bubbles which would otherwise consume a greater amount of electrode active area therefore blocking the transfer of electrons (Mazloomi et al., 2012). A greater force is applied to the nucleating gas bubbles and the bubbles are forced to leave the electrode at a smaller diameter compared to a base case making use of lower pressure operation. This reduction in bubble residence time and the resulting rapid disengagement rate all contribute to the overall reduction of the ohmic resistance loss represented in Equation (8) (Mazloomi and Sulaiman, 2012).

A drawback of pressurised operation is that the electrolytic housing would need to be designed in accordance to operate at the desired elevated pressure without incurring both a structural failure and additional CAPEX costs. Therefore the correct material, geometric shape and thickness need to be considered for pressurised operation to be feasible (Ganley, 2009). High pressure however, provides a benefit of being capable of performing high temperature electrolysis. As mentioned before, high temperature is beneficial as it results in the decrease in the required equilibrium voltage and resultantly, an improved electrical efficiency (Zeng and Zhang. 2010). It is known that if a certain temperature is exceeded, a solution will start to vaporise; therefore operating above the vapour pressure will ensure that the electrolytic solution remains liquid.

2.7.3. Electrode Gap

Noted earlier, in Equation (4), is the relationship of the electrode gap and the ohmic resistance generated. It is clear to see that a reduction in the gap between the electrodes will constitute a lower electrical resistance (Mazloomi and Sulaiman, 2012). A limitation is

however present in how much of a reduction is possible which is dependent on a number of parameters. The presence of a diaphragm/membrane between the electrodes and the gas bubbles between the electrodes is proportional to the chosen operating current density dependant on the cell potential. These parameters have the effect of dictating a stable operating electrode gap by the occurrence of a phenomenon known as 'void fracture' (Nagai et al., 2003b). Void fracture is defined as the sudden loss in the electrode active area due to the buildup of gaseous product on the surface of electrodes. The increase in the fraction of gas bubbles between the electrodes leads to an increase in the electrical resistance in the aqueous solution and a decrease in stack efficiency (Nagai et al., 2003b). The result is illustrated in the following figure taken from Nagai et al., (2003b):

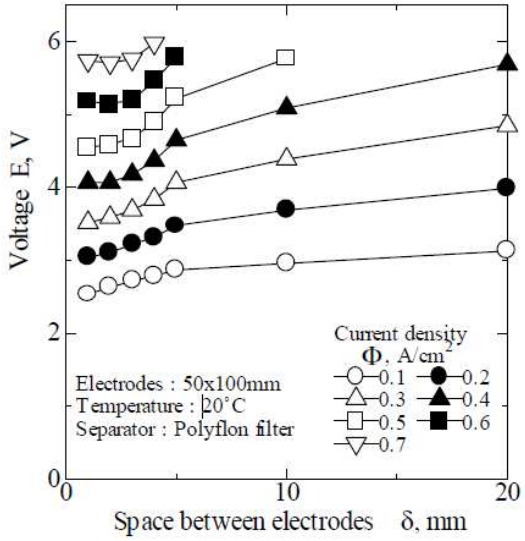

Figure 10: Effect on cell performance for an experimental set-up utilising a separator (Nagai et al., 2003b)

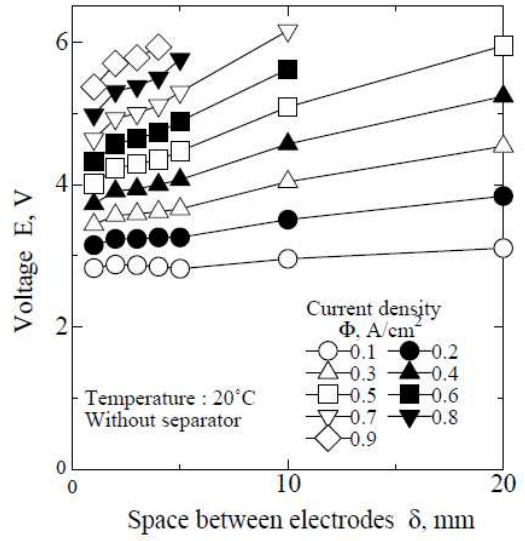

Figure 11: Effect on cell performance for an experimental set-up utilising no separator (Nagai et al., 2003b)

From the above plots it is noted that using a separator within an experimental set-up yields a large resistance as a greater benefit for current densities noted at lower voltages. An optimum electrode gap exists in the region of 1-2mm which records the lowest voltages for the tested current densities. Additionally, it is evident that the higher current densities produce a larger electrode gap due to the effects of void fracture.

The occurrence of void fracture has been attempted by various electrolyser designs to curb the resistance caused by employing a 'zero gap' configuration that involves placing the electrodes close and together separated by means of a very thin hydroxide conducting membrane (Pletcher and Li, 2011). These designs are generally more efficient than existing designs however, they are substantially more costly and complex (Yde et al., 2013). The use of zero gap systems for alkaline electrolysis however is still under development due to the inability of these membranes to operate effectively in contact with pure water. Acid membranes have been found to operate maximally when in contact with pure water and therefore have formed the basis for PEM electrolysis (Pletcher and Li. 2011). An indication into the potential of reducing the electrode gap to a few microns is noted in the fact that these electrolysers have been recorded to exceed current densities of 1000 $mA.cm^{-2}$ operating at voltages below 2 VDC (Pletcher and Li. 2011).

Modification of the surface of electrodes by increasing the surface wettability has been shown to improve the minimum electrode gap possible before void fracture takes place (Nagai et al., 2003a). The treatment of electrodes however, may alter the overvoltage contribution yielding no improvement in efficiency. This is an area of limited knowledge and is still open to extensive investigation.

2.7.4. Size and Alignment of Electrodes

With reference to Equation (19), an important variable reducing the ohmic drop between the electrodes is the total area available for reaction or the active area. By increasing the size of the electrodes, and consequently increasing the area of overlap, a reduction in resistance can be produced (Mazloomi and Sulaiman, 2012). There is a limitation to this however, as Mandin et al., (2008), reports that there is a significant increase in bubble accumulation in the

upper region of the electrodes. This would result in void fracture occurring and a reduction in efficiency would be observed with an increase in electrode height. It is therefore ideal to increase the size of the electrodes, and simultaneously reducing the height in order to maximise cell performance (Mazloomi and Sulaiman, 2012).

Electrode configurations seem most ideal when electrodes are positioned parallel to one another with no presence of an 'edge'. The influence of geometric variables may have substantial influence on the current distribution uniformity of the electrode, altering the overall process efficiency (de Maubeuge, 2011). The electrode gap, as discussed before, is a governing parameter of current distribution uniformity as it is reported that the influence of geometric inconsistencies is magnified at smaller electrode gaps (de Maubeuge, 2011).

Edge effects are described by de Maubeuge (2011), to be the condition where electric current lines are concentrated at the edge of the electrodes. Similarly, current will also become concentrated at irregular areas of the electrode that serve to reduce the current path between electrode faces. It is therefore a requirement that electrodes be modified to insulate these edge regions in order to modify current paths to promote a uniform current distribution across the electrode face. The following diagram illustrates the typical current path formed between electrode faces with insulated edges taken from de Maubeuge (2011):

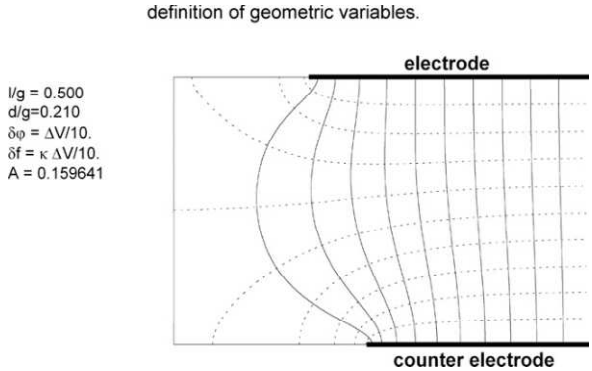

Figure 12: Normal insulating wall and counter electrode width configuration, potential distribution and electric current lines respectively as dashed and continuous curves (de Maubeuge, 2011)

de Maubeuge (2011) goes on to demonstrate the effect of placing a barrier between the electrode and counter electrode to note the influence of the current path:

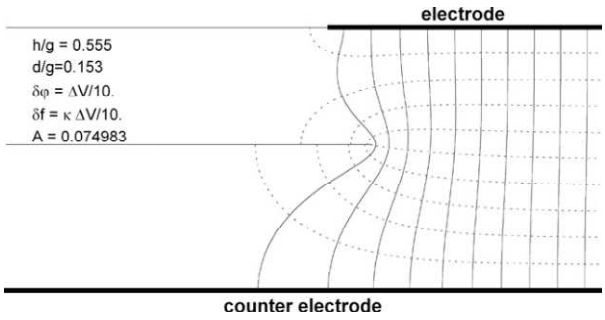

Figure 13: This parallel mask configuration, potential distribution and electric current lines respectively as dashed and continuous curves (de Maubeuge, 2011)

Placing a physical barrier between the electrode faces represents a pronounced obstacle to the flow of current. This barrier contributes to the additional resistance of which the over-potential will compensate for. The additional resistence therefore demonstrates why electrolysers utilising diaphragms (typically associated with alkaline electrolysers), that are non-conductive with regards to ions, may generate inefficient operation as numerous obstacles are present.

2.7.5. Bubble Resistance

In current electrolysers, the issue of void fracture remains a large contributor of performance issues associated with current electrolyser technologies. It is said that ohmic resistance is proportional to the fraction of product bubbles between the electrodes (Mazloomi and Sulaiman, 2012). This resistance can be quantified by modification of Equation (19) (below) to represent the partial lengths emanating from the electrode surface, taking into account the variations of product gas fractions (Mazloomi and Sulaiman, 2012):

$$R = \frac{\rho \sum l_i}{A} \dots\dots\dots (19)$$

Where, l_i represents the partial lengths of electrolytic layers with various product gas concentrations, ρ is the resistivity (Ω.m) and A (m^2) is the cross sectional surface area of the partial length.

Mazloomi and Sulaiman (2012) provide a graphical representation of the resistance dependence of the product gas fractions:

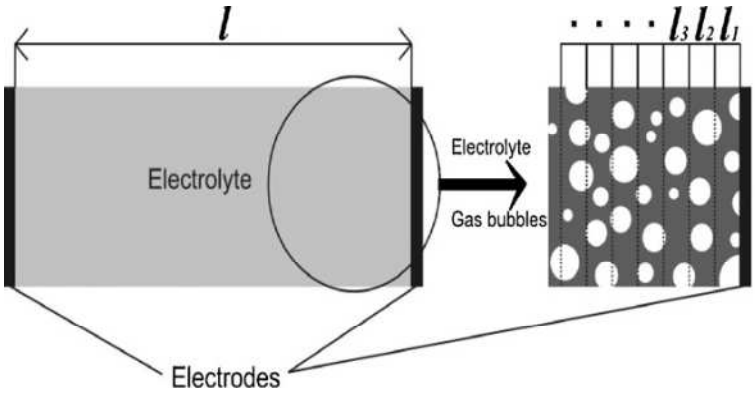

Figure 14: The void fraction formation in the electrolyte (Mazloomi and Sulaiman, 2012)

The following photograph taken from Nagai et al., (2003b) provides graphical evidence of the phenomena shown in Figure 14, and the change in gas fraction from the surface of the electrode can be seen:



Figure 15: Microscope image of bubbles emanating from a hydrogen cathode (Nagai et al., 2003b)

From the above illustration, the concentration of gas is greatest nearest to the electrode surface. The resistivity factor in Equation (20) will therefore be a combination of the resistivity of the electrolytic solution and that of the product gas bubbles. The sum of the individual partial lengths of Equation (20) will therefore make up the total resistance of the bi-phase electrolyte contained between the anodic and cathodic electrodes (Mazloomi and

Sulaiman, 2012). This resistance is therefore expected to vary with different operating current densities.

Bubble evolution on the surface of electrodes results in the loss of effective electrode area. The current path through the electrolyte is extended as the current is required to flow around the produced gas bubbles (Lumanauw, 2000). The size of the bubble emanating from the electrode surface is a function of the viscosity which is dependent on the temperature, concentration of the electrolytic solution, the operating pressure of the electrolysis stack and the operating current density (Nagia et al., 2003). As the operating current density increases, an increase of the bubble diameter is observed. The bubble rise velocity is affected by the increase in temperature for bubbles predominantly found in moderate concentrations. The subsequent decrease in viscosity with increasing temperature, allows the buoyancy force of the bubble to overcome the drag force imposed by the liquid electrolyte to a greater extent. (Nagia et al., 2003). An increase in pressure, however, increases the solubility of product gas within the electrolytic, solution according to Henry's law. Therefore an increase in temperature and a decrease in pressure would be potentially beneficial in reducing the fraction of gas present between the electrodes, themselves allowing for improved electron transfer between electrode faces (Mazloomi and Sulaiman, 2012).

The electro-catalyst surface properties would also have implications on the residence time of a bubble on the electrode surface. The wettabilty of the surface has several repercussions with regard to the adhesion properties of the product gas bubbles. A surface that is easily wettable will result in the liberation of smaller bubbles. In contrast, a surface that is not easily wettable results in easier nucleation of product gas bubbles and hence larger bubbles will be released from the surface (Nagia et al., 2003). Differences in bubble sizes have been demonstrated with mesh type, porous mesh type and plate electrodes; the largest gas bubbles are released from plate type electrodes. Mesh type electrodes therefore release smaller gas bubbles. Plate type electrodes additionally, have a more even bubble size distribution in contrast to mesh type electrodes. The surface roughness has also shown to increase the size of the released product bubbles (Lumanauw. 2000).

Ideally it is required that the product gas bubble disengages from the material surface as rapidly as possible to increase the effective reactive area for additional gas formation. Apart from the above solutions, additional solutions involve introducing an ultrasonic field or vibration device that overcomes the adhesion force of the gas bubbles to metal surfaces

(Mazloomi and Sulaiman, 2012). The increase in solution velocities is a simple, but potentially energy intensive solution, as the force applied to the product gas bubbles increases the liberation rate and reduces the evolved bubble diameter (Lumanauw, 2000).

Currently, electrolyser nominal current density operating thresholds are limited, due to the presence of a greater fraction of gas bubbles between the electrodes. This results in the occurrence of void fracture leading to the sudden loss of performance due to the loss of effective reactive surface area (Millet and Grigoriev, 2013). The presence of a diaphragm or membrane for electrolysis systems limits current density thresholds further as a balance must be maintained between the operating current density and the electrode gap (Nagai et al., 2003a). Zero gap systems, involving the presence of a very thin membrane utilising gas diffusion electrodes, do not readily suffer similar effects in the reduction of electrode gap, however the presence of the gas diffusion layer (GDL) results in an additional factor of resistances, as product gas bubbles must first move through the GDL before extraction from the electrolyser unit using pure water (Pletcher and Li, 2011). Gas diffusion electrodes allow for operating current density thresholds obtained, to be higher than conventional AWE electrolysers, however thresholds on the magnitude of current densities still apply. Membraneless type electrolysers in theory serve to overcome this issue as no product gas bubbles of diffusion issues are present between or within the electrodes. The elimination of product gas bubbles between the electrodes is fundamental, however the requirement of a separator that demonstrates high conductivity and eliminates cross gas contamination by demonstrating resistance to pressure, temperature, chemical and mechanical degradation is imperative (Mazloomi and Sulaiman, 2012).

2.7.6. Separator Material

The presence of a separator material between the electrodes hinders the performance of the electrolyser as it inhibits the free flow of current between electrodes and the accumulation of ions in solution which could lead to conditions of void fracture (Mazloomi and Sulaiman, 2012). Correct performance of the diaphragm or membrane depends on the material's ability to resist corrosion, chemical and mechanical degradation. Often the conductivity of the

separation material is several times lower than that of the electrolytic solution which adds to the resistance in the flow of ions (Mazloomi and Sulaiman, 2012).

An early separator material, regarded as the best separator in the 90's which involved the use of asbestos as the separator material, is currently still in use. Asbestos proved to be highly wettable and porous, demonstrating good separation properties of the product gases (Rosa et al., 1995). The hazardous and toxic nature has since discounted the use of asbestos, and lead to the development of alternative materials. At present, possible suitable materials for both alkaline and proton exchange electrolysers has been developed in the form of different polymers and solid type electrolytes, however their durability and stability are yet to be proven (Jensen et al., 2008).

Modern separators used for electrolysers make use of ion exchange membranes, where the membrane can be either cationic or anionic depending on the type of electrolyser. The most common cationic membrane is referred to as Nafion and demonstrates increased thermal stability and tensile strength over earlier membrane materials (Rosa et al. 1995). It is not only a requirement for a separator to demonstrate a low power consumption and excellent durability, but additionally, the quality of hydrogen needs to be preserved and maintained for long term performance. Currently purity exists for alkaline electrolysis technologies especially those making use of a zero gap configurations (Manabe et al., 2012). Challenges still exist in developing a membrane that is capable of long term stable operation with acceptable cross gas mixing resistance at elevated temperatures, concentrations (for both the electrolyte and gas fractions) and pressures.

2.7.7. Electro-catalysts for Hydrogen and Oxygen Evolution Reactions

It has been shown theoretically that the most optimal hydrogen electro-catalyst appears on the apex of a volcano diagram (Yde et al., 2013). A volcano plot shows the adsorption strength of hydrogen to a particular catalytic surface. If hydrogen bonds too weakly to the surface of the metal or perhaps too strongly, a decrease in electro-activity can be observed, hence the generalised shape of volcano diagrams. The theoretical plot for hydrogen below demonstrates

common metals used to maximise the electro-activity of the hydrogen evolution reaction (HER):-

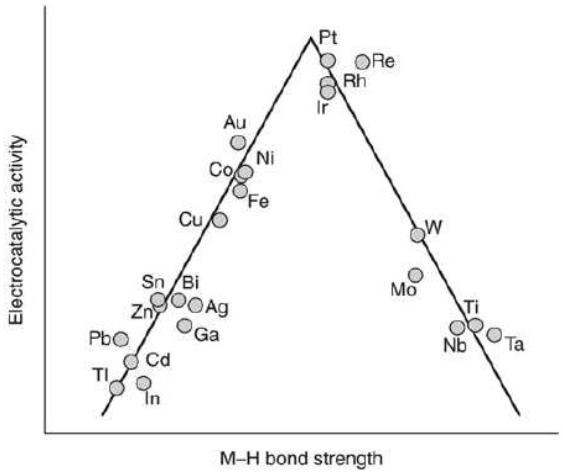

Figure 16: Volcano plot for the hydrogen evolution reaction (Yde et al., 2013)

As observed in the above plot, platinum has the highest possible metallic catalytic activity (Figure 16) for the hydrogen evolution reaction as it possesses intermediate adsorption energy to the metallic surface. A number of platinum group metals (PGM) follow thereafter, such as ruthenium and iridium. A number of non-PGM metals demonstrate maximised catalytic performance for the HER such as nickel, cobalt and iron. PGM metals are highly expensive and contribute greatly to the cost of an electrolyser stack. They are commonly used in proton exchange membrane electrolysers (PEM), utilising an acidic ionic transfer medium. The non-PGM materials lend themselves well to alkaline systems using hydroxide ions as the charge transfer medium (Yde et al., 2013).

Similarly as shown in Figure 16 (above), a volcano plot exists (Figure 17 below) for the oxygen evolution reaction (OER) (Lee et al., 2013):

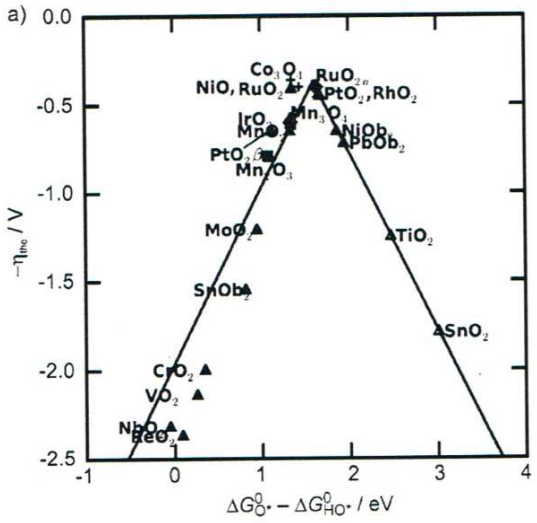

Figure 17: Volcano plot for the oxygen evolution reaction (J. Lee et al., 2013)

The above illustration shows the optimal catalysts. In contrast to the hydrogen evolution reaction, the volcano plot for the oxygen evolution reaction examines the adsorption energies of the hydroxide (OH^-) ion to the surface of an electro-catalyst (Man et al., 2011). Oxide catalyst materials are found to be selective to maximising performance for the oxygen evolution reaction. Figure 17 notes the two theoretically optimal catalysts for the oxygen evolution reaction as Spinel Cobalt oxide (Co_3O_4) and ruthenium dioxide (RuO_2). It is important to note however that certain catalysts may be optimal in terms of performance proven in theory; however severe durability and stability issues may be incurred when the catalyst is applied in reality (Yde et al., 2013). Similar to the hydrogen evolution reaction, some PGM metallic oxides, composed of iridium, platinum and ruthenium, are regarded as the best OER materials in alkaline and acidic media (Lee et al., 2013). Oxides are ideal purely because it proves difficult to oxidise them further, however PGM oxides prove fairly expensive to use in construction of electrodes for alkaline water electrolysis (Lee et al., 2013).

The corrosion properties of cathodic and anodic materials for AWE can be examined theoretically by examining Pourbaix diagrams. Pourbaix diagrams are a plot of the pH of the medium in which the material will be immersed and the potential applied to the metal (Yde et al., 2013). Regions of thermo-chemical stability can then be identified easily. Since this investigation deals primarily with alkaline water electrolysis, the Pourbaix diagrams of the highest catalytically active HER non-metals have been taken from Yde et al. (2013).

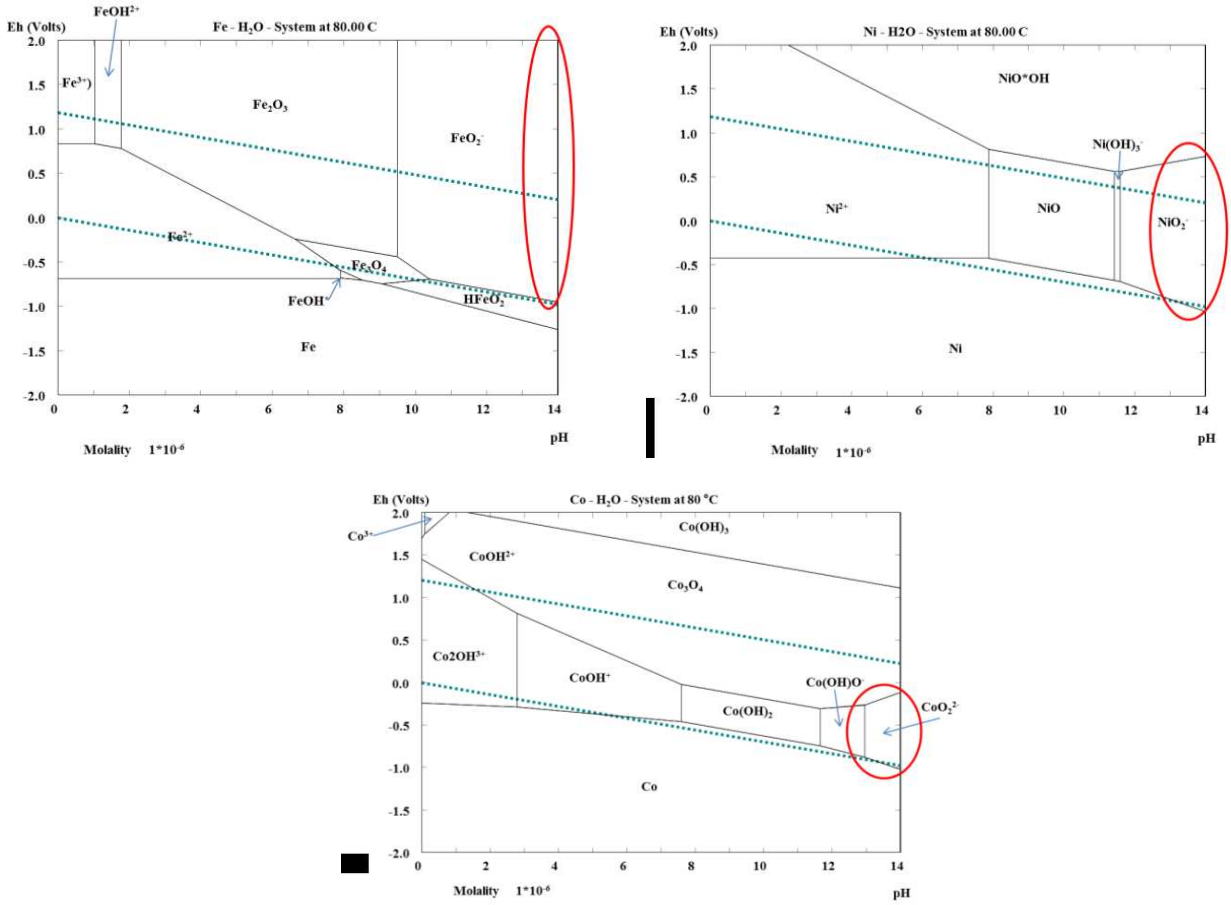

Figure 18: Pourbaix diagrams at 80°C for Iron (above-left), Nickel (above-right) and cobalt (bottom), in a water system (Yde et al., 2013)

From Figure 18 (above), regions of instability have been highlighted in high alkaline solutions. It is known from experimental investigations that nickel demonstrates high corrosion resistance in highly alkaline solutions, and is commonly used as the material of choice for alkaline electrolysis, which therefore disagrees with the above electrochemical theory (Marini et al., 2012). Although Pourbaix diagrams provide an indication as to electrochemical stability, it provides no indication as to the rate of corrosion as it is well known that the rate of corrosion for nickel occurs very slowly.

Particular types of nickel catalysts have been developed which create structures for maximising the catalytic surface area. Nickel is regarded as the most practical and desirable catalyst when it comes to both the cathodic and anodic reactions. Additionally the use of porous nickel electrodes maximises the three phase contact area, which increases the effective surface area of the electrode, to achieve higher power densities and operating current densities (Lee et al., 2013). Raney nickel has been found stable in alkali conditions for both the anodic and cathodic catalysts (Marini et al., 2012).

Raney nickel is created by starting with a nickel-aluminum alloy which is thereafter treated with concentrated sodium hydroxide (NaOH). This treatment leaches the aluminum from the alloy leaving behind a high surface area structure of nickel metal. The pores created in the catalyst are of significant consideration. As mentioned previously, the oxygen reaction, (Equation (14)) is the limiting reaction for the overall water electrolysis reaction represented by Equation (2). Due to the larger molecule size of oxygen, pore blockage is substantially more prevalent in reference to the hydrogen molecule (Appleby et al., 1978). Raney nickel can be additionally used as a catalyst support by undergoing doping of a more active element such as molybdenum or cobalt. This has been shown by Salvi et al., (2011) to improve the activity of the Raney nickel significantly.

Other compounds used typically for catalysts for alkaline water electrolysis are spinel oxides (such as the aforementioned catalyst spinel cobalt oxide (Co_3O_4)) and perovskite type oxides ($LaCoO_3$). These compounds possess high activity, availability, low cost, thermodynamic stability, low electrical resistance and environmental friendliness (Lee et al., 2013). All catalysts are known to possess a threshold of performance, whereby no further increase in performance is possible. Additional increases in performance can be alternatively achieved through the maximisation of the effective electrode area by use of sintered or porous type electrodes (Mazloomi and Sulaiman, 2012). Compared to smooth nickel electrodes, woven or porous sintered type nickel electrodes demonstrated 30 times more activity, which indicates that a significant activity improvement can be achieved by improvement of the effective surface area of electrodes (Mazloomi and Sulaiman, 2012).

Jensen et al., (2008) defines the requirements for an effective electrocatalyst quite clearly. The catalytic surface needs to provide for the simple discharge and adsorption of hydrogen or hydroxide ions from and to the surface. A large surface area needs to be present between the catalyst surface and the electrolytic solution and an adequate number of sites need to be present for the nucleation of product bubbles. A reasonable means of detachment of product bubbles from the electrode surface needs to be prevalent in order to maximise the effective reactive surface area of the electrode. Achieving the aforementioned would result in a catalyst with a superior production rate per unit volume.

3. METHODOLOGY

3.1. Overview

The technology design and operating principle is based on two circular porous mesh electrodes opposing one another, similar to any existing electrolyser technology. However the fundamental difference with the Hydrox Holdings Ltd. technology used for this investigation is that there is no need for the use of a membrane/separator to ensure that the evolved gases remain separate which comprises the propriety nature of the technology.

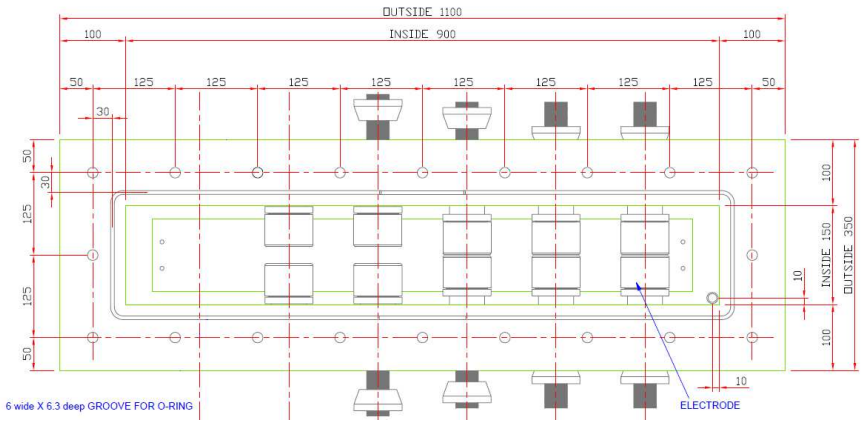

Figure 19: Electrode geometry and assembly procedure within the HH electrolyser apparatus

A dedicated test rig was constructed to evaluate this electrolyser design configuration (Figure 19). The electrolyser apparatus, consisting of six electrode assemblies, serves to introduce flow in a non-preferential manner to all the electrode assemblies. It also allows for accurate adjustment and alignment of the electrode gap. Within the electrode assembly, filtration mesh of plain dutch weave type procured from Ofolan (Titanium supplier) and Hebei Nanrui Filtration company (pure nickel supplier) with an absolute aperture micron rating of 120 microns and a warp and weft wire diameter of 0.35 mm and 0.25 mm respectively, is inserted and tensioned. The nickel purity is 99.5 % and that of the titanium is 99.9 %. The assembly

is used to provide tension and electrical power to the mesh electrodes inserted between the conductive nickel 200 head and polypropylene tensioning cover. A 30 mm opening on the frontal face of the polypropylene tension cover allows for the region of electrochemical reaction.

The electrolytic solution enters the assembly from a pressurised chamber which allows for non-preferential flow to each electrode assembly that governs the primary operating principle. The hydrogen and oxygen gas formed from each electrode assembly is then carried within the electrolytic solution which then reports to the respective gas/liquid separators for separation. Filtration mesh, which constitutes the porous media for reaction, allows for the effective geometric area for reaction to be maximised. The available geometric area is 4.304 square centimeters per square centimeter cross sectional area. This translates into an overall available geometric area of 30.42 cm^2 for the 30mm diameter electrodes used for this investigation.

Current density, as reported in this report, is determined as the ratio of the total current (passing through a single pole pair of electrodes) to the flat cross sectional area available for charge transfer (in this case, the 30 mm cross sectional area of the porous electrodes).

The importance of maintaining an effective electrolytic velocity across the electrodes is to ensure that conditions do not evolve that could lead to void fracture. Similar techniques are used to enhance performance for existing electrolyser technologies. It is therefore important to ensure that the fraction of gas between the cathodic and anodic electrodes is minimised. An adequate flow velocity would provide the advantage of spacing the electrodes as close as 1mm apart. Flow velocity, referred to in the results that follow, makes reference to the average flow velocity over the cross sectional area of the mesh material. All flow velocities reported will be based on this calculation basis, although it is understood that the fluid dynamics may interpret that flow which may be more selective to certain areas.

3.2. Process Flow Diagram Description

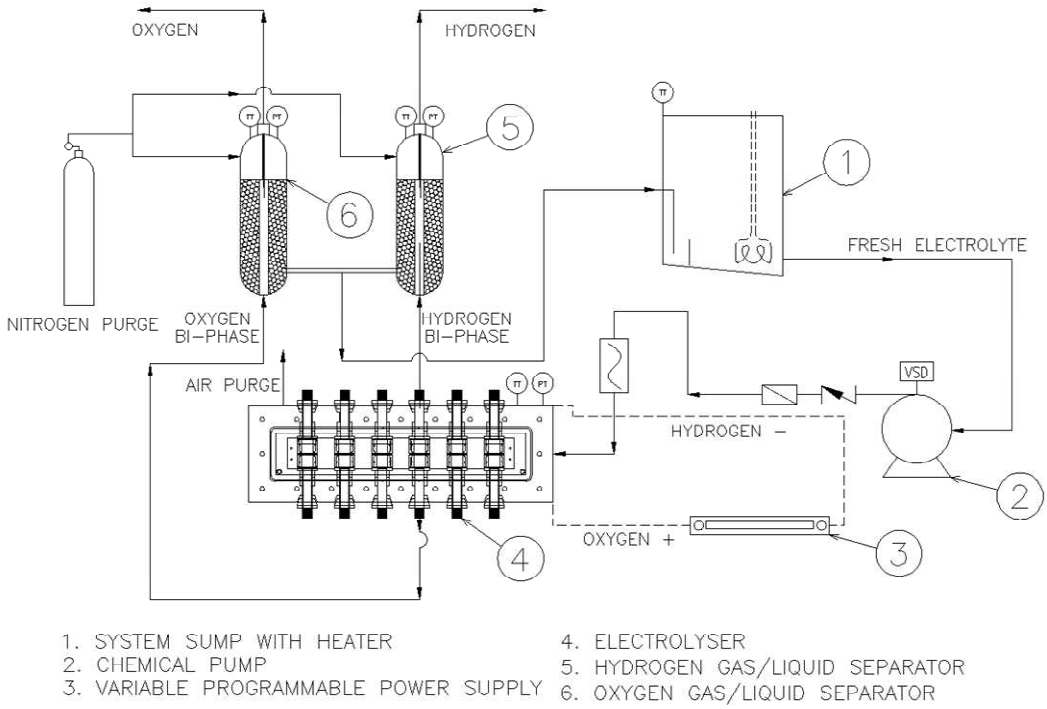

Figure 20: Process flow diagram of the Hydrox Holdings Ltd. membraneless test rig

A simplified process flow diagram of the test rig used to test performance variables is depicted in Figure 20 (above). Temperature is controlled with the use of a variable temperature control element and flow rate is measured with reference to an electro-magnetic flow meter. Applied voltage on the electrode pairs is controlled and monitored by means of a variable/programmable power supply (2.4 kW TDK), with two electrode pairs having been employed in all instances. Electrolyte is circulated through the system by a chemical pump, and the flow rate can be controlled by a variable speed drive or diaphragm valve installed in the system. The resulting product gas is separated from the electrolytic solution by the respective oxygen and hydrogen gas/liquid separators, subsequent to which the electrolytic solution is circulated back to the system sump for re-heating/storage. A nitrogen purge system has been installed on the system separators to remove contaminant atmospheric gases prior to gas purity testing to prevent contamination within gas samples. The electrolytic concentration and temperature is monitored with the use of a Boeco PT-380 mV/pH meter. Temperature and pressure gauges have been installed on the system for each gas/liquid

separation vessel and on the electrolyser for gas flow rate correction reference to supplier calibration curves.

The membraneless test rig has been constructed out of polypropylene plastic, and where necessary, stainless steel 316 and nickel 200 (Figure 21) have been employed. The test rig was machined to the highest tolerances to ensure accuracy of electrode alignment. It is capable of operating at electrolytic solution flow rates of 12 m^3/hr at temperatures up to 80 °C and maximum electrolytic concentrations of up to 50 wt% potassium hydroxide (Supplied by Kayo Fine Chemicals, with the alkalinity of the potassium hydroxide flakes being 90.2 %). Electrode pairs can be tested independently or in conjunction with other electrode pairs. The electrode gap is variable from 10 mm to gaps as small as 0.5 mm. Distilled water (type 1 water quality supplied by Minema Chemicals) with a maximum specific conductance of 0.05 µS/cm (ASTM, D1193-91) was used throughout.

a **b**

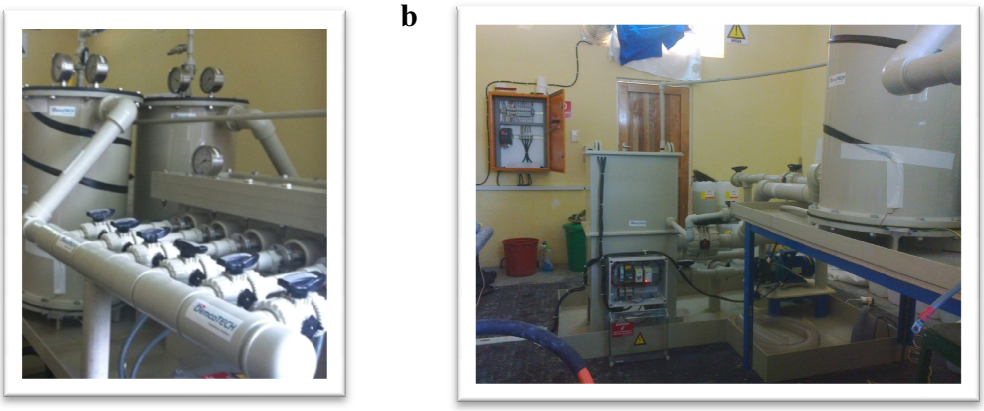

Figure 21: Illustrations of (a) The electrolyser apparatus and product gas L/G separators (b) The process ancillaries showing the system sump, chemical pump and control panels

Water electrolysis was conducted employing several electrode materials, i.e. industrially pure nickel (Hebei Nanrui Filtration company), platinum plated stainless steel 316 (Silvex Surface Technologies), nickel plated stainless steel 316 (A&A Plating), stainless steel 316 (Merco Industries), MMO (Metal-Metal Oxide) plated titanium (NMT Electrodes with titanium substrate from Ofolan), and platinum plated titanium (NMT Electrodes with substrate titanium from Ofolan) under various conditions and atmospheric pressure. The MMO (Metal-Metal Oxide), catalyst comprises of RuO_2, IrO_2 and TiO_2 in the ratio 35/10/55 for the anodic

electrode. This MMO catalyst for the purpose of this research and the reported results has been denoted as Ir-RuO_2, since the iridium and ruthenium serve to be the active components for enhancing the kinetics of the oxygen evolution reaction.

The test rig was not designed to operate under pressure and in excess of 80 °C, and in that regard, all runs were conducted at atmospheric pressure and temperatures up to 80°C. In order to deduce the optimal operating conditions for the chosen electrode diameter of 30 mm, the following parameters were controlled: electrolytic concentration, electrolytic temperature, electrolytic flow velocity, electrode gap, electrode material and DC voltage.

The test rig records and controls voltage and current data by means of a device/software interface using Labview^{TM} 2013. By data logging the results to an excel spreadsheet, experimental accuracy can be quantified and analysed. All other variable measurements such as flow rate, pressure, temperature and concentration were manually read off instruments and inputted noting all fluctuations in values. Experiments were repeated a minimum of three times to note the precision and repeatability of results. Gas purity analysis was conducted by AirSep Labs, employing an Agilent 6890 gas chromatograph.

3.3. Experimental Apparatus

Although the design, fabrication and commissioning of the Hydrox Holdings Ltd. (HH) electrolysis test rig is not the focus of this paper, the design considerations and brief design method can be referred to in *Appendix B.* The following is a brief description of the major process components and their basic function and flexibilities within the process.

3.3.1. Electrolyser



Figure 22: Membraneless alkaline electrolyser apparatus

The electrolyser (Figure 22) utilising the membraneless technology is designed in a manner to incorporate a variation of electrode sizes from 30 mm to 150 mm in diameter. For the purpose of this investigation, an electrode diameter of 30 mm was chosen to eliminate the effects of a non-uniform pressure drop across an electrode face. The mounting method of the electrodes within a tensioning assembly ensures that electrode faces are always parallel to one another since the electrolyser has been machined to highest tolerances. The electrolyser incorporates shell strengthening that ensures that no warping of the vessel takes place during fluctuations of pressure and temperature.

The design of the electrode assemblies themselves ensures that edge effects are avoided, which would bring about preferential product gas formation along the periphery of the electrode face. The threaded tube and lock nut system allows for the accurate adjustment of electrode heads to a defined electrode gap.

The electrolyser incorporates a distribution plate above the electrolytic solution inlet to allow for uniform flow and pressure dynamics. This is to ensure that the electrolytic flow to each of the electrodes is similar to avoid electrodes operating at performances that are vastly different from one another.

The electrolyser makes use of independent pole pair selection valves and electrical connections to allow flexibility when selecting the desired electrode pole pairs for testing.

3.3.2. Gas/Liquid Separators

A. B.

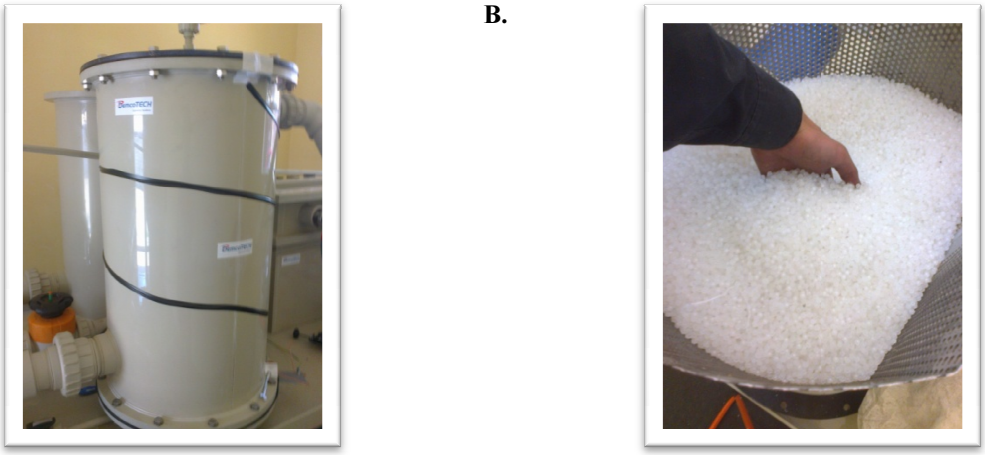

Figure 23: (a) Hydrogen gas/liquid separator (b) Packing media contained within gas/liquid separators

The main function behind a vertical type packed bed separator (Figure 23) is to maximise the contact area of the electrolytic solution, so that a small film of liquid forms around the packing media for effective removal of product gas. The removal of micro-bubbles from an electrolytic solution is an area not yet extensively investigated, and therefore conventional methods of gas/liquid separation are not ideal to perform this type of separation.

The gas/liquid separation vessels are oversized to ensure that efficient separation takes place at both high flow rates and low flow rates of electrolyte. The system is fitted with a nitrogen purge system to ensure that all trapped air within the vessels is purged, before experimental tests take place, due to the wide flammability limit of hydrogen gas. The system is designed to reduce the velocity of electrolytic solution collecting in the separator sump to ensure a reduced likelihood that product gas is re-entrained into the 'liberated' electrolytic solution.

The separators have been designed in a manner to self-regulate the electrolytic fluid level by means of a gravity recycle loop to the electrolytic sump. The separators are fitted with gas rotameters, pressure gauges and temperature gauges for the determination of evolved product gas flow rates from the process.

3.3.3. Electrolytic Sump

A



B



Figure 24: (A) Electrolytic Sump (B) Circulation of electrolytic fluid within sump electrolytic sump apparatus

The sump allows for the storage of the electrolytic solution when not in use, along with the submergence of a chemical heating system that is responsible for the regulation of temperature during operation. The system sump is the access point at which measurements of pH/mV or temperature can be performed before liquid is circulated to the electrolyser. The sump serves as an additional vessel for micro-bubble settling in the event that not all micro-bubbles are removed from the electrolytic solution during gas/liquid separation. A baffle plate disallows micro-bubbles from having a direct line to the pump suction. As a consequence, entrained micro-bubbles are forced to the solution surface before the electrolytic solution recycles back to the electrolyser.

The large system volume for the sump acts as a buffer against rapidly changing concentrations that would otherwise affect the performance of the electrolyser as concentration increases over time. The system incorporates a closed recycle loop for the mixing of potassium hydroxide reagent. The large surfaces of the sump help absorb the majority of the heat given off during the dissolution of potassium hydroxide flakes to prevent over heating of system components.

3.4. Reagents and Material Stability

Careful consideration was provided into the selection of materials for the various major equipment pieces. Operating lifetime and corrosion resistance are fundamental factors in determining the suitability of materials in the extreme operating conditions when considering the design of a new electrolyser. If conditions are prevalent that will allow the structure of the electrolyser to thermally or chemically degrade, the electrolyte will become contaminated as a result, and the reaction mechanism and system performance will alter due to the presence of contaminant materials. With reference to chemical resistance charts, the suitability of materials has been correlated as a check list to ensure that the maximum operating limits of materials will not be exceeded.

Table 2: Material compatibility determined from material corrosion resistance tables for potassium hydroxide solutions

Materials of Construction	Maximum operating temperature (C)	Maximum Operating Concentration (wt%KOH)
Polypropylene	100	60
Polyethylene	60	60
Polyvinyl Chloride	60	25
Chlorinated Polyvinyl Chloride	100	60
Polytetraflouroethylene	250	60
Polycarbonate	60	20
Perspex	50	50
Acrylic	50	50
Stainless Steel 316	100	50
Staniless Steel 304	100	27
Polysulfone	100	50
EPDM	100	50

With reference to Table 2 (above), it is clear that for the desired maximum operating conditions of 80°C and 50 wt% potassium hydroxide, Polypropylene (PP), Chlorinated Polyvinyl Chloride (CPVC) and Polytetraflouroethylene (PTFE) are the few plastic materials that exhibit good chemical resistance. None of these plastics are defined as translucent plastics which are more ideal for monitoring internals of process apparatus. As a consequence a plastic such as Perspex was used for this purpose for process components with intermittent contact with electrolytic solution, and during times of continuous contact, the temperature was limited to a maximum of 50°C to prevent degradation of the material.

Metallic components used in the test rig construction were comprised solely of stainless steel 316/316L which demonstrates a superior corrosion resistance due to its high nickel content. Molybdenum additionally enhances pitting and crevice corrosion to a greater extent.

Additional conductive components were subsequently manufactured out of pure nickel for enhanced material stability.

3.5. Experimental Procedure

3.5.1. Initial Plant Commissioning and Safety Checklist

Before any experimental investigation can proceed, a number of safety requirements and commissioning tests need to be performed on equipment before tests can be conducted in a safe manner. A tabulated breakdown of the checklist was developed, in correspondence to ISO 22734-1 (Hydrogen generators using water electrolysis process), detailing the most important criteria for hydrogen generation equipment, before operation. For a more detailed breakdown of the commissioning and safety checklists, please refer to *Appendix D*.

Table 3: Safety and commissioning main point checklist

Mechanical Equipment	
Material Requirements	• Mechanical stability and strength • Resistance to chemical and physical action
Enclosures	• Rigidity and durability • Environmental tolerances and adequate insulation properties • Fire Resistance and adequate ventilation • Easy access for maintenance • Containment of hazardous liquids and materials
Pressure Bearing Components	• Adequate design to contain explosive, flammable or toxic fluids • Separation of oxygen and hydrogen constituent components • Process vessels and piping designed to withstand maximum pressure with adequate safety margins
Electrical Equipment, Wiring and Ventilation	
Fire Proof and Hazard	• Prevention of accumulation of ignitable mixtures through thorough

Protection	ventilation • System start-up purge with inert gas such as nitrogen • Gas detection system
Electrical Requirements	• Proper insulation and isolation of exposed electrical conductors • Where insulation is not possible, clear marking • Grounding and bonding of equipment • Circuit protection by means of circuit breakers, fuses and overload relays
Operator Controls	
Control Philosophy	• Provision for starting, stopping and reset of plant operation • Emergency stop to bring plant to a safe status • Programmable electronic equipment only for monitoring and testing • Alarms to sound in the event of hazardous conditions
Ionic Transport Medium	
Electrolyte	• Electrolyte must be chemically stable with respect to environment and to support a long plant operating lifespan • No introduction of undesirable reaction within other materials or undesirable side reactions • Means to cater for the safe sustainable disposal of electrolyte
Personnel Protection	
Equipment Protection	• All live and moving parts to incorporate insulation or guarding • All non-insulated parts to be located, guarded and mounted to reduce risk of contact
Personnel Protection Equipment	• Acid proof overalls and shoes to be provided when operating equipment • Eye, respiration and hand protection when dealing directly with equipment containing corrosive chemicals
Pre-Commissioning and Commissioning Tests	
Pre-commissioning Tests(Cold commissioning)	• Physical inspection of equipment, controls and connections • Initial cold commissioning checks including pump directional checks, control panel start up and power supply start up
Commissioning Tests	• Pressure testing of equipment components for both gas and liquid containing vessels (usually performed by manufacturer/supplier) • Leakage test of equipment components for both gas and liquid containing (performed upon completion of plant assembly) • Temperature/heating tests • Water tests using potable water will be used to test the above • Performance tests with electrolyte once above has been performed to measure hydrogen and oxygen rate and quality

3.5.2. Test Parameters and schedule for Parameter Optimisation

Apparatus used for this investigation has been outlined in Section 3.3 above, along with the operating and control philosophy. A schedule of experiments was developed for which a single experimental parameter became the focus variable, and its effect on cell performance noted through a variation of applicable additional test parameters.

3.5.2.1. Electrolytic Concentration Optimisation

Initial tests were based on finding the optimal concentration range of potassium hydroxide (KOH) electrolyte on a mass percent basis. The following constant and variable test conditions form the basis of identifying the optimal concentration range. Test parameters that are constant for this experimental investigation are assumed to have little or no influence on cell performance with changing concentration of potassium hydroxide. Test parameters that are variable however are assumed to possess trends regarding the cell performance with a variation in potassium hydroxide concentration.

Table 4: Constant and variable test parameters for electrolytic concentration optimisation

Constant Test Parameters		
Test Variable	*Unit*	*Variable Range*
Electrode Material	-	Stainless Steel 316
Electrode Gap	mm	3.5
Variable Test Parameters		
Test Variable	*Unit*	*Variable Range*
Electrolytic Concentration (Focus)	mass% KOH	20; 30; 40; 50
Temperature	°C	40,50,60,70,80
Flow Velocity	$m.s^{-1}$	0.1; 0.2; 0.3; 0.4; 0.5; 0.6
Cell Potential	VDC	1.765; 1.9; 2; 2.5; 3; 4

Upon completion of the above tests, remaining tests were performed at the deduced optimal concentration. This investigation serves to find the concentration of potassium hydroxide that maximises conductivity of the electrolyte that will have the same relative contribution when experimental conditions are adapted. It is therefore independent of changes in electrode catalytic materials, temperature, electrode gap and flow velocity, as the resistivity factor seen

in Equation (19) will vary for changing temperatures, however the resistivity will remain constant for a fixed electrolytic concentration (Allebrod et al., 2012).

The additional intention of this investigation was to note the effect of electrolytic flow velocity and the increase in temperature on cell performance. Test velocities were initially chosen to extend to the highest possible flow velocity to show that an upper limit exists where a drop in cell performance is noted due to deviation of the electrodes parallel nature. It is however not practical from a commercial sense to operate at electrolytic flow velocities this high as the parasitic load contribution of the electrolytic circulation pump would be too high. Hereafter the velocity was restricted to a practical range of flow velocities.

3.5.2.2. Selection of Catalytic Material

Once the optimal electrolytic concentration was determined, it was then possible to optimise performance with regard to a catalytic material for the anode and cathode that maximises rate kinetics for the oxygen evolution reaction and hydrogen evolution reaction. A number of catalytic combinations were chosen as suggested by literature for testing.

Table 5: Constant and variable test parameters for catalytic material optimisation

Constant Test Parameters		
Test Variable	*Unit*	*Variable Range*
Electrolytic Concentration	mass% KOH	30 wt%
Electrode Gap	mm	3.5
Variable Test Parameters		
Test Variable	*Unit*	*Variable Range*
Electrode Material	-	Combinations (Anode, Cathode): (SS316,SS316); (Ni plated SS316, Ni plated SS 316); (Ni 200, Pt Plated SS316); (Ni 200, Ni 200); (Ir-RuO_2 plated Ti, Pt plated Ti)
Temperature	°C	50,60,70,80
Flow Velocity	$m.s^{-1}$	0.075; 0.1; 0.15
Cell Potential	VDC	1.765; 2; 2.5; 3; 3.5

This investigation aims to reveal the optimal electro-catalysts for the above stated conditions. The major portion of the research aims at improving the efficiency of electrolysers, however, the implication is to use PGM catalysts along with large size plants; which imply high capital expenditure (Marini et al., 2012). Operating at higher potentials implies greater operating current densities, while smaller plant size and lower capital expenditure is carried out at the expense of efficiency. The optimal catalyst will therefore be subdivided into another in a lower potential range, and a catalyst that maximises performance in an elevated performance range. It will be important however, to closely study the effects of corrosion on catalysts operating in the higher potential range.

3.5.2.3. Electrode Gap Optimisation

A reduction in the electrode gap reduces the current path between parallel electrodes and therefore reduces the ionic resistance of the electrolyte as already mentioned with reference to Equation (19). The electrode gap is closely dependant on a phenomenon referred to as void fracture, which in the case of the membraneless electrolyser operating principle, is mitigated by operating at enhanced electrolytic flow rates. The fraction of gas bubbles increases between the electrodes as the current density increases, therefore more flow velocity would be required to remove the gas bubbles between the electrodes to mitigate the possibility of void fracture. This parameter will therefore be closely compared to the flow velocity of electrolytic fluid and a change in temperature which would have the positive result of reducing the fluid viscosity.

The catalyst of choice for this investigation was nickel 200 due to its ease of availability, resistance to corrosion in an alkaline environment, general use as an electrode for alkaline electrolysers and cost effectiveness when compared to other available catalysts (Jensen et al., 2008).

Table 6: Constant and variable test parameters for electrode gap optimisation

Constant Test Parameters		
Test Variable	*Unit*	*Variable Range*
Electrolytic Concentration	mass% KOH	30 wt%
Electrode Material	-	Ni 200
Variable Test Parameters		
Test Variable	*Unit*	*Variable Range*
Electrode Gap	mm	0.8; 1.3; 2.5; 3.5; 4.5; 5.5
Temperature	°C	50,70
Flow Velocity	$m.s^{-1}$	0.075; 0.1; 0.15
Cell Potential	VDC	1.765; 2; 2.5; 3; 3.5

The electrolytic temperature was restricted to 50°C and 70°C, to note whether the viscosity change of the electrolytic solution has any influence in changing the optimal electrode gap for the pure nickel electrodes. From this investigation, it is possible to note the minimum electrode gap requirement, at a constant electrolytic flow velocity required, in order to operate at a set current density threshold.

3.5.2.4. Three Dimensional Electrodes for Performance Enhancement

Expanding from the definition for current density for this investigation, and the enhancement for rate kinetics as suggested in the literature review, an increase in geometric area of the electrodes would increase the current density as calculated on a cross sectional basis. In theory, the geometric calculated current density should decrease due to the distance increase of the outer electrode from the nearest opposite face. This would therefore result in a variation of specific current density[6], throughout the thickness of the electrode. However the membraneless technology, similar to technologies utilising porous electrodes or gas diffusion electrodes, aims to maximise the cross sectional current density as explained in Section *2.5 Basis for Current Density,* in order to reduce the overall stack volume. The possibility of using three dimensional electrodes to achieve this optimisation was investigated and the relative benefit quantified with the increase in thickness.

[6] Current density calculated for a planar surface of a three dimensional electrode at a specified distance from the electrode face.

Table 7: Constant and variable test parameters for three dimensional electrode performance optimisation

Constant Test Parameters		
Test Variable	*Unit*	*Variable Range*
Electrolytic Concentration	mass% KOH	30 wt%
Electrode Material	-	Ni 200
Electrode Gap	mm	2.5 mm
Variable Test Parameters		
Test Variable	*Unit*	*Variable Range*
Number of mesh layers	#	Single; Double; Triple
Temperature	°C	70
Flow Velocity	$m.s^{-1}$	0.15
Cell Potential	VDC	1.765; 2; 2.5; 3; 3.5

The relationship with temperature would have been well established in prior investigations, and it was therefore suspected that there would be no further need to establish data over the full original temperature range. Therefore a temperature from the higher temperature range was selected to test the additional performance increase with regard to the three dimensional mesh electrodes.

3.5.3. Additional Test Parameters

3.5.3.1. Gas Purity Analysis

Once the majority of parameters were optimised, the gas purity of hydrogen and oxygen with changing flow velocity was investigated. As per the membraneless technologies operating principle, the purity of the produced hydrogen and oxygen depends on the operating current density and the flow velocity. A condition demonstrating stable performance was chosen based on results from the above parameter optimisation investigations. The chosen current density and temperature is representative of the worst case scenario in order to determine whether the technology is capable of operating with superior gas purities at most tests parameter conditions.

Table 8: Constant and variable test parameters for gas purity analysis

Constant Test Parameters		
Test Variable	*Unit*	*Variable Range*
Electrolytic Concentration	mass% KOH	30 wt%
Electrode Material	-	Ni 200
Electrode Gap	mm	2.5 mm
Current Density	$mA.cm^{-2}$	3500
Variable Test Parameters		
Test Variable	*Unit*	*Variable Range*
Temperature	°C	Room temperature
Flow Velocity	$m.s^{-1}$	0.075; 0.1; 0.15
Cell Potential	VDC	Dependant on current density threshold

3.5.3.2. Medium Term Stability Tests

The feasibility of many electrode catalyst combinations depends on the catalysts ability to maintain stable performance for an extended duration of time with little change in the polarisation[7]. The material deemed the most practical and stable material for the alkaline membraneless electrolyser was tested over a set duration of time.

Table 9: Constant and variable test parameters for medium term stability testing

Constant Test Parameters		
Test Variable	*Unit*	*Variable Range*
Electrolytic Concentration	mass% KOH	30 wt%
Electrode Material	-	Ni 200
Electrode Gap	mm	2.5 mm
Testing Duration	hrs	250
Temperature	°C	60
Flow Velocity	$m.s^{-1}$	0.075
Current Density	$mA.cm^{-2}$	3500

The electrode stability was tested at a deemed stable current density of 3500 $mA.cm^{-2}$ in order to do a thorough analysis of the electrode stability. The temperature was limited to 60°C in order to minimise the evaporation of liquid electrolyte from the system. 250 hours seemed sufficient to note any severe increases in polarisation of the tested catalytic material for the amount of allocated time for the test.

[7] Polarisation of a catalyst refers to the additional potential increase from the initial stable potential for a specific duration of testing.

3.5.4. Test Methodology

Once the desired test parameters were selected for a specific test run according to the above optimisation investigations, the system was prepared to match these parameters. Initially the electrodes are inserted and adjusted to match the desired electrode material and electrode gap. Once performed, the electrolytic solution is then prepared using the methodology outlined in *Appendix C*. The system can then be heated and circulated at the desired test temperature and flow velocity. Once completed, a general procedure can be employed to generate the test data for an experimental run.

3.5.4.1. Recording System pH and mV

Before each experimental run, it is ensured that a measurement of both pH and mV are recorded along with the system temperature. The Boeco PT-380 pH/mV portable probe consists of a stainless steel temperature probe capable of recording temperatures up to 120°C and pH values ranging between -2 to 16.

These probes are submerged into the electrolytic solution, ensuring that all measurement sensitive parts are fully submerged. The meter requires a length of time before a constant reading is registered. These readings will be represented for each experimental run in order to note whether any significant fluctuation in concentration is evident.

3.5.4.2. Recording System Temperature, Flow Rate and Pressure

System temperature is recorded simultaneously with mV and pH recordings as noted above. Temperature is the limiting factor that prevents the meter from taking an immediate reading. In some cases the meter is found to create an untrue hold result. In this situation, it can either be requested to re-measure the values, or to ensure that the highest recorded temperature be accepted as the true system temperature. This temperature can be cross referenced with the

temperature gauge located on the top of the reaction unit. Heating of the plant can be set by altering the temperature value on the selection knob located on the heating control panel. This value will be compared with the measured reference sensed by the temperature probe.

System flow is easily recorded with the use of the digital display on the electromagnetic flow meter. Flow values and fluctuations are regularly recorded with changing voltage conditions during experimental runs. System flow, as mentioned previously, will be accurately controlled by the variable speed drive for the pump and in addition, if required, by a diaphragm valve located on the feed line to the electrolyser. The flow velocity of the electrolytic solution is then calculated by dividing the flow rate with the exposed electrode area open to electrolytic flow.

Located adjacent to the temperature gauge, will be the electrolyser's pressure gauge. This gauge provides an estimate for system pressure which is recorded at every change in flow, temperature and concentration condition. Pressure is noted to be dependent on numerous external variables such as mesh gauge and aperture size.

3.5.4.3. Recording System Voltage and Current

Once the system temperature, flow rate and pH/mV is recorded, the system is then ready to conduct the experimental run. During the experimental run, fluctuations in system parameters will be recorded.

Labview™ 2013 provides the engine with which software is generated that creates the possibility to externally control and data log voltage and current of the Genesys 2.4kW programmable power supply. The software provides a data logging capability for which both parameters can be monitored over any length of time. Labview™ provides the capability to interface with many hardware devices through the development of a virtual instrument interface. From this interface, conditions of the device can then be monitored and controlled.

The developed programme displays a graphical chart/analysis by which fluctuations in readings can be noted. This will be specifically important for noting when a steady state condition has been reached. The programme will have numerous flexibilities in either

maintaining a constant voltage and noting the fluctuation in current or in contrast maintaining a constant current, and noting the variation on voltage. Once an experimental test run has been concluded, reference can be made to the data logged file to note final values of current or voltage, along with fluctuations in voltage and current measurements.

An excel spreadsheet has been developed for each experimental investigation whereby measured and theoretical data can be inserted. Standard deviations, graphical representations and uncertainties are automatically calculated and generated.

3.6. Analytical Procedure

For each of the set experimental conditions, experiments were repeated 3 times to gain a sense of the repeatability of experimental results. Experimental analysis of results was performed by calculating the standard deviation and uncertainty for each data set. Reference was made to Peters (2001) regarding the methodology for analysis of the data. Collection of data for experimental analysis will always have bias[8] associated with it caused by human error. Mathematically it is conceptualised as Equation (20):-

$$Measured\ Value = True\ Value \mp error \dots\dots\dots (20)$$

The error in the above expression is a measure of the inherent variation in the phenomena observed due to numerous factors interfering with the measurement. The simplest method to reduce the error of a recorded value is to replicate the conditions at which the result was recorded. A benchmark for a minimum of three recordings has been set for each set of experimental conditions. This will serve to note whether results are repeatable and precise. An average will be taken for the recorded values and noted as the experimental result. A sample average is calculated via the following expression:-

$$\bar{x} = \frac{\sum_{i=1}^{n} x_i}{n} \dots\dots\dots (21)$$

Where:-

[8] Bias is defined as discrepancies that exist between data values due to external influences that may affect the precision or accuracy of a data set.

$\bar{x}$:- Mean average for a set of data

xi:- single data point

n:- number of recorded data points

The standard deviation is another useful means of interpreting the precision of results by noting a range within which a certain percentage of the results falls within. Standard deviation is calculated via the following expression:-

$$s^2 = \frac{\sum_{i=1}^{n}(x_i - \overline{x})^2}{n-1} \dots\dots\dots (22)$$

The degrees of freedom, dependent on the number of recorded values are determined by *n-1* where *n* is the number of values in a data set. The standard error of the mean is a means of determining the uncertainty[9] associated with the particular test conditions. The standard error can be determined by the following equation:-

$$s_{\bar{x}} = \frac{s}{\sqrt{n}} \dots\dots\dots (23)$$

By taking the standard mean and multiplying it by the relevant *t* value determined from a confidence interval table will yield the uncertainty or error associated with the recorded values:-

$$\bar{x} = t_{n-1:a/2} s_{\bar{x}} \dots\dots\dots (24)$$

Where:-

t:- Confidence interval factor

Table 10: Confidence interval table (Peters, 2001)

Confidence Interval Table			
Degrees of Freedom	*CI = 90%*	*CI = 95%*	*CI = 99.5%*
1	6.314	12.706	127.32
2	2.92	4.303	14.089
3	2.535	3.182	7.453
4	2.132	2.776	5.598

[9] The uncertainty of a data point defines the precision or the error of that data point determined from the average of that data set.

By examining Table 10, it can be seen that a confidence of 90, 95 or 99.5 percent can be selected. It was decided that a confidence of 95% would be sufficient for data analysis. This means that the recorded value would have a 95% likelihood of appearing in the indicated error range.

This calculation method yields an equation by which the precision of the result can be clearly analysed by examining the uncertainty factor.

4. RESULTS AND DISCUSSION

4.1. Optimisation of Electrolytic Concentration

Experimental results have been completed in sequence of increasing concentration from 20wt% to 50wt% potassium hydroxide solution. The optimal concentration for optimising the performance of the alkaline water electrolysers has been determined for the tested parameters represented in Table 4. It was noted during experimental tests that after a time duration greater than 12 hours, the stainless steel 316 electrodes experienced severe performance drops. Additionally, performance tests concerning 50 wt% potassium hydroxide at a temperature of 80°C,were not performed due to the material operability limits of the system chemical pump being exceeded.



Figure 25: KOH crystal formation at high concentration and temperature resulting in rapid degradation of the chemical pump mechanical seal.

This therefore required the subsequent replacement of the mechanical seal of the chemical pump. These conditions were also found to increase wear on the Hydrox Holdings Ltd. pilot plant due to the aggressive corrosive nature of the lye solution at these elevated temperature

conditions. Careful consideration is therefore stressed when considering the design of alkaline hydrogen electrolysers in aggressive conditions even if these conditions prove to maximise the performance of these systems.

As mentioned above, the stainless steel 316 electrodes required frequent replacement in order to produce reliable results across the range of tested concentrations as results inevitably were seen to be unreliable due to large deviations in hypothesised trends. The following table therefore indicates the instances during testing where electrodes underwent severe deactivation[10] and were therefore replaced:

Table 11: Points of deactivation and subsequent electrode replacement during the investigation of determining the optimised electrolytic concentration for stainless steel 316 electrodes

Concentration (wt% KOH)	Temperature (°C)
20	40,50,60,70,80
30	40,50,80
Deactivation of Electrodes (Subsequent Electrode Replacement)	
30	60,70
40	40,50,60,70,80
Deactivation of Electrodes (Subsequent Electrode Replacement)	
50	40,50,60,70,80

From the above table, it can be noted that electrode deactivation was enhanced through operation at predominantly the higher temperature scale as a result of elevated operating current densities and aggressive conditions. The first instance of this phenomenon was noted at a concentration condition of 30 wt% KOH and a temperature of 80°C. These conditions were resultantly not re-tested and therefore the degree of performance degradation can be noted in the experimental results that follow. The lower temperature scale, below 70°C, will therefore be used in order to demonstrate concentration trends and trends associated with flow velocity and temperature.

[10] The process whereby a catalyst has become poisoned or has undergone electrochemical deposition and therefore the catalytic nature of the electrode is defined by the newly plated/deposited material.

4.1.1. Concentration Fluctuation and Monitoring

The method for monitoring concentration change as described in Section *3.5.4.1. Recording System pH and mV,* was used in order to note whether there is any significant change in concentration as experimental testing progresses. The system electrolytic volume amounting to approximately 175 liters of electrolytic solution suggests that at the low amperage, no significant change in concentration should be observed with the water losses attributed to evaporation, leaks and the consumption of water due to electrolysis. It was the aim of recording the change of conductivity of the solution, as a function of time, to demonstrate whether a significant change was noted. This however was performed on the assumption that contaminants within the solution were present in reduced concentrations not possessing considerable influence on the function of the PT-380 pH probe used.

A measurement of mV/pH was performed prior to each experimental run. These results demonstrate the change in pH/mV (indicative of concentration[11]) measurements over the selected duration of experimental testing. An average was taken between three measured results for each temperature and flow condition. These were then subsequently compared to the theoretically determined results at the appropriate temperature as determined from a standard solution. The following plots illustrate the change in pH and mV readings as experimental results progressed.

[11] Concentration can be linked to the pH of the solution by the empirical correlation pH = -log $[OH^{-1}]$, and therefore a directly proportional relationship exists.

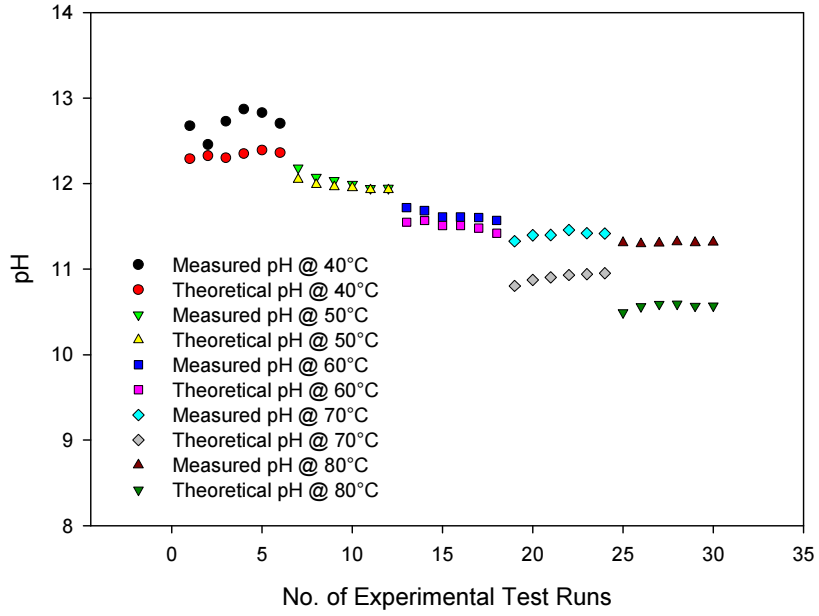

Figure 26: Change in pH for progressing experimental runs for the performance investigation for stainless steel 316 electrodes and 20 wt% potassium hydroxide

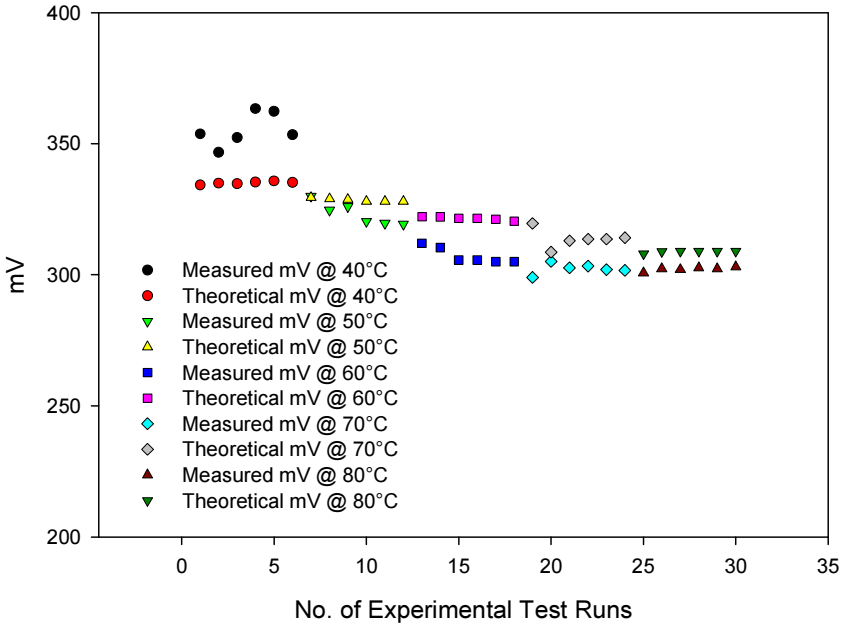

Figure 27: Change in mV for progressing experimental runs for the performance investigation for stainless steel 316 electrodes and 20 wt% potassium hydroxide

Results for 30, 40 and 50 wt% potassium hydroxide can be made reference to in *Appendix E.1*. Theoretical data points create a linear relationship as a function of temperature as determined from the calibration data. It is noted that for both trends for pH and mV readings illustrated

on Figure 26 and Figure 27, the readings decrease with increasing temperature. Deviations between theoretically determined data and experimentally determined data are not exact, however deviations are shown not to be significant, therefore concentrations could be assumed to remain constant as the same trend is followed for each concentration investigation. The only notable difference, where initially measured values for each temperature are high and decrease exponentially to a linear trend, is associated with 50 wt% potassium hydroxide concentration in Figure E5 and Figure E6. The aggressive conditions of this elevated concentration showed observable degradation of the measurement probe. Other observable phenomena include outliers, however these results were not consistent with the general developed trends.

4.1.2. Concentration as a Function of Flow Velocity and Temperature

From literature it is evident that, for a temperature range between 0-100°C, the conductivity of an immobilised potassium hydroxide solution peaks at 35 wt% potassium hydroxide (Allebrod et al., 2012). It is clear that out of the four concentrations tested, 30 wt % potassium hydroxide generated the highest recorded current densities for the tested voltage range employing stainless steel 316 mesh electrodes **(**Figure 28, Figure 29, Figure 30 and Figure 31**)**. As stainless steel was initially easily accessible, it was chosen as the material of choice for early testing of electrolytic concentrations and trends associated with flow velocity and temperature. It is evident that similar findings are obtained compared to results obtained from literature (Marini et al., 2012) for the Hydrox Holdings Ltd. test rig employing stainless steel 316 electrodes. Although polarisation data has been shown for flow velocities of 0.1 $m.s^{-1}$ and 0.3 $m.s^{-1}$ and temperatures of 50°C and 70°C the trend for the additional tested temperatures (40°C, 60°C and 80°C) and flow velocities (0.2 $m.s^{-1}$, 0.4 $m.s^{-1}$, 0.5 $m.s^{-1}$ and 0.6 $m.s^{-1}$) are replicated. These additional results can be made reference to in *Appendix E.2.*

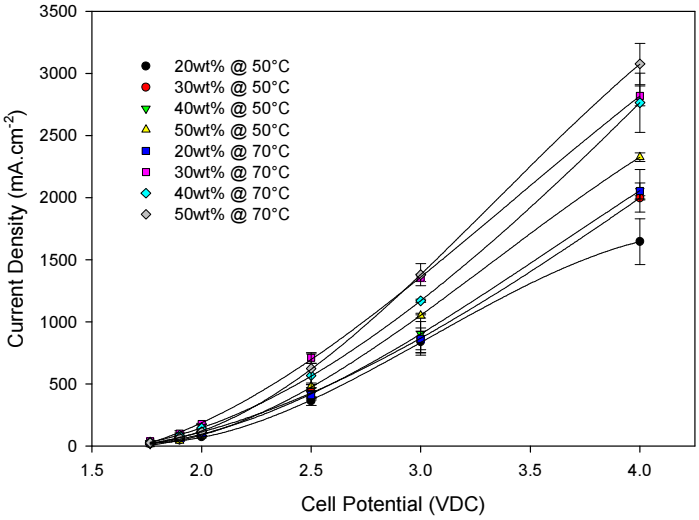

Figure 28: Polarisation curves of test rig as a function of potassium hydroxide (KOH) concentration at a temperature of 50°C and 70°C, an electrode gap of 3.5 mm and a flow velocity of 0.3 m.s^{-1} for stainless steel 316 electrodes.

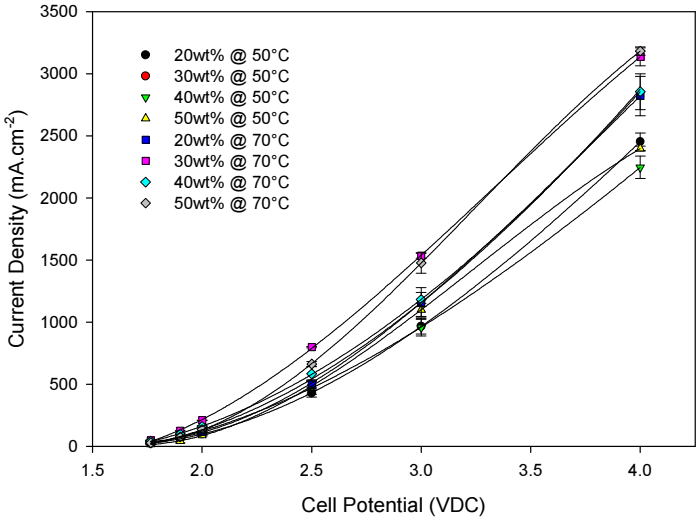

Figure 29: Polarisation curves of test rig as a function of potassium hydroxide (KOH) concentration at a temperature of 50°C and 70°C, an electrode gap of 3.5 mm and a flow velocity of 0.1 m.s^{-1} for stainless steel 316 electrodes.

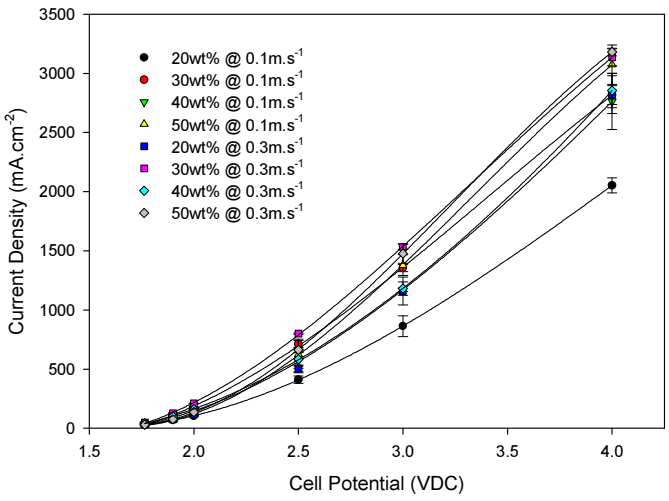

Figure 30: Polarisation curves of test rig as a function of potassium hydroxide (KOH) concentration at a flow velocity of 0.1m.s^{-1} and 0.3 m.s^{-1}, an electrode gap of 3.5 mm and a temperature of 50°C for stainless steel 316 electrodes.

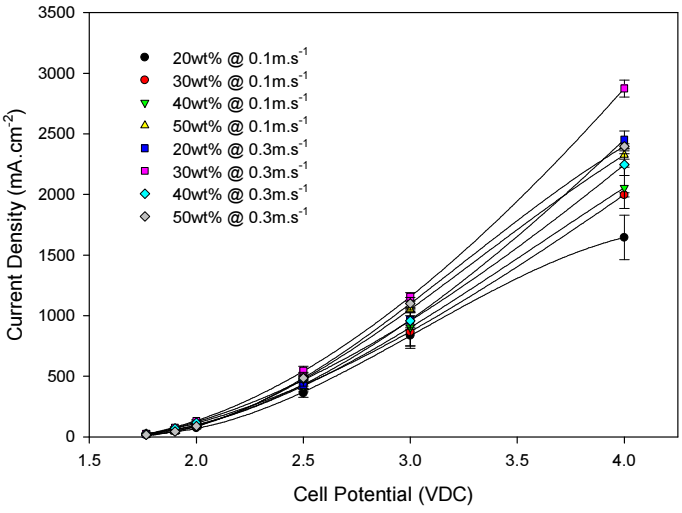

Figure 31: Polarisation curves of test rig as a function of potassium hydroxide (KOH) concentration at a flow velocity of 0.1m.s^{-1} and 0.3 m.s^{-1}, an electrode gap of 3.5 mm and a temperature of 70°C for stainless steel 316 electrodes.

The above illustrations are representative of the same data, making reference to the change in optimal concentration as a function of firstly, temperature illustrated in Figure 28 and Figure 29, and secondly as a function of flow velocity illustrated in Figure 30 and Figure 31. Similar results are obtained for 30 and 50 wt% KOH for the voltage region smaller than 3 VDC (Allebrod et al., 2012), however for the highest tested voltage of 4 VDC and 50 wt% performance was marginally superior in contrast to 30 wt% KOH. For each investigated temperature, it was clear that 30 wt% potassium hydroxide exhibited the highest current density with the exception of the higher tested voltage range. Stainless steel 316 underwent chromium leaching at 80°C and as a result an inferior performance was generated for 30 wt% potassium hydroxide at this temperature condition and 40 wt% potassium hydroxide proved notably superior (Figure 32):

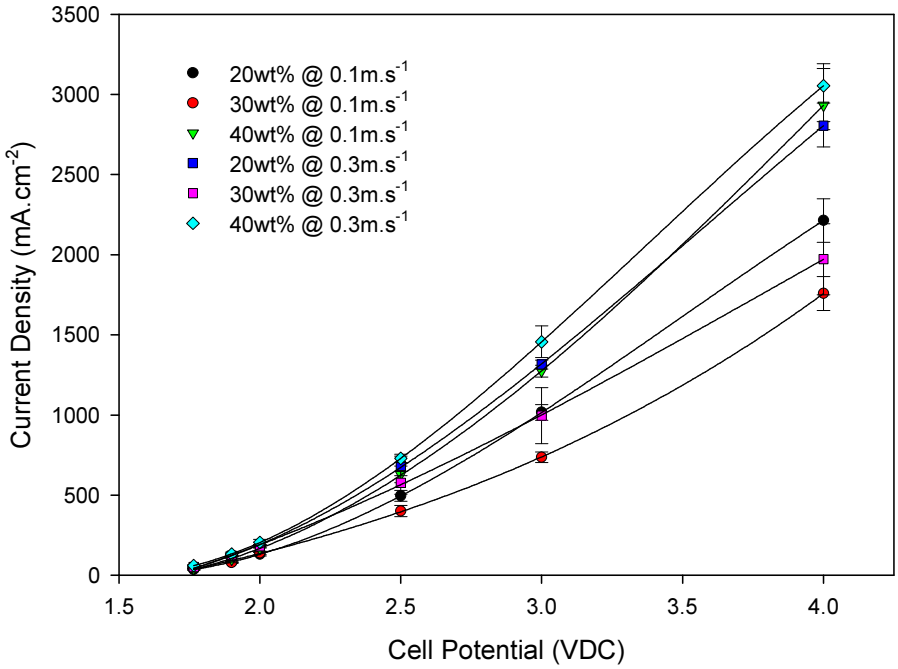

Figure 32: Polarisation curves of test rig as a function of potassium hydroxide (KOH) concentration at a flow velocity of 0.1m.s^{-1} and 0.3 m.s^{-1}, an electrode gap of 3.5 mm and a temperature of 80°C for stainless steel 316 electrodes.

The use of stainless steel was originally thought relevant as the choice of material for applications in alkaline water electrolysis. Referring to the empirical results generated, specifically in the above Figure 32, instances of sudden drops in performance observed after a mere 12 hours of variable voltage operation suggests that electrochemical phenomena

associated would ultimately limit long term operational feasibility. This observed de-activation produced results deemed as unreliable and therefore the subsequent replacement of electrodes was required at intervals where deactivation was noted. Upon close observation of the electrodes themselves and their conductive parts, the anode, responsible for oxygen formation has altered appearance from stainless steels general silver sheen to a bronze appearance as illustrated in Figure 33 below.



Figure 33: Left: - General silver sheen of the cathodic conductive head. Right: - Altered appearance to a bronze appearance of the anodic conductive head.

The physical appearance of the electrolytic solution had undergone a colour change from a clear solution to a yellow/green coloured solution as a result of leached chromium ions as illustrated in Figure 34 below:



Figure 34: Left: - Clear electrolytic solution. Right: - Contaminated appearance of electrolytic solution

With an increase in temperature the conductivity of the electrolytic solution increases (Allebrod at al. 2012) and the reaction kinetics of the hydrogen and oxygen evolution reactions increase, as well as mass transfer of ions through the solution occurs at an increased rate. A notable decrease in the overpotential required for a set hydrogen generation rate is subsequently observed (Zeng and Zhang, 2010). The positive effect of increasing the temperature of the electrolytic solution is clear from Figure 28 and Figure 29. It is therefore favourable to operate at as high a temperature as possible, as cell performance and efficiency increases with temperature. Temperature furthermore benefits the overall process by reducing the pressure drop of the solution flowing through the system components and thereby increasing the ease at which bubbles are evolved from the electrode surface, which in turn increases the effective reactive area available. High temperature and pressure operation could not be investigated thoroughly, due to the design constraint of the current test facility, but it is foreseen that these applied increases in these parameters will dramatically add to the efficiency improvement of alkaline water electrolysis systems and of the HH electrolyser technology.

4.2. Effect of Electrolytic Temperature and Electrolytic Flow Velocity

Alkaline water electrolysis is known to increase in efficiency with increasing temperature and electrolytic flow velocity. This is true in the fact that the electrical efficiency may improve, as a larger portion of the total energy required for the reaction is supplied in the form of heat energy once the operating voltage exceeds 1.48 VDC[12]. Every existing electrolytic system makes use of an electrolytic fluid re-circulation pump, which in many electrolysers, is simply used to extract produced gases out of the electrolyser unit and for the constant supply of fresh electrolyte to the electrolytic unit. With HH electrolyser technology, it uses this electrolytic fluid at a substantially higher fluid re-circulation rate so as to improve the rate at which product bubbles are removed between electrodes, and from electrode surfaces to further improve the effective reactive area available for electrochemical reaction. The following results demonstrate the trends associated with increasing the electrolytic temperature and electrolytic flow rate at a constant cell potential for the potentials of 2 VDC and 3 VDC for

[12] The thermo neutral voltage as discussed in 2.3. Water Electrolysis Thermodynamics

both 30 wt% KOH and 40 wt% KOH. Additional results pertaining to a cell potential of 2.5 VDC can be made with reference to Appendix *E.3.*

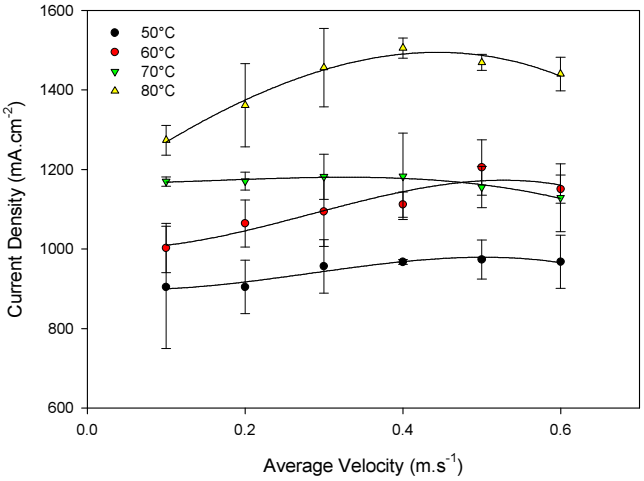

Figure 35: Current Density versus Average Velocity of electrolytic fluid as a function of electrolytic temperature at an electrolytic concentration of 30 wt%, a cell potential of 2 VDC and for stainless steel 316 electrodes.

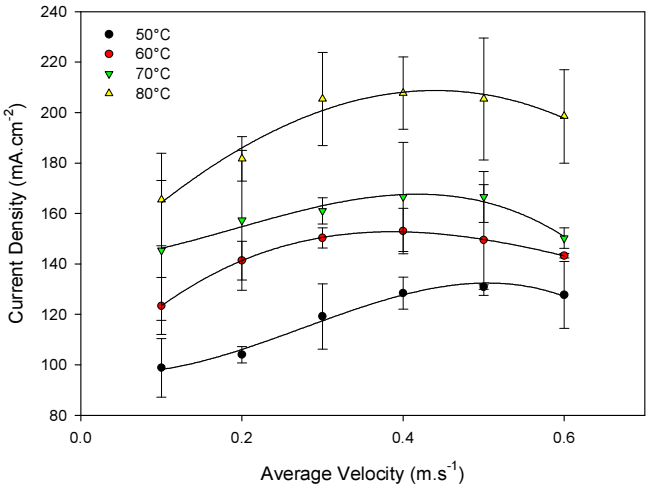

Figure 36: Current Density versus Average Velocity of electrolytic fluid as a function of electrolytic temperature at an electrolytic concentration of 40 wt%, a cell potential of 2 VDC and for stainless steel 316 electrodes.

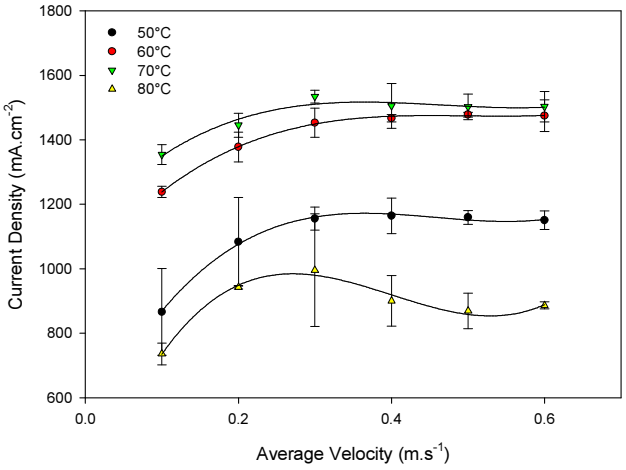

Figure 37: Current Density versus Average Velocity of electrolytic fluid as a function of electrolytic temperature at an electrolytic concentration of 30 wt%, a cell potential of 3 VDC and for stainless steel 316 electrodes.

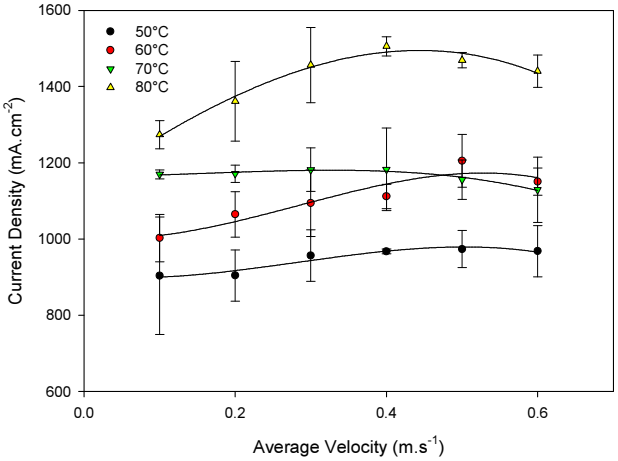

Figure 38: Current Density versus Average Velocity of electrolytic fluid as a function of electrolytic temperature at an electrolytic concentration of 40 wt%, a cell potential of 3 VDC and for stainless steel 316 electrodes.

Although the increase of electrolytic flow velocity through the electrode mesh has a notable increase in cell performance as noted in Figures above, the increase is not as substantial as that resulting from increased temperature. From the results above that an optimal flow velocity exists for which current density is maximised, after which no additional benefit is provided for the increase in flow velocity beyond that point. As the temperature increases, the optimal flow velocity is extended to the higher flow velocity range. This therefore suggests that the mechanism governing this improvement is related to pressure exerted on the mesh electrodes. When the pressure exceeds a certain critical point, a deviation in the parallel nature of the electrodes is experienced resulting in a breakdown of the uniform field created between the parallel electrodes. The sudden drop in efficiency with regard to 30 wt% KOH at 80°C can be clearly noted when referring to Figure 37, where 80°C is still observed to maximise performance at the lower voltage range However, a sudden loss in performance is noted with regard to the higher voltage range.

As mentioned in the section above, the increase in electrolytic temperature is known to increase the rate kinetics of all chemical reactions. Results therefore demonstrate an increase in current density for all tested cell potentials and as a result, it is expected that the highest temperature of the tested experimental range should produce the highest current density. Equation (19) as quoted from Mazloomi and Sulaiman (2012) shows that the ohmic resistance is directly related to the resistivity of the solution. Resistivity has a proportional relationship to temperature, observed as decreasing with the increase in temperature. It must be highlighted however that the total energy required by the electrolysis of water, as noted in the literature review, is a combination of the Gibbs free energy and Entropy as illustrated in Equation (7) (Dieguex et al., 2008).

The increase in electrolytic temperature additionally improves the stack performance by increasing the electrolytic solution flow rate past the mesh electrodes for a set pressure drop. By increasing the flow velocity, an increase in the disengagement rate of the product gas is observed (Mazloomi et al., 2012). A gas meniscus is formed on the material surface and is reduced in thickness with the increase in electrolytic fluid velocity which reduces the probability of void fracture whereby potential cross gas contamination and a loss of effective reactive area can take place (Mazloomi et al., 2012). The benefit of the reduction of residual gas between or within electrodes notes that a smaller electrode gap can be employed at substantially higher current densities, which consequently benefits cell efficiency. Operating

at unrealistic high liquid throughputs will require considerable work for pumping. Therefore, an adequate velocity of 0.1 $m.s^{-1}$ (the average velocity across a single electrode face) ensures an efficient practical requirement for pump work and still promotes stable performance and adequate gas purity.

The effects of temperature and flow velocity have been demonstrated in the sections above. The remaining results sections will focus predominantly on optimisation in the practical range of electrolytic fluid velocity and in the higher temperature range to demonstrate optimal performance. All remaining results as a function of various temperatures and flow velocities can be made to references in *Appendix E.*

4.3. Optimisation of Electrode Materials

In the pursuit of optimised cell performance a number of different cathodic and anodic materials, that are cost effective and easily obtainable, were tested in the HH AWE test rig. The chosen materials for the investigation are representative of materials that would typically be used in existing commercialised electrolysis test-rigs. Data has been reported for 70°C as data for stainless steel at 80°C demonstrated unstable behavior as reported in sections above.

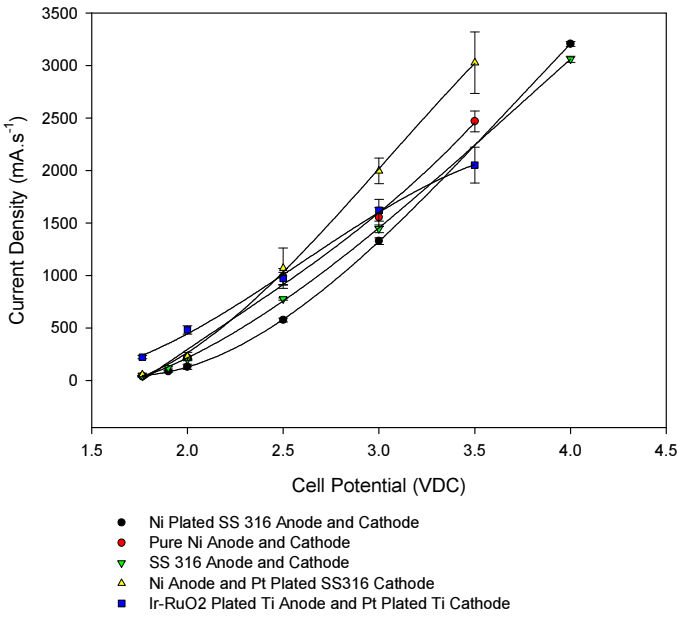

Figure 39: Polarisation curves of test rig as a function of cathodic and anodic material for a temperature of 70 °C, a flow velocity of 0.1 $m.s^{-1}$, an electrode gap of 3.5 mm and 30 wt% potassium hydroxide (SS: stainless steel).

From the use of nickel on the anode and plated platinum on the cathode maximised cell performance at voltages greater than 2.5 VDC under prevailing conditions (Figure 39). Using a material that is selectively electro-catalytic for either the hydrogen or the oxygen evolution reaction, will collectively increase the reaction rate kinetics of the overall water electrolysis reaction (Miles, 1975). Based on volcano plots highlighting electrocatalytic activity, platinum is known for its superior properties in maximising the hydrogen evolution reaction rate (Yde et al., 2013). The oxygen evolution reaction, on the other hand, is known to be the limiting reaction within the overall water electrolysis reaction. Nickel, commonly used as the general catalyst for anodic reactions in industry, has been reported to have a higher catalytic activity for the oxygen evolution reaction compared to platinum, and it is therefore expected that using platinum for the anode will not yield results superior to pure nickel (Wang, 2005).

Metal oxides, however, are suggested to dramatically improve the catalytic response of the oxygen evolution reaction (Man et al., 2011), and in that regard additional optimisation for the membraneless electrolyser is possible. Based on theoretical calculations the optimal suggested catalysts exhibiting the highest degree of catalytic activity is RuO_2 and Co_3O_4. It should however be considered that catalysts that are suggested to be theoretically optimal may not always perform as well when subjected to real experimental conditions in terms of durability and stability (Man et al., 2011). An MMO anode, used in conjunction with a platinum plated cathode, is seen to yield superior results at voltages below 2.5 VDC (Figure 39). Above this voltage, however, other material combinations are seen to improve cell performance.

In using this advanced catalytic combination for the membraneless cell it is evident that a current density of 257 $mA.cm^{-2}$ is achieved at 1.765 VDC under atmospheric conditions and 70 °C, which compares favourably to current commercial alkaline electrolysers performance (Jensen et al., 2008). With the use of pure nickel electrodes for both the anode and the cathode, at similar conditions to the PGM catalysts, a substantially lower current density of 51.9 $mA.cm^{-2}$ at 1.765 VDC, however it is evident, that with the membraneless technology, the favorable PGM catalysts perform poorly in comparison to the pure nickel electrodes at elevated voltages with reference to Figure 39.

Due to complexities experienced with regard to stainless steel as mentioned in the above Section 4.1 that deal with the *Optimisation of Electrolytic Concentration*, the conductive components responsible for the conducting charge to the mesh electrodes were replaced with

a more stable alternative to prevent electrode poisoning[13]. Initially bench tests were performed in order to justify the stability of material in the lye solution when a charge is conducted through them. A beaker test filled with 40 wt% potassium hydroxide solution was used to perform this check with two equally spaced mesh electrode plates. No physical separation of the gas was accounted for, to allow oxygen gas (generally responsible for the formation of metal oxides on the cathode) to occupy the entire liquid volume of the beaker. The following configuration was produced as illustrated in Figure 40 below:



Figure 40: Bench top experimental set-up configuration for the determination of a suitable stable conductive material

The electrolytic solution was clear initially before a potential difference was applied across the electrodes. Upon producing a potential difference of 2.5VDC across the mesh plates it was observed that the solution turned milky purple in appearance. The source of this contamination came solely from the anodic electrode. It was thereafter observed after a duration of 2 hours, that the cathodic electrode had become plated by a black deposit presumed to be a metal oxide as shown in Figure 41 below:

[13] The process described previously as the deposit/plating of a material less/more catalytically active onto the existing catalyst.

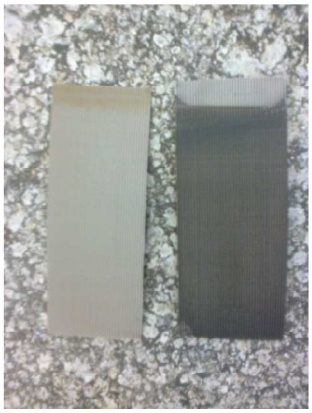

Figure 41: Left – Anodic electrode responsible for oxygen evolution, Right – Cathodic electrode responsible for hydrogen evolution

Once the solution had been allowed to settle, the solution was observed to have turned a characteristic yellow/green tinge which is characteristically associated with Hexavalent chromium leaching into solution. It was observed that when a separator was placed between the electrode plates, the electrode plates remained clear of deposits indicating that the presence of oxygen gas in the vicinity of the reducing cathodic electrode was responsible for the deactivation behavior associated with stainless steel electrodes. The same experiment was performed with nickel star shaped electrodes, and after a duration of testing exceeding 24 hours at a voltage of 2.5VDC and no physical barrier between the electrodes, the electrodes were observed to be deposit free as shown in Figure 42 below:



Figure 42: Nickel star shaped electrodes as observed after a beaker test at 2.5VDC for a testing duration exceeding 24 hours.

The conductive components of the electrolyser test rig were therefore machined out of industrially pure nickel (Ni 200) in order to obtain accurate results with respect to catalytic material that is particularly sensitive to catalytic poisoning.

4.4. Effect of the Variation in Electrode Gap and Electrolytic Flow Velocity

For the HH AWE technology the electrode gap, electrolytic flow velocity, and current density are interdependent, which means that the electrode gap and electrolytic flow velocity need to be optimised in order to maximise current density (Nagai et al., 2003a). During operation, at low electrolytic flow velocities, a decrease in efficiency was observed which is due to the increase in the fraction of produced gas bubbles between the anodic and cathodic electrodes. This results in (i) a sudden loss in the electrode active area under minor bubble formation between the electrodes, and (ii) the hampering ionic flow between the electrodes under severe bubble formation between the electrodes (Mazloomi and Sulaiman, 2012). It is therefore obvious that an effective electrolytic flow velocity across the electrodes is to be maintained, not only to limit the effect of void fracture, but also to prevent cross gas contamination which is an associated problem with many membrane technologies (Jensen et al., 2008). Operating conditions therefore need to be avoided that result in void fracture (Figure 43a), but the electrolyser needs to be operated under conditions that serve to reduce this effect (Figure 43b).

a. b.



Figure 43: Pictures of (a) Evidence of void fracture taking place between an electrode pair for an electrode gap of 2.5mm, current density of 3000mA/cm^2 and below the recommended fluid velocity of 0.075m.s^{-1} (b) the reduction of void fracture between an electrode pair for an electrode gap of 2.5mm, current density of 3000mA/cm^2 and above the recommended fluid velocity of >0.075m.s^{-1}

The above figures serve to provide a graphical illustration of the formation of a gas meniscus on the porous electrode surface. Once the solution velocity overcomes a certain minimum required fluid velocity, the meniscus reduces in thickness and is speculated to be removed rapidly from the electrode surface in order to prevent a gas meniscus forming on the surface of the electrode.

As a result of the flow of electrolytic solution, resulting in the formation of a negligible gas meniscus, a relatively small electrode gap (<1mm) can be obtained and together with operating at the optimal electrolytic concentration of 30 wt% potassium hydroxide a reduction in the total ohmic resistance can be achieved (Jensen et al., 2008). The relationship between the mentioned variables for the reduction in ohmic resistance is demonstrated in Equation (19) (adopted from Mazloomi and Sulaiman, 2012).

The material resistivity of the gaseous constituent of the electrolyte between the electrodes is substantially greater than the material resistivity of the electrolytic solution itself (Mazloomi and Sulaiman, 2012), which substantiates the benefit achieved by maintaining a negligible gas meniscus on the frontal face of the electrode.

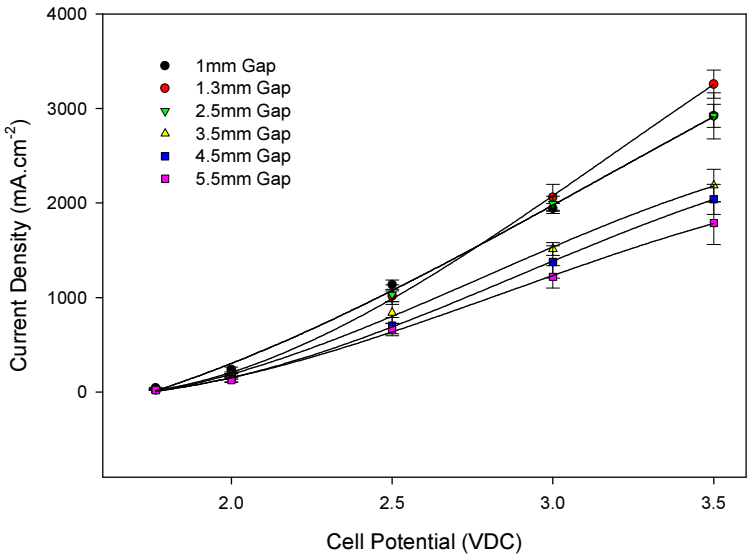

Figure 44: Polarisation curves of a membraneless stack as a function of electrode gap for pure nickel electrodes at a temperature of 50 °C, 30wt% potassium hydroxide and a flow velocity of 0.15 m.s^{-1}.

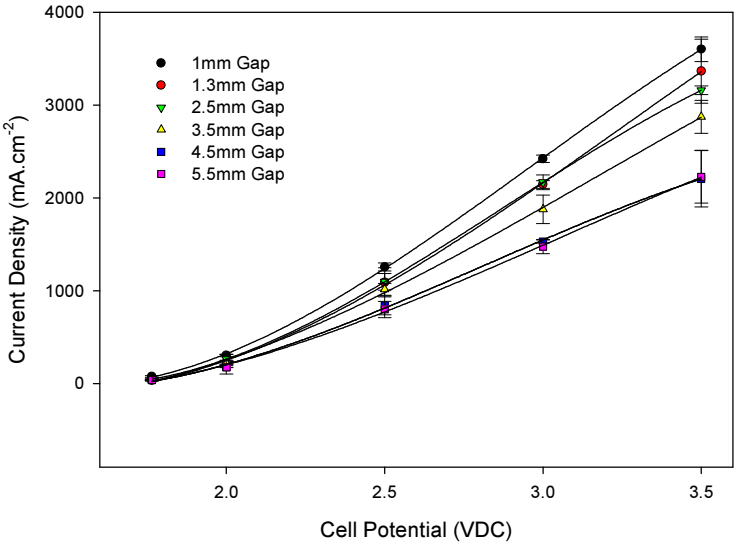

Figure 45: Polarisation curves of a membraneless stack as a function of electrode gap for pure nickel electrodes at a temperature of 70 °C, 30wt% potassium hydroxide and a flow velocity of 0.075 m.s^{-1}.

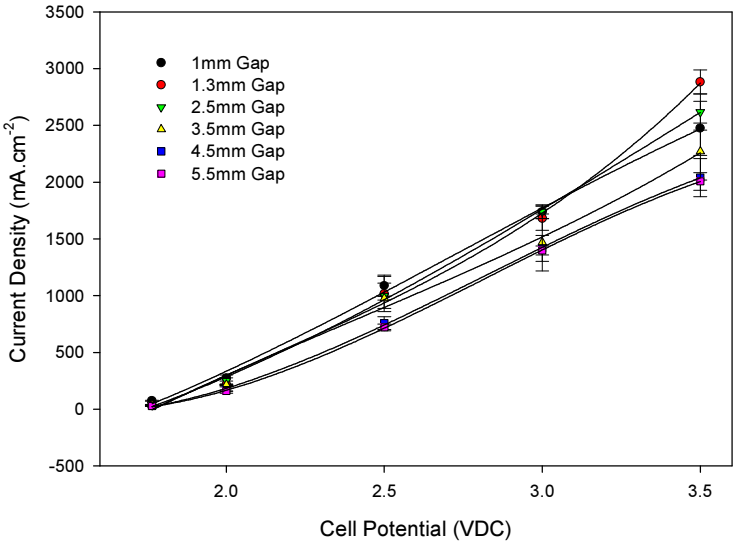

Figure 46: Polarisation curves of a membraneless stack as a function of electrode gap for pure nickel electrodes at a temperature of 70 °C, 30wt% potassium hydroxide and a flow velocity of 0.15 m.s^{-1}.

On evaluating current densities for different electrolytic flow velocities and electrode gaps (Figure 44, 45 and 46) it is clear that the electrode gap does not affect current density as much as electrolytic flow velocity appears to. This effect is greatest at high applied potentials and least at low potentials, which would allow for reduced pump energy requirements at low applied potentials. Extracting the data for a single flow velocity, i.e. 0.15 m.s^{-1} from Figure 46, the diminished effect that the electrode gap has on current density at low applied potentials is clear.

From Figure 45 it is clear that electrodes operating under a large current density (3000 mA.cm^{-2}) and low fluid velocity (0.075 m.s^{-1}), will favour a larger electrode gap due to the presence of a thicker gas meniscus. Electrodes, however, operating within the same current density range, but under an enhanced flow velocity (0.15 m.s^{-1}), will favour a smaller electrode gap. For smaller current densities at lower cell potentials (< 2.5 VDC), the results indicate that fluid velocity has little benefit in improving performance, and the electrode gap will dictate the resulting performance. This is due to sufficient electrolytic fluid velocity that removes product gas from the electrode surface preventing any substantial build-up of a gas meniscus.

A small band of fluid velocity exists and caused by a sudden change between the conditions void fracture and of separated gas meniscuses at high current densities. The degree of improvement in current density is dictated by Equation (19) and has shown to increase for increasing fluid velocities (Figure 45 and 46). Only a limited improvement in current density is observed with increasing fluid velocity from 0.075 $m.s^{-1}$ to 0.15 $m.s^{-1}$, which means that operating at fluid velocities beyond 0.15 m.s-1 will create unrealistic high liquid throughputs that will require considerable pumping work. Ultimately, an optimisation problem will present itself between the overall system efficiency and stack efficiency, identifying the optimal fluid velocity for minimising power demand of both the stack and of the system pump. Results recommend a minimum required operating velocity of 0.075 $m.s^{-1}$ in order to maintain stable operation and high gas separation efficiency.

The temperature increase from 50°C to 70°C would result in a difference in solution viscosity which would have an influence on the rate at which product bubbles are removed from the mesh electrode surface. An obvious benefit of operating at increased temperatures is the positive effect on the thermodynamics resulting in a reduction of the equilibrium voltage (Allebrod et al., 2012). However, at increased temperatures the gas bubble size is increased, which reduces the rising velocity for standard plate electrolysers (Mazloomi and Sulaiman, 2012). For the Hydrox Holding Electrolyser, which portrays operation similarities to standard plate electrolysers, the disengagement rate and nature of the bubbles emanating from the electrode surface is dependent on the electrolytic flow velocity and the viscosity of the solution, which is also dependent on both the concentration and temperature of the electrolytic solution (Mandin et al., 2008). The difference in performance illustrated between Figure 44 and Figure 46 for a flow velocity of 0.15$m.s^{-1}$ shows in the generated current density between the two temperatures with the greatest influence accounted for by the change of the electrode gap. Larger electrodes gaps are favoured at lower temperatures due to the effect of viscosity on the bubble evolution rate and indirectly on the diameter.

Current density, therefore, has the greatest bearing on the electrode gap as higher current densities result in higher gas evolution rates, which in turn will cause the gaseous meniscus on the surface of the electrodes to increase in thickness. If the electrode gap is too narrow, a breakdown in performance and stability is observed due to void fracture (Nagai et al., 2003b).

By increasing the flow velocity, an increase in the disengagement rate of the product gas from the electrode surface is observed (Mazloomi et al., 2012), and the gas meniscus formed

on the material surface is reduced in thickness (within the gap) reducing the probability of void fracture whereby potential cross gas contamination and a loss of active area can take place (Mazloomi et al., 2012).

4.5. The Effect of Increasing the Effective Area for Reaction

As noted by Mazloomi and Sulaiman (2012), increasing the geometric area by means of pitting, chemical roughening or physical roughening of an electrode surface, an increase in current can be achieved at a fixed voltage. Appleby et al., (1978) demonstrates gas diffusion electrodes for enhancing the geometric area for chemical reaction. Since the HH technology utilises mesh electrodes, the concept was investigated by increasing the layers of mesh in order to increase the geometric area of the electrode. As results have proven optimal at a flow velocity of 0.15 $m.s^{-1}$ and more reliable with the HH test rig at 70°C, an investigation was performed in doubling and tripling the mesh layers in order to determine the percentage improvement in cell performance.

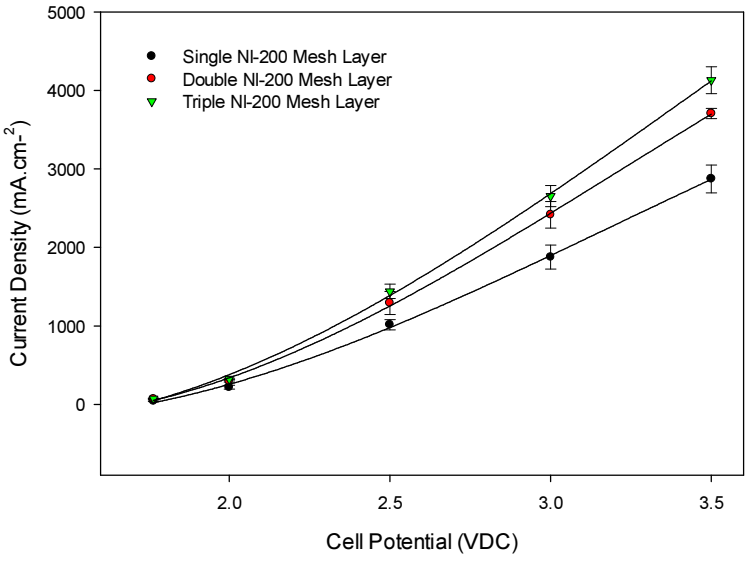

Figure 47: Polarisation curves of the test rig stack as a function of electrode geometric area for pure nickel electrodes at a temperature of 70 °C, 30wt% potassium hydroxide and a flow velocity of 0.15 m.s-1

The

greater the effective electrode area, the greater the number of active sites available for gas evolution. It is important to note however that the thicker the electrode, the further the rear of the electrode becomes from the opposing polarity electrode surface and hence the lower the activity within these areas. Figure 47 illustrates that a maximum electrode thickness exists for which the last layers of the electrodes contribute very little to the total gas production. It is noted that by doubling the geometric electrode area, a justifiable improvement in cell performance is obtained, however adding an additional layer has no significant additional improvement. Appleby et al., (1978) notes that pore blockage in gas diffusion electrodes is one of the major contributors to the non-utilisation of layers further away from the opposing faces.

4.6. Gas Purity Analysis

Analysis of hydrogen obtained at an operating current density of 3500 $mA.cm^{-2}$, an electrode gap of 2.5 mm, and an electrolytic temperature of 30 °C, revealed high purity (Table 12). This analysis was conducted at a lower temperature due to the presence of excessive caustic vapours in the product gas that could potentially damage sensitive analytical equipment. It is clear that gas purity is a function of the electrolytic flow velocity when considering the Hydrox Holdings Ltd. AWE technology, and it decreases with decreasing flow velocity that is directly linked to gas meniscus build-up between the electrodes ultimately resulting in void fraction and cross gas contamination. At an average flow velocity of 0.1 $m.s^{-1}$ across the electrode surface a hydrogen gas purity of 99.8 vol% is obtained, which is comparable to current industry standards that incorporate gas purification equipment (Zeng and Zhang, 2012). Furthermore, no carbon footprint was recorded, which could render the need for additional purification systems obsolete compared to other existing membrane technologies. The absence of carbon components provides compatibility of this alkaline water technology with fuel cells.

Table 12: Gas purity of hydrogen and oxygen as a function of electrolytic fluid velocity over the electrode face.

Electrolytic Flow Velocity ($m.s^{-1}$)	Hydrogen Purity (vol %)	Oxygen Purity (vol %)
0.200	99.8	98.8
0.100	99.8	96.7
0.075	99.0	97.6

During experimental testing, a sudden reduction in pressure for the oxygen liquid-gas separator was incurred which accounts for the divergence of generalised behaviour for the oxygen gas purity in Table 12.

4.7. Medium Term Stability

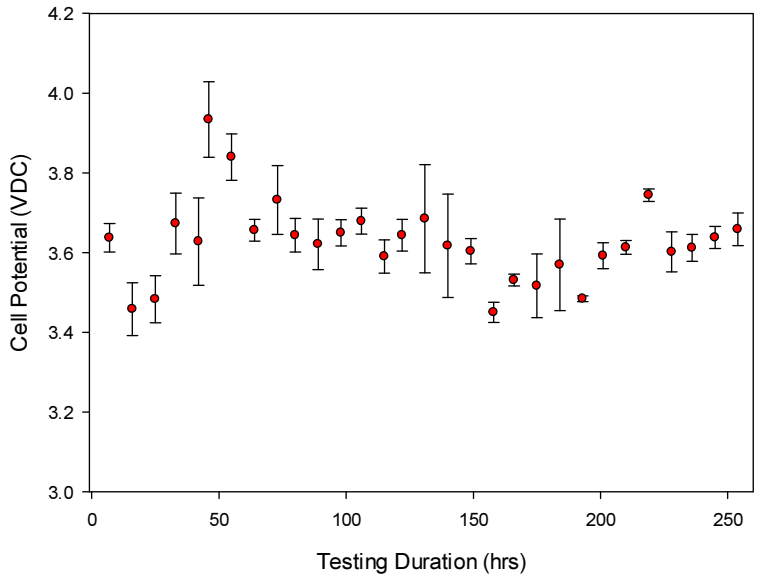

Figure 48: Stability curve for cell potential as a function of testing duration for pure nickel electrodes at a flow rate of $0.075 m.s^{-1}$, an electrode gap of 2.5mm, 60°C and 30 wt% potassium hydroxide

Jensen et al., (2008) notes a number of catalyst combinations capable of maximising performance of electrolysers, however little is reported with respect to long term electrode stability or electrode efficiency drop. All tests range within the region of 100 to 400 hours of continuous operation. Typically, the electrode efficiency drop is measured by subjecting the electrolyser either to a constant current density and noting the cell potential increase with time, or selecting a constant voltage and noting the drop of current density with time. This drop in the catalytic effectiveness of the electrode can caused by numerous phenomena, two of which have been found to be most prominent in this investigation and they are the physical corrosion of the electrode surface resulting in a loss of effective reactive electrode area as well as the poisoning of the electrode surface by depositing a material of lower catalytic activity onto the original catalyst.

Pure nickel electrodes were selected to perform a medium term stability test as nickel proved to be the most stable material in an alkaline environment to a reasonable degree of resistance to contaminants within the system. With reference to Figure 48 (above), it is clear that after a time duration of little over 250 hours, the end voltage result is similar to initial voltages measured at the start of the test. The fluctuation between the lowest and the highest cell potential is ~400mV. The overpotential increase of the final and initial values amounted to be ~20mV, which in essence concludes that nickel within an alkaline environment displays high stability, and has the potential to be used as an effective electrolyser catalyst for an alkaline membraneless system as has successfully been demonstrated in conventional alkaline systems (Mazloomi and Sulaiman, 2012).

4.8. Stack Efficiency, Specific Energy Consumption and Technology Comparison

In employing the optimal set of results for (i) the maximum flow velocity of 0.15 $m.s^{-1}$ with the associated minimum electrode gap of 1 mm using pure nickel electrodes, (ii) the minimum flow velocity of 0.075 $m.s^{-1}$ in addition with the associated maximum electrode gap of 2.5 mm again using pure nickel electrodes, and (iii) the minimum flow velocity of 0.075 $m.s^{-1}$ with the associated maximum electrode gap of 2.5 mm using MMO anodes, the

generated current densities are plotted as a function of the higher heating value efficiency of hydrogen **(**Figure 49**)**. The theoretical (Equation (25)) and actual (Equation (26)) revealed higher heating value efficiencies were determined using the equations (adapted from Zhang et al., (2010)):

$$\eta_{theoretical}=\frac{n_{H_2,out,theoretical\ HHV}}{E} \ldots\ldots\ldots (25)$$

$$\eta_{actual}=\frac{n_{H_2,out,actual\ HHV}}{E} \ldots\ldots\ldots (26)$$

Where nH_2, is the measured volumetric flow rate of hydrogen in Nm^3/hr deduced from theoretical and actual volumetric flow rates; *HHV* is the higher heating value of hydrogen that equals 3.54 kWh/Nm^3 (Zeng and Zhang, 2010) and E is the total electrical energy input into the electrolyser alone in kW.

From Figure 49 it is clear that below 2.2 VDC, Ir-RuO_2 anodes and Pt cathodes produced the highest current densities, while pure nickel anodes and cathodes produced the highest current densities in excess of 2.2 VDC. Current alkaline electrolysers run typically at ~2.0 VDC and the typical operating current densities range between 200 mA.cm^{-2} and 500 mA.cm^{-2} (Millet and Grigoriev, 2013). Employing Ir-RuO_2 anodic and Pt cathodic electrodes **(**Figure 49**)** the HH technology delivers a maximum recorded current density of 220 mA.cm^{-2} (at 1.8 VDC) and 474.40 mA.cm^{-2} (at 2.0 VDC) at a flow velocity of 0.075 m.s^{-1}, a temperature of 70°C and an electrode gap of 2.5 mm. At these similar operating conditions, employing pure nickel electrodes, current densities of 51.9mA.cm^{-2} (at 1.8 VDC) and 242.9 mA.cm^{-2} (at 2 VDC) shows that at the lower voltage range, PGM catalysts outperform the simplistic nickel electrodes.

A fundamental difference for the membraneless technology is prevalent for the higher potential range reference to Figure 49. Even though operation is more inefficient at higher potentials, higher current densities are achieved which implies that a significantly smaller volume electrolyser can be utilised for a set hydrogen production output. Use of a smaller volume electrolyser constructed out of readily available materials leads to a substantial reduction in capital costs which has positive repercussions for the end selling price of hydrogen if the hydrogen was produced from a renewable source of energy.

With reference to the lower potential range for the HH electrolyser, it can be noted that the technology produces current densities comparable to that of current alkaline electrolysers. It is furthermore expected that a significant additional increase in performance can be obtained that will likely exceed 500 mA.cm^{-2} at 2.0 VDC, by using improved catalysts that are specifically selective to the hydrogen evolution and oxygen evolution reactions along with increasing the temperature of the electrolytic solution (Miles, 1975).

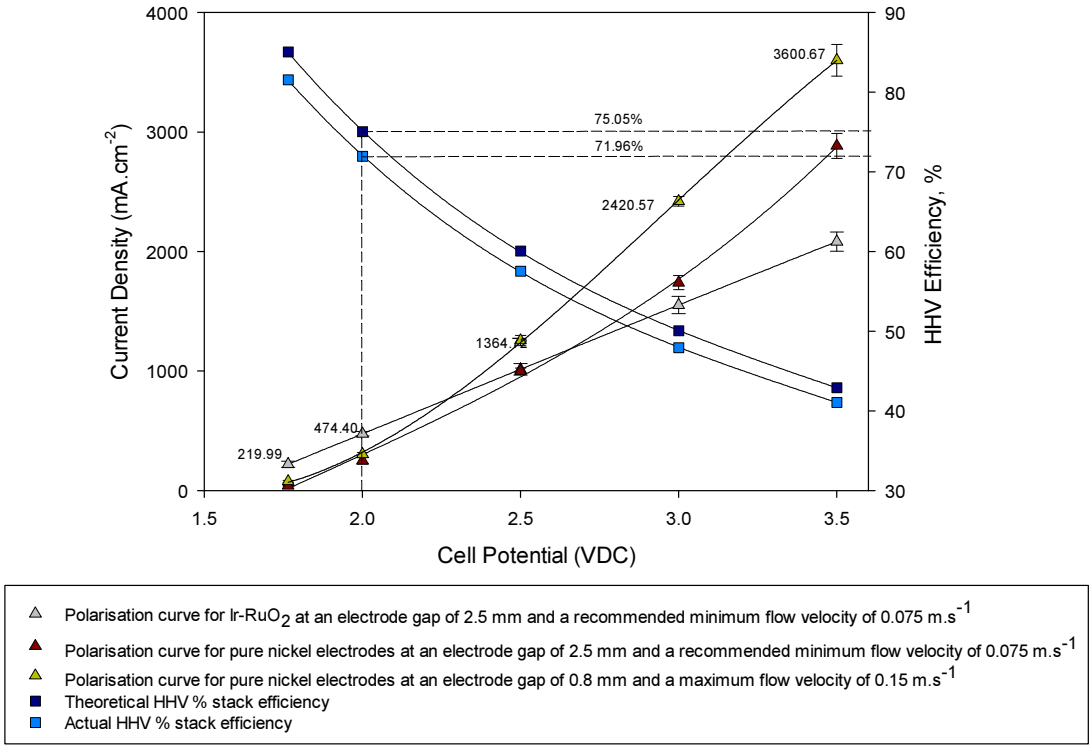

Figure 49: Optimal polarisation curves for (i) the minimum electrolytic flow velocity of 0.075 m.s-1 at an electrode gap of 2.5 mm (For PGM catalysts and Ni Catalysts), and (ii) the highest demonstrated flow velocity of 0.2 m.s-1 at an electrode gap of 0.8 mm (for Ni catalyst only), as a function of theoretical and actual HHV stack efficiency at 70 °C and 30 wt% KOH

In a comparison of the voltage-current and power consumption relationship of the Hydrox Holdings Ltd. AWE electrolyser to that of the main water electrolysis technologies (Figure 50), it is evident that conventional alkaline and high temperature solid oxide electrolysers have nominal operating current density thresholds of approximately 500 mA.cm^{-2}, while

PEM technology has a typical nominal operating upper limit of approximately 1200 mA.cm^{-2} (Millet and Grigoriev, 2013). In contrast, the Hydrox Holdings Ltd. AWE technology displayed stable performance (with the use of pure nickel electrodes) at current densities easily exceeding 1500 mA.cm^{-2}. The HH technology is therefore capable of similar performance trends as that of conventional alkaline water electrolysis technologies, but the different in being capable of exceeding current density thresholds of even PEM electrolyser systems. As previously discussed, the membraneless technology therefore demonstrates potential for greatly reducing the required scale of equipment required for high hydrogen gas outputs at the expense of efficiency, which with additional development of a non-PGM catalyst, could be improved to become competitive with exiting PEM electrolysers.

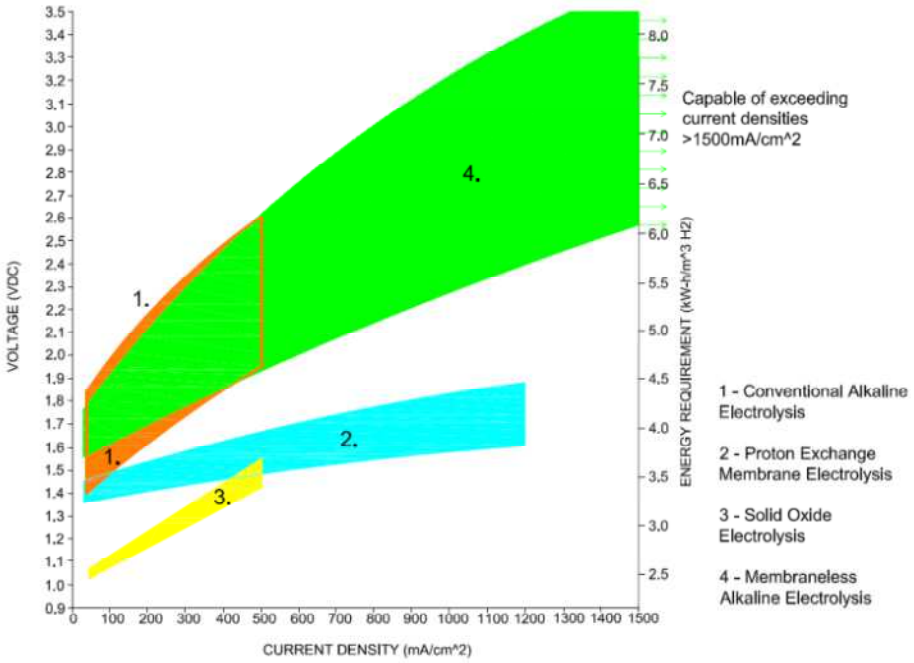

Figure 50: Polarisation curves and specific energy consumption of main water electrolysis technologies: (1) industrial alkaline electrolysers (70 – 95 °C), (2) solid polymer electrolysers (90 – 110 °C), (3) high temperature solid oxide electrolysers (900 °C), (4) current polarisation region for the Hydrox Holdings AWE technology for the temperature range of 50-80°C

5. CONCLUSIONS

5.1. Future Work

- The Hydrox Holdings Ltd. electrolyser, being predominantly manufactured out of polypropylene plastic, does therefore allow for pressurised operation. Future work will therefore include the effect of pressurised operation.
- The longevity of electro-catalytic materials needs to be investigated. As noted, some catalysts have the potential to produce high current densities at high efficiencies; however no indication has been made as to the operational stability of these catalysts.
- The medium temperature range needs to be investigated, however material compatibility at the higher temperature range > 100°C will need to be considered before performing electrolysis at these elevated temperatures.
- A solid grounding for the minimum attainable flow velocity can be re-investigated by the use of larger electrodes and thorough gas purity investigations.
- Pressurised operation of the membraneless technology can be considered in an attempt to note whether pressurised operation is possible coupled with low pressure storage methods.

5.2. Conclusions to Research

An investigation into the variation of conditions of performance influencing variables has revealed a number of optimal operational conditions for water electrolysis generators. Typically, operation at elevated temperatures is ideal in order to greatly improve the electrical efficiency of water electrolysers. Catalytic materials that are both cost effective and which provide a surface morphology characterised by a large number of active sites is vital in order

to maximise the hydrogen output per cross sectional unit surface area. Electrodes are desirably placed as close together as possible, but not at the expense of incurring void fracture and cross gas contamination. Utilising methods capable of increasing the rate of bubble removal from not only the electrode surface, but between the electrodes themselves is ideal for limiting the magnitude of induced ohmic resistance. Based on the materials of construction, the optimally deduced electrolytic concentration has been determined to be in the region of 30 wt% potassium hydroxide. All of the above optimal variable ranges have been found to agree well with literature findings.

Alkaline water electrolysis technology in general is highly promising due to the numerous advantages over PEM and solid oxide water electrolysis technologies. These advantages include (i) cost effective materials for construction, (ii) simplified overall design that result in a reduction of capital cost and lower maintenance, and (iii) durable and robust technology capable of a superior life of plant compared to other technologies. However the optimisation of performance influencing parameters for alkaline water electrolysis technologies can be universally applied to both solid oxide and proton exchange membrane technologies. Smaller electrode gaps, and cost effective superior electrolytic materials will prove key in improving the operating thresholds of alkaline water technologies.

Parameters that were investigated using the membraneless pilot plant included: a range of electrolytic temperatures, concentrations, flow velocities, various types of electro-catalytic materials, a range of electrode gap dimensions and gas purity analysis using Gas Chromatography methods (GC). An optimal electrolytic solution flow velocity range was identified to be in the order of 0.075-0.1m.s^{-1}, which resulted in an optimal gap of ~2.5mm and a resulting gas purity of >99 vol%. Operating at higher flow velocities (> 0.1-0.2 m.s^{-1}) allows for the use of a smaller electrode gap of ~0.8mm.

Employing Ir-RuO_2 and Pt for the anodic and cathodic electrodes respectively, current densities of 220 mA.cm^{-2} (at 1.765 VDC) and 474 mA.cm^{-2} (at 2 VDC) were verified at an electrode gap of 2.5 mm, temperature of 70°C and a minimum recommended flow velocity of 0.075 m.s^{-1}. At the same experimental conditions, using pure nickel for the anode and cathode electrodes yielded current densities of 51.9 mA.cm^{-2} (at 1.8VDC) and 242.9mA.cm^{-2} (at 2 VDC) at an electrode gap of 2.5mm, temperature of 70°C and a flow velocity of 0.075m.s^{-1}.

The Hydrox Holdings Ltd. Membraneless technology, demonstrates comparable performance to existing alkaline technologies, however the greatest potential for the membraneless technology is believed to be in high hydrogen production output rates at elevated potentials by using renewable energy for the purpose of reducing the cost to produce hydrogen.

The aim for all electrolysers is to achieve a simplified construction, the optional use of non-precious metal catalysts for electrode cost reduction, the capability of operating at high current densities and a membrane that is robust and capable of long term operation which will lead to the development of a cost-effective compact alkaline electrolyser that would have an enormous potential.

REFERENCES

Allebrod F., Chatzichristodoulou C., Mollerup P.L., Mogensen M.B. (2012) Electrical conductivity measurements of aqueous and immobilized potassium hydroxide, *International Journal of Hydrogen Energy*, vol 37, pp. 16505 – 16514

Appleby A.J., Crepy G., Jacquelin J. (1978) High efficiency water electrolysis in alkaline solution, *International Journal of Hydrogen Energy*, vol 3, pp. 21-37

Berry G.D. (2004) Hydrogen production. In: Encyclopaedia of energy, vol 3. San Diego (CA): Elsevier-Academic Press, pp. 259-63

de Maubeuge H.L. (2011), Influence of geometric variables on the current distribution uniformity at the edge of parallel plate electrodes, *Electrochimica Acta*, vol 56, pp. 10603-11

Dieguez P.M., Ursue A., Sanchis P., Sopena C., Guelbenzu E., Gandia L.M. (2008) Thermal performance of a commercial alkaline water electrolyser: Experimental study and mathematical modelling, *International Journal of Hydrogen Energy*, vol 33, pp. 7338-54

Doherty T., Sunderland J.G., Roberts E.P.L., Pickett D.J. (1996) An improved model of potential and current distribution within flow-through porous electrode, *Electrochimica Acta*, vol 41, pp. 519-26

Eunnyeong H., Kim J., Cho S. (2012) Selecting hydrogen producing methods using fuzzy analytic hierarchy process with opportunities, costs and risks, *International Journal of Hydrogen Energy*, vol 37, pp. 17655-62

Fragkou V., Ge Y., Steiner G., Freeman D., Bartetzko N., Turner A. (2012) Determination of the real surface area of a screen-printed electrode by chronocoulometry, *International Journal of Electrochemical Science*, vol 7, pp. 6214-20

Ganley G.C. (2009) High temperature and pressure alkaline electrolysis, *International Journal of Hydrogen Energy*, vol 34, pp. 3604-11

Glatt E., Rief S., Wiegmann A., Knefel M., Wegenke E. (2009) Structure and pressure drop of real and virtual metal wire meshes, Berichte des Fraunhofer ITWM Nr. 157

Ivy J. (2004) Summary of electrolytic hydrogen production, Milestone Completion Report, National Renewable Energy Laboratory, NREL/MP-560-36734

Jarzabek G., Borkowska Z. (1997) On the real surface area of solid electrodes, *Electrochimica Acta*, vol 19, pp. 2915-2918

Jensen J.O., Bandur V., Bjerrum N.J., Jensen S.H., Ebbesen S., Mogensen M., Tophoj N., Yde L. (2008) Pre-investigation of water electrolysis, Joint Study Report, Technical University of Denmark and DONG Energy, PSO-F&U 2006-1-6287

Kjartansdottir C.K., Nielsen L.P., Moller P. (2013) Development of durable and efficient electrodes for large-scale alkaline water electrolysis, *International Journal of Hydrogen Energy*, vol 38, pp. 8221 – 8231

Lee J., Jeong B., Ocon J.D. (2013) Oxygen electrocatalysis in chemical energy conversion and storage technologies, *Current Applied Physics,* vol 13, pp. 309-321

Lumanauw D. (2000) Hydrogen bubble characterisation in alkaline water electrolysis, master's thesis, University of Toronto, Publication No. 0-612-54129-0

Man I.V., Su H., Calle-Vallejo F., Hansen H.A., Martinez J.I., Inoglu N.G., Kitchin J., Jaramillo T.F., Norskov J.K., Rossmeisl J. (2011) Universality in Oxygen Evolution Electro catalysis on Oxide Surfaces, *Chemcatchem*, vol 3, pp. 1159-65

Manabe A., Kashiwase M., Hashimoto T., Hayashida T., Kato A., Hirao K., Shimomura I., Nagashima I. (2012) Basic Study of Alkaline Water Electrolysis, *Electrochimica Acta*, vol 100, pp. 249-256

Mandin P., Aissa A.A., Roustan H., Hamburger J., Picard G. (2008) Tow phase electrolysis process: from the bubble to the electrochemical cell properties. *Chemical Engineering and Processing: Process Intensification*, vol 10, pp. 1926-32

Marini S., Salvi P., Nelli P., Pesenti R., Villa M., Berrettoni M., Zangari G., Kiros Y. (2012) Advanced alkaline water electrolysis, *Electrochimica Acta*, vol 82, pp. 384 – 391

Mazloomi K., Sulaiman N.B., Moayedi H. (2012) Electrical efficiency of electrolytic hydrogen production, *International Journal of Electrochemical Science*, vol 7, pp. 3314 – 3326

Mazloomi S.K., Sulaiman N. (2012) Influencing factors of water electrolysis electrical efficiency, Renewable and Sustainable Energy Reviews, vol 16, pp. 4257-63

Miles M.H. (1975) Evaluation of electro catalysts for water electrolysis in alkaline solutions, *Electro analytical and interfacial electrochemistry*, vol 60, pp. 89 – 96

Millet P., Grigoriev S. (2013) Water electrolysis technologies, *Renewable hydrogen technologies*, vol 2, pp. 19 – 40

Monsouri K, Ibrik K., Bensalah N., Abdel-wahab A. (2011) Anodic dissolution of pure aluminium during the electro coagulation process: influence of supporting electrolyte, initial pH and current density, *Industrial and Engineering Chemistry Research*, vol 50, pp. 13362-72

Mueller-Langer F., Tzimas E., Kaltschmitt M., Peteves S. (2007) Techno-economic assessment of hydrogen production of hydrogen production processes for the hydrogen economy for the short and medium term, *International Journal of Hydrogen Energy*, vol 32, pp. 3797-810

Muzhong S., Bennett B., Ding Y., Scott K. (2011) A concise model for evaluating water electrolysis, *International Journal of Hydrogen Energy*, vol 36, pp. 14335-41

Nagai N., Takeuchi M., Kimura T., Oka T. (2003) Existence of optimum space between electrodes on hydrogen production by water electrolysis, *International Journal of Hydrogen Energy*, vol 28, pp. 35 – 41

Nagai N., Takeuchi M., Nakao M. (2003) Influence of bubbles between electrodes onto efficiency of alkaline water electrolysis, proceedings of PSFVIP-4, F4008, Chamonix, France

Peters C.A. (2001) Statistics for Analysis of Experimental Data, Environmental engineering processes laboratory manual, Princeton university, NJ 08544

Pletcher D., Li X. (2011) Prospects for alkaline zero gap water electrolysers for hydrogen production, *International Journal of Hydrogen Energy*, vol 30, pp. 1 – 16

Salvi P., Nelli P., Villa M., Kiros Y., Zangari G., Bruni G., Marini A., Milanese C. (2011) Hydrogen evolution reaction in PTFE bonded Raney-Ni electrodes, *International Journal of Hydrogen Energy*, vol 36, pp. 7816-21

Schulenburg H., Durst J., Muller E., Wokaun A., Scherer G.G. (2010) Real surface area measurement of Pt3Co/C catalysts, *Journal of Electro analytical Chemistry*, vol 642, pp. 52-60

Sinnot R.K. (1999), Coulson and Richardson's Chemical Engineering, 3rd Edition, Bulington, Butterworth-Heinemann, 398-492

Skogestad S. (2009), Chemical and Energy Process Engineering, 1st Edition, Florida, CRC Press, 237-250

Sogaard M., Odgaard M., Skou E.M. (2001) An improved method for the determination of the electrochemical active area of porous composite platinum electrodes, *Solid State Ionics*, vol145, pp. 31-35

Ragunathan P., Mitra S.K., Nayar M.G. (1981) Porous nickel electrodes in water electrolysis 1. Electrode preparation and polarization studies in strong alkali, *International Journal of Hydrogen Energy*, vol 6, pp. 487-96

Rosa V.M., Santos M.B.F., da Silva E.P. (1995) New materials for water electrolysis diaphragms, *International Journal of Hydrogen Energy*, vol 20, pp. 697-700

Wang B. (2005) Recent development of non-platinum catalysts for oxygen reduction reaction*, Journal of Power Sources*, vol 152, pp. 1-15

Wang M., Wang Z., Gong X., Guo Z. (2014) The intensification technologies to water electrolysis for hydrogen production, *Renewable and Sustainable Energy Reviews*, vol 29, pp. 573-88

Wendt H. (1990) Electrochemical hydrogen technologies: Electrochemical production and combustion of hydrogen, Elsevier, Amsterdam, The Netherlands

Yde L., Kjartansdottir C.K., Allebrod F., Mogensen M.B., Moller P., Hilbert L.R., Nielsen P.T., Mathiesen T., Jensen J., Andersen L., Dierking A. (2013) 2nd generation alkaline electrolysis, Final Report, EUDP 63011-0200

Zeng K., Zhang D. (2014) Evaluation the effect of surface modification of Ni based electrodes for alkaline water electrolysis, *Fuel*, vol 116, pp. 692-98

Zeng K., Zhang D. (2010) Recent progress in alkaline water electrolysis for hydrogen production and applications, *Progress in Energy and Combustion Science*, vol 36, pp. 307 – 326

Zhang H., Lin G., Chen J. (2010) Evaluation and calculation on the efficiency of a water electrolysis system for hydrogen production, *International Journal of Hydrogen Energy,* vol 35, pp. 10851 – 10858

Y. Zhao Y., C. Ou C., J. Chen J. (2008) A new analytical approach to model and evaluate the performance of a class of irreversible fuel cells, *International Journal of Hydrogen Energy,* vol 33, pp. 4161-70

APPENDIX A - ACTIVITY COMPARISON OF MESH ELECTRODES VERSUS PLATE ELECTRODES

Introduction

A simplified experimental apparatus was constructed with the purpose of relating the activity of stainless steel 316 plate electrodes to that of stainless steel 316 mesh electrodes. It was expected that if that the current densities are normalised with respect to the geometric area, the current densities for the chosen voltage range should be approximately the same for both the mesh and the plate. This is expected since all experimental parameters are similar except for the geometry of each electrode. In a prior experiment, it was found that the solid plate electrode demonstrated a higher current density for the entire tested potential range when contrasted to the mesh electrode pair. It was concluded that the cause for the lower current density for the mesh electrodes was solely due to the influence of product gas bubbles becoming trapped in the structure of the mesh. It was therefore decided to perform an accurate test that would mimic a flowing system to verify whether these findings are grounded.

Experimental Set-up

The original set-up was concluded to be unreliable due to the small size and the excessive heat given off by the reaction which presented increasing current densities over time. It was therefore decided to produce a new set-up through the capability of simulating flow with the use of a mechanical agitator and an ability to regulate temperature by submergence of the system in a water bath to keep the temperature constant.



Figure A1: Prior Simplified Experimental Set-up



Figure A2: Experimental set-up with mechanical agitator for activity determination investigation



Figure A3: Agitation system in motion moving fluid over the porous mesh electrodes



Figure A4: Experimental system in correct configuration for activity determination investigation

The agitation system was not only observed to move solution past the electrodes, but simultaneously also through the mesh electrode. The rate of agitation was vigorous, ensuring the best possible scenario for rapid removal of gas bubbles from the mesh electrode. Most of the electrode remained submerged in the electrolytic solution, the section that remained exposed served as the connector point for the electrical clips. This area of the exposed electrode and the area covered by the ceramic spacers were accounted for when geometric area was calculated. The following is data referring to the physical dimensions of each electrode:

Table A1: Physical Parameters of mesh and plate electrodes for activity determination investigation

Mesh Electrode		
Parameter	Unit	Value
Electrode Gap	mm	11
Electrode Length	mm	61
Electrode Width	mm	48
Electrode Thickness	mm	0.855
Submerged Region	mm	42
Plate Electrode		
Parameter	Unit	Value

Electrode Gap	mm	11
Electrode Length	mm	60.5
Electrode Width	mm	47.5
Electrode Thickness	mm	1
Submerged Region	mm	42

The plate electrodes were re-polished with 1200 grit water paper to ensure that the surface is potentially featureless since impurities may contribute to inconsistencies in experimental results.

Results

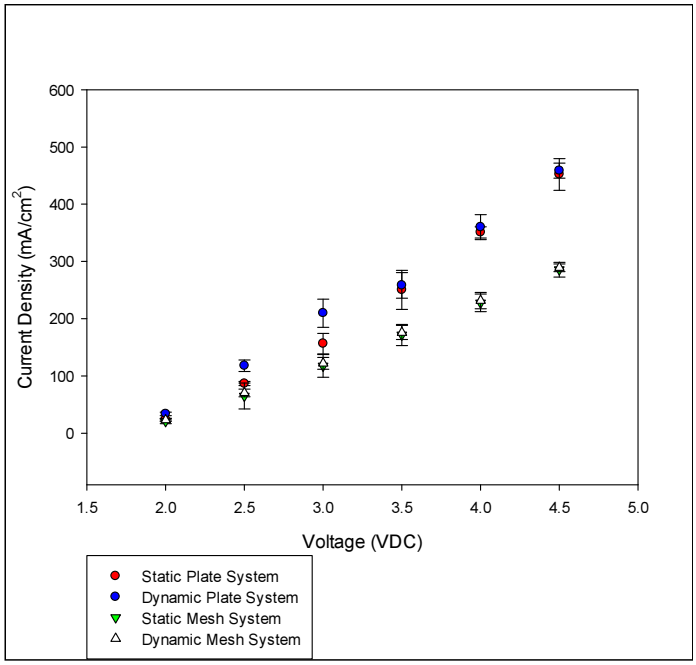

Figure A5: Current density versus cell potential for various tested systems for the determination for activity rations between mesh and plate electrodes in static and dynamic systems

It was again apparent that the mesh system for both the static and dynamic systems demonstrated activities that were lower than the plate system. The effect was less evident at lower potentials; however an increase in current density increased the difference between the current densities evolved by the mesh and plate. As expected, an increase in current density was seen at set potential with agitation of the electrolyte for both the plate and mesh systems.

The increase however was not significant enough to result in a dynamic mesh system superseding the current densities produced by the static plate system as hypothesised.

Table A2: Dynamic versus static ratios for various tested systems

Comparison Factors (Static Mesh Vs. Dynamic Mesh)	
Voltage (VDC)	Ratio (Dynamic/Static)
2	**1.1128**
2.5	**1.0819**
3	**1.0373**
3.5	**1.0247**
4	**1.0185**
4.5	**1.0119**

Comparison Factors (Static Plate Vs. Dynamic Plate)	
Voltage (VDC)	Ratio (Dynamic/Static)
2	**1.426**
2.5	**1.360**
3	**1.339**
3.5	**1.030**
4	**1.026**
4.5	**1.014**

Comparison Factors (Static Plate Vs. Dynamic Mesh)	
Voltage (VDC)	Ratio (Dynamic/Static)
2	**1.005**
2.5	**0.813**
3	**0.824**
3.5	**0.749**
4	**0.667**
4.5	**0.657**

It is noted that the dependence of current density is less pronounced for a mesh system whether static or dynamic. A plate system has a greater dependency at lower potentials. However, inevitably the difference is superficial at higher potentials. A comparison of a static plate system to a dynamic mesh system reveals that at low voltages, little difference is seen. However at high potentials, a decrease in current density is noticed for the dynamic mesh system in contrast to the static plate system. Agitation is therefore not adequately beneficial enough to provide the required increase in current density to allow a dynamic mesh system to perform better than a static plate system. Therefore the static plate system demonstrates superior activity compared to the dynamic mesh system for the tested potential range despite the larger available surface area of the mesh.

APPENDIX B - DESIGN CONSIDERATIONS OF THE APPARATUS COMPRISING THE HYDROX HOLDINGS LTD. ELECTROLYSER TECH RIG

B.1. Electrolyser Apparatus

Introduction

The basis for design of the electrolyser was accomplished by reference to an existing Hydrox Holdings Ltd membraneless concept test rig. Through the detailed examination of the electrolyser design and function, it was noted how the original design could be improved to provide superior electrolyser flexibility for comprehensive experimental testing. The following lists the additional design considerations:-

- Larger electrode surface areas for conclusive testing ensuring that error is minimised through a representative electrode test size. This can be achieved by either increasing the electrode surface area, or increasing the number of pole pairs.
- Larger threaded nipples to ensure that electrodes can be added of any size and a mechanism for adjusting the electrode gap was allowed for.
- Sufficient spacing between the pole pairs along with a sufficiently large vessel to accommodate larger electrodes when desired.
- The introduction of electrolyte into the electrolyser through a single port below a flow distribution plate for uniform pressure distribution within the unit.
- A simple electrode exchange mechanism through efficient disconnection and reconnection of electrodes to the electrolyser shell.
- Stainless steel and polypropylene design for high resistance to hot caustic conditions within the electrolyser for reduced electrolyte contamination.

- The development of a modular design to investigate the feasibility of a modular principle through the application of the current electrolyser design.
- The insertion of a bleeding port and valve to remove excess gas from the electrolyser to eliminate any possible re-entrainment of air via the electrode assembly.
- The sloping of the electrolyser for complete electrode discharging and gas bleeding.
- The positioning of discharge piping above the operating level of liquid within the electrolyser to maintain complete liquid volume within the electrolyser and in addition, provide a mechanism to expel trapped gas.
- The independent operation of electrode pole pairs through isolated electrical and flow connections.
- A strong structural design of the electrolyser to ensure that the vessel does not warp under pressure during normal operation and if the electrodes become clogged.
- Observation ports at low temperature conditions to note behaviour within the electrolyser unit itself.

By re-designing the existing electrolyser to incorporate all of the above mentioned considerations, an electrolyser with superior flexibilities for thorough experimental investigation was constructed. The following flexibilities characterise the electrolyser reactor specifications for the test rig used for this investigation:-

- The fine adjustment of the electrolyser gap for gaps between 0.5 – 10 mm
- Improved distribution of electrolytic fluid throughout the length of the electrolyser.
- Re-enforcement and tensioning of electrode mesh to handle higher flow rates and larger electrode sizes without warping due to high flow rates.
- The simple removal and addition of electrodes by threaded connections and detachable electrical connections.
- The attachment of the electrode discharges onto the discharge manifold through threaded couplings to maintain the set electrode gap.

- The fine adjustment of the electrode gap for the specified electrode sizes with the use of high tolerance aligned electrodes with the use of tapered lock nuts to ensure that electrode position is securely fastened.

Brief sizing method of the electrolyser

The relative sizing of the electrolyser is generally dependant on the flow dynamics present within the unit to maintain a uniform pressure drop across the mesh electrodes. This is fundamental for equal hydrogen and oxygen generation across all available electrode surface areas. For the purposes of sizing the experimental test-rig to identify the optimal electrolytic reaction conditions, the sizing of the electrolyser is dependent on the power supply equipment constraints. The amperage rating on the equipment has a direct influence on the maximum allowable total area for the electrodes.

It was determined over a range of 0-150A what the maximum allowable electrode surface area is for the electrolyser. These values were used as a guideline for sizing the electrodes. Initially an ideal current density of 800 $mA.cm^{-2}$ would represent the design target for the new electrolyser test-rig. 800 $mA.cm^{-2}$ is selected on the basis that the test rig requires the ability to obtain higher than expected current densities when using a catalytic material. The estimated electrode sizes were calculated based on the required surface area necessary to obtain the ideal current density. It was then decided how many pole pairs were required to achieve the deduced electrode surface area:-

$$SA = \frac{I}{i} \dots\dots\dots (25)$$

Where,

SA - is the maximum allowable surface area for the electrodes (cm^2)

I - is the supplied maximum current to the system (A)

i - is the ideal exchange current density (A/cm^2)

B.2. Gas/Liquid Separation Apparatus

Introduction

After additional investigation, it was concluded that the baffle type horizontal separator was not effective enough to ensure complete liberation of heavy oxygen gas in the prescribed residence time. It was concluded that the separation mechanism was further crippled by pulling gas bubbles further into the electrolyte by using the baffled design. An existing separator constructed by Hydrox Holdings Ltd., made use of the concept of maximising effective surface area to create a thin film of liquid which accommodated effective product gas liberation. The choice of separator for the proposed experimental test-rig was therefore based on this concept and was modified to improve this separation mechanism. A number of advantages can be noted with this particular design:-

- Simple in construction, simple to modify for improved separation technique if additionally required by replacing or altering the packing.
- Type of separator does not require the substantial volume compared to the horizontal type separator.
- Small residence time required for the complete liberation of product gas.
- The use of small chemically resident balls results in low reagent flow rate, ensuring that gas is not forced back into the electrolyte. A large surface area ensures effective separation at high flow rates.
- Flexibility to process high and low flow rates of electrolytic solution.
- Design flexible to observe the separation process within the separator.
- Separators regulate their own liquid level through basic design considerations and additional regulatory methods such as gravity controlled discharge.
- Optional pressure functions for a pressurised system.

The following lists the disadvantages with the design:-

- Small residence time within the separator subject to the length and area of the separator may result in residual gas in the electrolyte. This may require the use of alternate packing or additional separation steps.
- A large volume of gas amongst the plastic balls for high contact to air may result in extensive heat loss.
- A single stage separation process may not be adequate enough for complete product gas removal. The separation efficiency is dependent on unit volume.

These separators are smaller in size compared to the original proposed horizontal gas/liquid separators. They are more simple and rugged in design for ease of flexibility if it is desired that the separation medium be altered. The dispersal of solution in the form of a thin film of electrolytic solution should ensure that the vast majority of solution be liberated when passed through the packed media.

Brief sizing method of the gas/liquid separators

The following assumptions are made on which to base the preliminary design of the vertical separators:-

- Maximum possible hydrogen and oxygen production rate for separation.
- Higher flow rates of electrolyte of 200L/min greater than what is predicted as adequate.
- The submersion of balls into the electrolytic solution to ensure that no product gas is entrained into the solution through turbulent action.
- Product bubble sizes within a bubble size range of 0.1mm to 0.05mm.
- The densities of product gases are reported at STP to account for higher temperature conditions.
- The densities and viscosities of the potassium hydroxide electrolyte are at STP at a concentration of 40%wt to account accurately for higher temperatures and lower concentration conditions.
- The column is sized according to the pressure drop equation as described by Ergun for a low pressure drop through the separator to ensure that frictionless

flow predominates so that less liquid is trapped within the voids of the packed beds.

- An area of wettability has been assumed to be 100% of the exposed area available. This characteristic should balance with the frictional effects of the solution moving through the packing.

In order to obtain the relative sizing of the separation units for oxygen and hydrogen, the method employed by Sinnot, (1999) for sizing packed columns, with respect to their pressure drop and solution velocity is used to provide a preliminary design concept for each separator. Two important concepts determine whether the design chosen is adequate:-

- The pressure drop through the packing of the packed column related to the velocity of the electrolyte.
- The film thickness formed on the plastic balls which determine how long it would take to liberate the product gas bubble.

The behaviour of fluid through the packing is dependent on the voidage between the spherical plastic balls. This has a strong dependence on whether liquid becomes entrained within the packing. In addition to the design of packed columns, the area of wettability is determined by the surface area exposed. This area can be related to the pressure drop within the packing by determining the specific surface area available:-

$$S = \frac{6}{d} \ldots\ldots\ldots (26)$$

Where:-

S = The specific surface (m^{-1})

d = The diameter of the spherical packing media (m)

Voidage is determined by examining the following table:-

Table B1: Voidage characteristics related to the diameter of the packing media taken from Sinnot (1999)

No.	Description	Specific surface area $S(m^2/m^3)$	Fractional voidage, e (−)	Permeability coefficient B (m^2)
	Spheres			
1	0.794 mm diam. ($\frac{1}{32}$ in.)	7600	0.393	6.2×10^{-10}
2	1.588 mm diam. ($\frac{1}{16}$ in.)	3759	0.405	2.8×10^{-9}
3	3.175 mm diam. ($\frac{1}{8}$ in.)	1895	0.393	9.4×10^{-9}
4	6.35 mm diam. ($\frac{1}{4}$ in.)	948	0.405	4.9×10^{-8}
5	7.94 mm diam. ($\frac{5}{16}$ in.)	756	0.416	9.4×10^{-8}

It is noted that the voidage between the particles is related to the diameter of the packing media. Based on the size of the relative spherical particles, a relationship can be developed on how the fluid flows between the packing media.

A model was chosen based on both streamline and turbulent flow through packing media. The following equation taken from Sinnot, 1999, relates the fluid flow rate and to the pressure drop :

$$\frac{R_1}{\rho {u_1}^2} = 5{Re_1}^{-1} + 0.4{Re_1}^{-0.1} \dots\dots\dots (27)$$

Where:

$$\frac{R_1}{\rho {u_1}^2} = \frac{-\Delta P e^3}{lS(1-e)\rho {u_c}^2} \dots\dots\dots (28)$$

$$Re_1 = \frac{u_c \rho}{S\mu(1-e)} \dots\dots\dots (29)$$

Where:-

ΔP = The pressure drop across the bed (N/m^2)

l = The thickness of the bed (m)

u_c = The average velocity of flow of fluid (m/s)

μ = Dynamic Viscosity (kg/m.s)

e = Voidage Fraction

u_l = Average velocity of fluid through the pore channels

ρ = Density of the fluid (kg/m^3)

The above equations can be substituted and simplified to the following expression:-

$$-\Delta P = \frac{5lS^2\mu u_c(1-e)^2}{e^3} + 0.4\left[\frac{u_c\rho}{S\mu(1-e)}\right]^{-0.1}\frac{lS(1-e)\rho {u_c}^2}{e^3} \ldots\ldots\ldots (30)$$

This equation can be solved in order to determine what the pressure would be for a packed column characterised by streamline or laminar flow. It is ideal for this result to be as small as possible for a low friction packed type column.

In addition, the film thickness can additionally be calculated to note the time taken for gas bubbles to move out of the liquid film relative to the time taken for the liquid to settle under gravity through the packed column. The following equation was used to determine the liquid film thickness:-

$$\delta_H = \left(\frac{3Q_L\mu}{\rho g}\right)^{\frac{1}{3}} \ldots\ldots\ldots (31)$$

Where:-

Q_L = Volumetric flow rate of electrolytic fluid

δ_H = The liquid film thickness

g = Acceleration due to gravity

The above equation provides an indication of the liquid film thickness on the surface of the spherical packing. Equation (8), as demonstrated in the procedure above, can then be used to determine the bubble rise velocity and in turn the time taken for a product gas bubble to escape from the electrolytic solution. This can be related to the time that the electrolytic solution spends within the separator.

B.3. Electrolytic Storage Sump

Introduction

The presence of a sump within the electrolyser test rig system serves the following functions:-

- As a buffer tank to maintain a uniform concentration throughout long term testing durations by compensating for concentration change through large volume.
- A means of access to the electrolyte to note temperature and concentration by means of temperature and concentration probes.
- Heating of the electrolytic solution just before it enters the electrolyser for accurate temperature control.
- Protection of heating equipment through the integration of a level probe.
- A drainage point to purge the system of electrolytic solution, the sump was therefore being sized to incorporate its own normal operating volume and the volume of the remaining test rig components.
- A sampling point to take samples of the electrolytic solution for composition testing.
- A level controller for regulating the level of electrolyte within the separators.
- An additional tank to allow for separation of residual product gas before entering the electrolyser unit.
- A mixing tank to pre-mix the electrolyte to the desired concentration through a closed circuit system.

Below is an explanation of the various control functions of the sump:-

Level Control

The sump was initially designed to accommodate for added level control of the separators, however an alternate solution has been incorporated by allowing the separators to adjust their own level based on a gravity discharge system. This provides the benefit that the solution within the sump does not have to be regulated within strict liquid volume limits when operating normally. By adjusting the level within the sump more liquid is enclosed within the separator discharge pipe, which allows for any entrapped gas to settle out of the liquid within the sump. This was amended by the insertion of a baffle that ensures that no gas exits directly out of the sump to the suction of the pump. An additional level control is aimed at protection of the sump heating equipment. The heater has a distinct heating zone, that when exposed to the surrounding air can cause the heater to burn out. The level control ensures that this part of the heating element is always submerged to protect the heating element.

Temperature Control

A heating element was introduced into the tank design. Depending on the heating element type, it would either need to be secured or movable within the sump. The chosen heating element is secured within the system sump. Ideally, the surface area of the heater should be maximised for sufficient heating purposes. Temperature control can then be achieved through a temperature control panel that regulates the temperature with reference to the measured temperature from an installed temperature probe.

Concentration Control

It is required to note the concentrations of the potassium hydroxide solutions at appropriate times throughout the experimental procedure. Sufficient space was provided within the sump to obtain conductivity readings. It was required to calibrate the conductivity meter, however once performed, the concentration could easily be determined through simple reference to a developed calibration curve. To

limit the evaporation from the tank during high temperature operation, the installation of a sump lid with appropriate seals limited evaporation from the system to regulate a constant concentration more effectively.

Drainage Point

The sump and the sump pipe work provide the lowest common point to the major equipment pieces in the electrolyser test-rig set-up. It allows for the drainage of the majority of the fluid from a flexible hosing outlet located on the discharge section of pipe from the pump. The remaining fluid can be drained from the gravity drain of the system. The functionality of the process was achieved by ensuring that the liquid pumped from the sump, always moved to a high point to represent an accumulated head, and the drainage for liquid always moved towards the lowest point located below the sump. This allows for easy drainage of the fluid from the system. The sump also serves as the common point in which to store electrolytic fluid during standby periods. This liquid can then be effectively drained using the pump discharge point, with the remainder of the fluid drained from the gravity drainage point.

Brief sizing method of the electrolytic sump

The sizing of the sump is based on the following requirements:-

- It must accommodate a heater that has possible dimensions of 440x245x730mm.
- The option to insert a baffle to reduce solution turbulence at the liquid/gas interface and allow for additional residual gas removal.
- The insertion of temperature/concentration probes.
- The insertion of a safety level probe.
- A volume large enough to function as a buffer solution.
- A volume large enough to contain the sump and systems required volume of electrolyte.
- Simple access to the electrolytic solution.

It is important that the intended operating volume of the sump provides a depth sufficient for level control and for accommodation of the electrolytic heater and respective probes.

The sump comprises of two volumetric sections namely the boxed section and the discharge section. The boxed section accounts for majority of the sump volume, however the sloped discharge section ensures that all electrolyte escapes the system when the discharge valve is opened.

- Volume of boxed section:-

$$\mathrm{Vr} = \mathrm{sL}^2 * \mathrm{Lr} \ldots \ldots \ldots (32)$$

- Volume of Pyramidal discharge section:-

$$\mathrm{Vp} = \frac{1}{2}\mathrm{sL}^2 * \mathrm{h} \ldots \ldots \ldots (33)$$

Where,

Vr – The volume of the rectangular section (m^3)

sL – Is the square length (m)

Lr – The length of the rectangular section (m)

Vp – Is the volume of the pyramidal section (m^3)

h – The perpendicular height of the pyramidal section (m)

By carefully varying the height of each section and determining the change in the volume of the sump, the relative operating depths can be deduced for the sump.

An indication of the heating requirements for the sump can be calculated through a simple energy balance (Skogestad, 2009). A certain amount of energy is required to increase the temperature of the solution from room temperature to the desired operating temperature. Heat is lost through the walls of the sump during the heating stage. The lost heat needs to be accounted for to compensate for heat loss from the system.

$$\mathrm{Q_{out}} = \mathrm{UA\Delta T} \ldots \ldots \ldots (34)$$

$$Q_{in} = mCp(T_1 - T_0) \ldots\ldots\ldots (35)$$

Where,

Q – Is the energy transfer (J)

U – Is the overall energy transfer coefficient ($W/m^2.K$)

A – Transfer area available (m^2)

Cp – The heat capacity (J/kg.K)

m – The mass of the electrolyte (kg)

T – Temperature of the electrolyte (K)

By adding the two equations above, the total approximate heating requirements is determined to provide a rough sizing for the heat requirement within the sump.

B.4. Electrolytic Circulation Chemical Pump

Introduction

The correct choice of pump is fundamental for overcoming the frictional forces developed within the experimental set-up. It was expected that the required head of liquid by the pump is relatively small for the suggested experimental set-up. It was required that a flow rate of at least 200L/min be capable for the required pumping system. A pump size was selected to generate a flow rate greater than 200L/min at the calculated head of liquid for an added safety factor. This ensures that the system is capable of the necessary flows of electrolyte even in cases of expansion and added

pressure drop factors. The liquid velocity within the system is controlled through the use of a manual control valve located after the pump set-up.

It is fundamental that the liquid is always pumped to the highest common point in the system, and that no point in the discharge section of the piping results in the entrapment of air. This requires additional bleeding systems which are undesirable for the achievement of a spontaneous system. Once pumped through the high point (bi-phase flow inlets to the separator), it is fundamental that the fluid moves continuously downwards in the gravity drainage system for liquid drainage back to the sump. This ensures that gas is not trapped within the system resulting in to complications. In order to accomplish this requirement, it is important that equipment is designed with a slight slope toward the common drainage point to ensure complete draining. It is further beneficial for drainage purposes to employ a marginal slope within the system piping to account for complete drainage of the system.

Brief sizing method of the electrolytic circulation chemical pump

In order to select the correct pumping curve, it is necessary to calculate the head of liquid required for the pump. The following assumptions were made to aid the process of sizing the electrolytic pump.

- The pump is designed for the maximum possible flow rate of electrolyte at 25°C and 40wt% KOH.
- The roughness factors for the piping are chosen on the basis of PVC piping at 0.0015mm.
- It is designed without considering the generation of gaseous products.
- The Reynolds number deduced that the flow in the pipes is a turbulent flow regime, therefore the alpha term within Bernoulli's equation is equal to 1.
- Control valves operate at a normal position of half closed.
- Ball valves operate at a normal position of fully open.
- Stagnant conditions within the electrolyser unit are assumed to be negligible fluid velocity, along with system units being infinitely large.

- Momentum balance from point 1, at the electrolytic fluid surface of the sump, to point 2, at the electrolytic fluid surface of the separators, as demonstrated in the diagram below:-

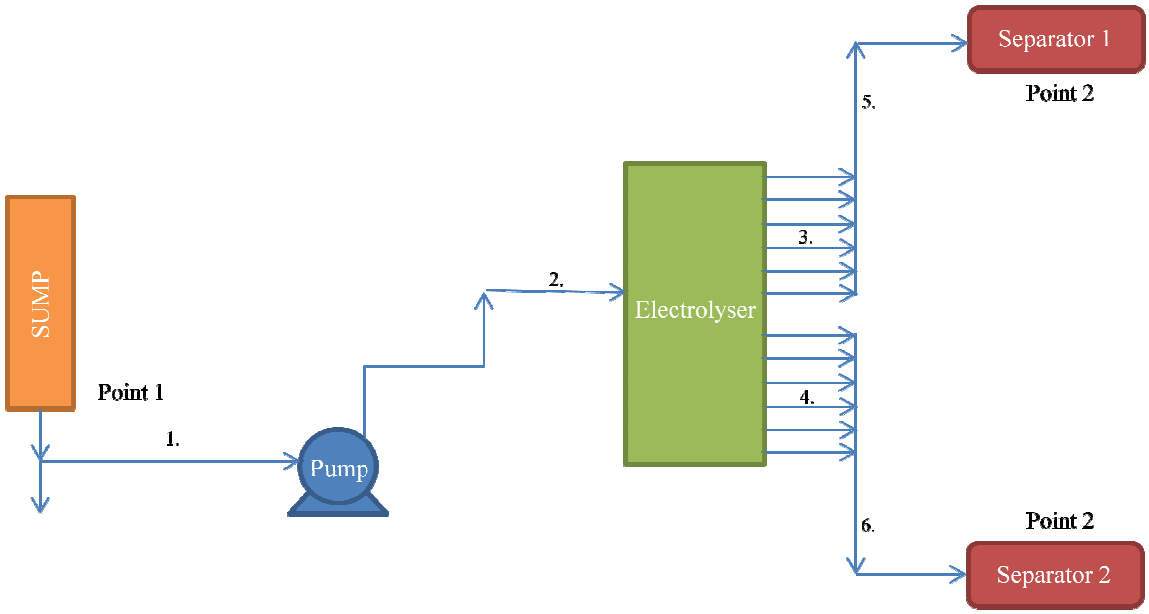

Figure B1: Momentum boundary conditions as defines for the sizing of the system chemical pump

The pressure head, which is the mechanical load required to generate a particular velocity of flow is calculated through the use of Bernoulli's equation, as mentioned in the section dealing with gravity drainage (Skogestad, 2009):

$$P_2 + \rho g z_2 + \rho \alpha_2 \frac{v_2^2}{2} + \Delta p_f = P_1 + \rho g z_1 + \rho \alpha_1 \frac{v_1^2}{2} + \Delta p_{lift} \dots\dots\dots (36)$$

Where,

P - is the pressure at the designated system point ($N.m^{-2}$)

ρ - is the electrolytic density ($kg.m^{-3}$)

g - is the gravitational constant ($m.s^{-2}$)

z - the height of the designated system point reference to the chosen reference point of the system (m)

α - is the laminar/turbulent flow correction factor

v - is the fluid velocity at the designated system point ($m.s^{-1}$)

Δp_f - is the friction loss term ($N.m^{-2}$)

Δp_{lift} - is the pressure head ($N.m^{-2}$)

The above equation is solved for the generated pressure head for the system between the discharge of the pump and the inlets to each separator. Individual pressure losses are determined for the denoted sections of piping. Once all the mentioned points have been inputted, it would be possible to compare the deduced head of liquid water by simple reference to system curves for diverse pump selections.

As illustrated in Figure B1, the various pipelines were subdivided into sections for easy reference. For each of these pipelines it is required to consider the friction loss associated with the following factors:-

- Pipeline Length
- Bends within the pipeline (90°, Tee or 45° bends)
- Valves within the pipeline (Ball valves, Check valves and Diaphragm valves)
- Contraction or Expansion points
- Pressure drop across the mesh electrodes (Glatt et al., 2009)
- Pressure drop across flow meters and strainers.

For the above friction drop contributing parameters, the following equation is used to determine the fanning friction pressure drop within each pipeline (S. Skogestad, 2009):-

$$\Delta p_f = 4f\frac{L}{D}\rho\frac{v^2}{2} \ldots\ldots\ldots (37)$$

Where,

f - is the friction factor read off from the Moody diagram or determined by the Colebrook equation

L - The length or equivalent length of the contributing parameter (m)

D - The hydraulic diameter of the pipeline. This can be determined through noting the relative roughness of PVC piping which amounts to 0.0015mm (m)

In order to determine the friction factor for the pipeline, it is necessary to calculate the Reynolds number. This can be determined through the following equation (Skogestad, 2009):-

$$Re = \frac{\rho v D}{\mu} \dots\dots\dots (38)$$

Where,

μ - is the kinematic viscosity of the electrolytic solution (kg/m.s)

Once the Reynolds number is known along with the roughness factor, it is possible to determine the friction factor. It is found that the flow regime is turbulent; therefore the Colebrook equation can be used to approximate the friction factor for turbulent flow regimes as derived from the Moody diagram. The Colebrook equation for the fanning friction factor is as follows (Skogestad. 2009):-

$$\frac{1}{\mathrm{f}^{0.5}} = -4\log\left(\frac{\frac{\varepsilon}{\mathrm{D}}}{3.7} + \frac{1.26}{\mathrm{Re}\sqrt{\mathrm{f}}}\right) \dots\dots\dots (39)$$

Where,

f – Is the friction factor

ε – Is the relative roughness of the piping material (mm)

D – Is the diameter of the piping (m)

By solving the above equation to be equal to 0, it is possible to use a solving technique to calculate the friction factor for each aspect contributing to the friction of the system. For valves, contractions, expansions and bends, an equivalent length factor is used as indicated in Skogestad. (2009) to determine the pressure drop due to friction.

The pressure drop due to fluid moving through the mesh electrodes provides a contribution to the friction caused due to fluid movement. This pressure drop is determined through a trend developed by Glatt et al., (2009). It is calculated what the theoretical and actual pressure drops would be of a liquid moving through a mesh. The following data was generated:

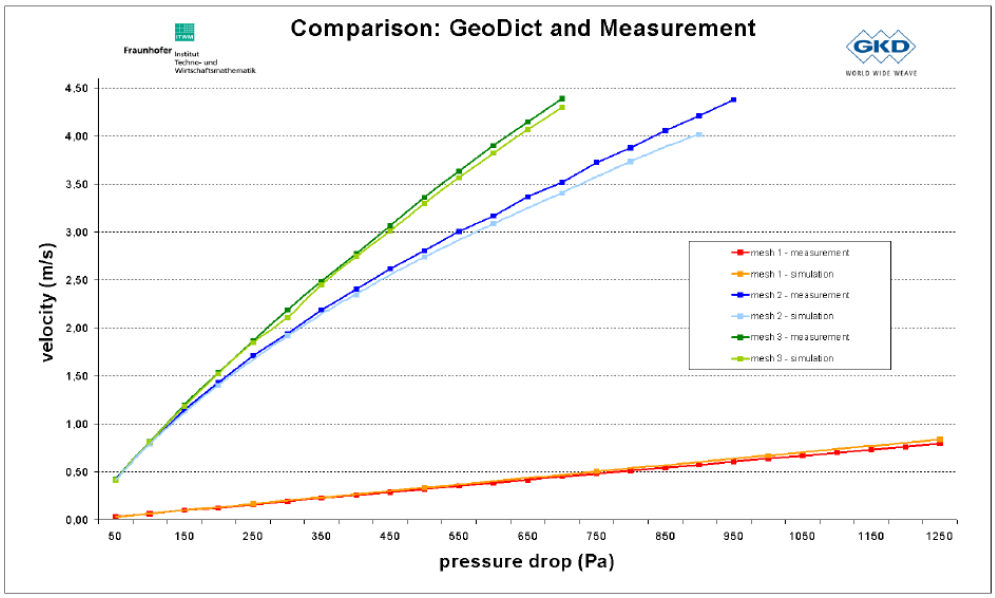

Figure B2: Velocity-dependant pressure drop for three different weave types of filtration mesh (E. Glatt et al. 2009)

Mesh 1 was chosen as it is characteristic of a twilled dutch weave with a configuration similar to what is used for the porous electrodes. This type of mesh develops the highest pressure drop relative to increasing velocity. It was also noted that the trend for this particular mesh is characteristic of a linear trend. It is therefore noted that a straight line extrapolation technique provides the pressure drop at the required velocity which would serve as an adequate approximation for the purpose of sizing the electrolyte pump:

$$P_{required} = \left(\frac{V_{require} - V_{min}}{V_{max} - V_{min}}\right)(P_{max} - P_{min}) + P_{min} \dots\dots\dots (40)$$

Where,

P - Is pressure drop across the mesh electrodes (Pa)

V - Is the velocity generated through the mesh electrodes (m/s)

This equation can then be added to the total generated pressure drop due to friction.

Once the pressure head has been calculated it can be converted to the head of fluid (mH2O) for the design specification for the required size of pump.

Several conditions were tested for identifying the worst case conditions within the system. These conditions were then plotted as system curves on the same plot as the pump curve to note intersection points to find the minimum required pump size.

B.5. Gravity Recycle Loop Piping

Introduction

As the system pump facilitates pumping of electrolyte between the electrolytic sump and the product gas separators, it is essential that the flow is balanced from the separator outlet back to the system sump. In order to achieve this efficiently without the need of additional equipment, conditions were created to make drainage possible under natural gravity. The effects of system pressure drop due to viscous solution flow needs to be overcome by the gravity feed for the flow of electrolyte back to the sump at an identical flow generated by the pump to the electrolyser. It is required that the exit piping from the outlet chamber of the separators be larger than the general process piping to ensure that at high flow rate, the solution escapes successfully to the sump without the requirement of excessive liquid head buildup. The liquid head therefore needs to be determined from the normal operating height of solution within the sump to the operating liquid height of solution within the separator.

Brief sizing method of the gravity recycle loop piping

As mentioned, the liquid flow rate needs to match or exceed the flow rate of the liquid in the discharge pumping circuit. In order to achieve this, it is essential to determine the ideal size of piping and the maximum fluid velocity through the drainage pipe to the system sump. In order for this to occur, a certain system head is required to ensure that the fluid is capable of reaching the desired fluid flow. The liquid height was determined by using Bernoulli's equation as demonstrated in the system pump sizing. The equation is adapted and solved for the following assumptions:-

- No pump work for the system.
- Inlet velocity of the surfaces of the separators remains negligible as it is assumed that the liquid height remains constant for both units.
- The liquid surface for the separators and the sump was noted as the two reference points on which to perform the mechanical energy balance.
- The calculation was performed for the worst case scenario of maximum flow rate; therefore it was assumed that the function was achieved at minimum flow conditions as well.

Bernoulli's equation is re-arranged to the following structure once the neglected terms have been removed from the expression (Skogestad, 2009):-

$$\Delta z = \frac{\frac{\alpha_2 {v_2}^2}{2}}{g} + \frac{\Delta pf}{\rho g} \dots\dots\dots (41)$$

Where,

Δz - is the change in solution levels between the separator and the sump (m)

v_2 - is the velocity of the fluid entering the sump (m/s)

g - is the acceleration due to gravity (m/s^2)

Δpf - is the friction drop through the piping system (N/m^2)

ρ - is the liquid density (kg/m^3)

This equation solves the desired height difference between the electrolytic solutions within the sump and separators for a particular pipeline size. The friction drop within the piping is fundamental in determining the required head of fluid to push the solution through at the desired velocity. It was found that the larger the piping, the smaller the required system head, as the pressure drop due to friction is significantly smaller. The frictional drop is determined in an identical manner as with the pump sizing section.

B.6. Flow Measurement

It was desired to place flow measurement instruments on the electrolytic feed line to the electrolyser and on the gas output lines leaving each separator. It was important to note that the liquid flow meter should be particularly resistant to the caustic potassium hydroxide solution during selection. It has been found that flow meters constructed out of polysulfone plastic with various PTFE and stainless steel 316 components are ideal for corrosion resistance. This preserves the long term use of the flow measurement instruments. It was essential that the additional components exposed to the electrolytic solution be composed of materials that are chemically resistant to the conditions experienced in the electrolyser test-rig.

The use of rotameters for liquid flow measurement has been discounted on the grounds that in order for these devices to operate efficiently, they should preferably be mounted in the vertical position. This however requires additional piping, and creates conditions for accumulation of gases within the pipe work. The use of horizontal liquid flow rotameters is a plausible consideration, however the calibrated springs are subject to high rates of erosion. Rotameters also require re-calibration of measured values to suit changing system conditions.

The selection of a flow measurement device that functions on the grounds of being independent of density and viscosity changes was a more viable option. Electromagnetic flow meters measure the velocity of solution through a known cross sectional area. These meters therefore are independent of changing density conditions. Vertically mounted gas rotameters were therefore chosen as the instrument of choice for gas flow measurement.

B.7. Temperature Measurement

Temperature control and measurement was achieved by a closed system within the sump, however it is essential that the temperature within the electrolyser be maintained at the desired limit. A temperature probe was placed in the electrolyser to provide an accurate feedback of temperature. The temperature could then be adjusted using the Teflon heating element located within the system sump. An additional check of temperature is performed using the Boeco PT-380 pH/mV probe.

Temperature determination on the product gas outlet streams is fundamental in determining the correction factor for gas flows exiting each separator. The temperature gauges are constructed out of stainless steel 316.

B.8. Pressure Measurement

Pressure gauges on the product gas discharge lines were used in determining accurate correction factors for gas flow out of the system with reference to standard atmospheric pressures. Pressure determination within the electrolytic feed line served the purpose of indicating whether any blockages had occurred in the liquid lines. Pressure measurement of exiting product gas from both separators was used in restructuring calibration data to corrected values. Pressure measurement was accomplished through the mounting of stainless steel 316 pressure gauges where necessary within the circuit.

APPENDIX C – ELECTROLYTIC COCENTRATION PREPARATION

Electrolytic concentration, for the purpose of this investigation, is measured and reported on a mass percent basis. The mass percent[14] of potassium hydroxide required to be mixed with a known mass of distilled water is determined through the following equation:-

$$M_T = M_{H20} + M_{KOH} \ldots\ldots\ldots (42)$$

Where:-

M_T:- Total mass of solution (kg)

M_{H2O}:- Total mass of distilled water solvent in the system

M_{KOH}:- Total mass of potassium hydroxide solute in the system

The mass of potassium hydroxide is a function of the total mass. Depending on the required mass percent of electrolyte, the potassium hydroxide variable in Equation (42) is substituted by the following:-

Table C1: Expressions for substitution when solving for potassium hydroxide mass for a particular concentration

Mass % KOH (%)	*Expression to Substitute*
20	$0.2M_T$
30	$0.3M_T$
40	$0.4M_T$
50	$0.5M_T$

Equation (42) is then solved by making the total mass the subject of the formula. Taking the difference between the total mass and the mass of distilled water in the system will yield the mass of potassium hydroxide required. Bulk suppliers of potassium hydroxide solute provide

[14] Mass percent refers to the mass quantity of the solute divided by the total mass of the solution which is the sum of the solvent and solute.

potassium hydroxide with varying concentrations between 85-91% by mass solute. This discrepancy is incorporated in determining the actual potassium hydroxide mass required. The uncertainty regarding the mixed concentrations will be noted, along with estimates for the loss of potassium hydroxide from evaporation and leakages within the system.

Potassium hydroxide concentration is monitored through the use of a pH/mV meter supplied from Boeco. The meter is capable of taking readings up to 100°C and 50wt% potassium hydroxide. Theoretically it should be possible to relate the measured pH to the concentration of hydroxide ions in solution. This is performed through the use of the following equation:-

$$pH = -\log([OH^-]) \dots (eq\ 43)$$

Where:-

[OH⁻]:- Is the molar concentration of hydroxide ions in solution

Standard solutions[15] have been accurately determined through the use of a sensitive balance that has accuracy up to three decimal places. By varying the temperature of these solutions, calibration curves were generated for each concentration and an average taken to generate an equation that will aid in determining the theoretical pH/mV of each reading taken under experimental conditions at any temperature within the desired temperature range.

By measuring the mV/pH value for each experimental run, a curve can be generated that will illustrate whether any significant change in concentration is present during experimental operations.

[15] A standard solution is a solution of known concentration prepared with the use of a sensitive mass balance.

APPENDIX D - SAFETY AND COMMISIONING CHECKLISTS AS DETAILED FROM ISO 22734-1

The following is a comprehensive list developed in reference to ISO 22734-1 Hydrogen generators using water electrolysis process: Part 1: Industrial and commercial applications. For each subheading, a description is provided detailing associated requirements, along with the intended solution employed during the design process of the Hydrox Holdings Ltd. membraneless water electrolysis test rig.

D.1. Mechanical Equipment Checklist

Table D1: Mechanical equipment checklist

Mechanical Equipment Checklist		
Sub-heading	*Description*	*Intended Solution*
General Requirements	• Hydrogen generator parts will be suitable for the temperature, pressures and conditions exposed to during operation. • Components should be clearly marked for description and precautions.	• All parts to be checked with compatibility of the specified operating conditions. • All parts labelled properly with the relevant information if required.
General Material Requirements	• Materials need to retain stability and strength. • Resist to chemical and physical action. • Be compatible to other materials for direct and indirect contact.	• Vessels and components need to be sized without compromise of strength. • Material compatibility should be considered. • General mechanical wear and corrosion resistance of material should be noted. • Auto-ignition temperature should be referred to.
Enclosures	• Minimum strength for the supporting structure should be determined. • Electrical enclosures need to be considered. • Fire resistance of materials for non-	• Manufacturers of major equipment will ensure that support is sufficient, sizing done with reference to standards. • Heat shrink and insulation will be used where appropriate.

	combustion. • Appropriate insulating materials for components. • Ventilation systems to remain unobstructed. • Containment of hazardous liquid leakages.	• Ventilation system will form a system on its own. • Drip trays will be employed to prevent leakage of hazardous liquid.
Pressure Bearing Components	• Components associated with mass need to have the required support. • Means of cleaning and drainage should be employed. • Areas of explosive components need high consideration for design and clear marking.	• Saddle clamps and supports to be employed where support is required. • All vessels equipped with gravity/pump drains. • Safety flame arrestors employed for flammable lines.
Piping, Fittings and Joints	• Process piping designed according to the necessary standards. • No deposits of contaminants within piping. • Operating temperature and pressure noted. • Elastic tubing and joints protected.	• Piping standards employed during design phase. • Pipes to be cleaned thoroughly during installation. • Materials of construction investigated. • Tubing under no load.
Electric Heaters	• Electric heaters protected sufficiently from aggressive conditions.	• Heater selection made under standard use for desired purpose.
Pumps	• Pumps protected sufficiently through construction of anti-static components and chemical resistant components.	• Pump selected under consideration for intended use.
Fans and Ventilators	• Fans and ventilators chosen for the application.	• Ventilators and ventilation to dilute hazardous gases to appropriate limits.

D.2. Electrical and Ventilation Equipment Checklist

Table D2: Electrical and Ventilation Equipment Checklist

Electrical and Ventilation Equipment Checklist		
Sub-heading	*Description*	*Intended Solution*
Fire and explosion hazard protection	• Hydrogen generators should be manufactured for the unintended release of hydrogen gas. • Area classification of the electrolyser unit. • Protection methods to prevent the accumulation of ignitable mixtures. • Ventilation preparation for	• Testing will be performed to ensure that no leaks are observed before experimentation. • Instructions and information will be given where appropriate. • Release rate needs to be at the optimal safe value. • The use of gas detection will be

	appropriate ventilation rate. • Ventilation of equipment for shut-down procedures. • Hydrogen and oxygen gas detection system.	accounted for around the electrolyser. • Equipment vents to be installed for venting gas. • Nitrogen purge systems installed for ventilation of equipment.
Electrical Equipment	• Protection against shock, fire and burns during operation and maintenance. • Grounding and bonding of equipment. • Circuit protection for electrical equipment through fuses, overloads and circuit breakers.	• Grounding chains and plates will be installed for electrical equipment for connection to casing. • Requirement for fire extinguishing will be accounted for.

D.3. Operator Controls Checklist

Table D3: Control systems and equipment checklist

Control systems Equipment Checklist		
Sub-heading	*Description*	*Intended Solution*
General	• Hydrogen test rig to be equipped with a control system that is designed and constructed so that the generator is safe and reliable and will prevent dangerous conditions from occurring.	• Each control loop will be detailed and marked as indicated by description and drawings.
Operator Controls	• Start-up procedure is only initiated once safeguards are in place. • Shut-down procedure has a stop control that will result in the safe controlled cessation of the hydrogen generator. • Emergency stop system to cease function of the electrolyser.	• Start-up and shut-down procedures will indicate the correct safe method of operating the electrolyser system. • Emergency stop of electrolyser and pump will be installed. • The necessary valves have been placed for safe start-up and shut-down.
Control function in the event of failure	• The hydrogen test rig should not start up unexpectedly. • The hydrogen test rig should stop immediately if the command is given. • Automatic or manual stop of system should be possible. • Protective devices should remain fully functional.	• The correct number of switches will be installed to ensure more than one method of start –up. • Emergency stop will cease all electrical supplies to the system; the majority of solution will then drain to the sump automatically. • Devices used will be specified to operate in conditions of experiment.

Correctable conditions	• The hydrogen generator may continue to operate from out of specification conditions that are corrected by reducing power level or changing the operating parameter.	• A number of methods has been employed to ensure that hazardous conditions are not induced.
Safety Components	• Safety equipment will incorporate the appropriate safety conditions as described by the manufacturer to ensure that the limits are maintained.	• Safety devices pre-programmed with desired safe limits. • Emergency shut-down in the event of unsafe breach of operating parameters.
Remote Control Systems	• Remote control systems operate the generator independently.	• No remote control system will be implemented as the system will be regularly inspected and will have the necessary safety modifications for safe shut-down.
Alarms	• When a condition affects the safe operation of the generator, an alarm signal should be received by the operator.	• Detection equipment should possess sufficiently loud equipment to be heard for hazardous gaseous conditions.

D.4. Ion Transport Medium Checklist

Table D4: Ion transport medium equipment checklist

Ion Transport Medium Equipment Checklist		
Sub-heading	*Description*	*Intended Solution*
Electrolyte	• The electrolyte needs to be chemically stable with respect to environmental degradation over the full range of operating conditions and over a defined lifetime of the hydrogen generator. • Not catalyse any parasitic side reactions either of a chemical or electrochemical form.	• The electrolytic medium has been checked with all components of construction for compatibility. • Research has been performed to note whether any undesired side reactions are present.

D.5. Personnel Equipment Checklist

Table D5: Personnel equipment checklist

Personnel Equipment Checklist		
Sub-heading	*Description*	*Intended Solution*

	• All live parts and/or moving parts shall be protected from access by unauthorised personnel. Live parts shall be highlighted by warning signs. • Guarding will be used to isolate live parts, maintenance only to be done on a de-energised system. • During experimental procedures, protective equipment to be worn at all time points.	• The required insulation of live parts will be performed. • All live wiring will be identified and highlighted by warning signs and colour coding. • Moving parts will be ensured to be guarded. • Laboratory, gloves, masks will be employed according to the requirements by the MSDS information.

D.6. Test Method Equipment Checklist

Table D6: Test method equipment checklist

Test Method Equipment Checklist		
Sub-heading	*Description*	*Intended Solution*
Basic Test Arrangements	• In conducting tests, the entire hydrogen generator, including any air filters, start up devices, venting or exhaust systems and all field furnished equipment shall be installed in accordance with the manufacturer's instructions.	• The system will be installed as shown and described by the detailed drawings allowed for by the supplier.
Reference test conditions	• Tests should be carried out between temperatures of 15°C and 35°C. • Relative humidity must not exceed 75%. • At an atmospheric pressure of 75kPa to 106kPa. • No hoarfrost, dew, percolating water, rain or solar radiation should be present.	• An initial hydrogen generation test will be performed in a controlled manner at room temperature and atmospheric pressure.
State of Equipment	• Each test should be carried out with equipment set-up for normal use. • Accessories will be either connected or not connected. • The correct use of required mains voltage. • Earthed terminals at all times. • Connections to be checked. • Equipment intended to be loaded	• The equipment will be operating at the minimum required operating volume initially with inert de-ionised water to note operating capability. • Connections and earthing cables will be inspected. • Equipment will be selected for standard use during operation.

	with a specific material in normal use, shall be loaded with the least favourable quantity, if a material is hazardous, another material may be loaded for testing.	
Functional Tests	• Conductive material should be present when performing these tests. • All functional tests to be performed as indicated by ISO 22734-1 10.1.4.3.	• Tests to be performed with electrolytic solution present. • Test equipment will be tested within the desired operating range.
Pressure Tests	• Pressure check on all pressure bearing parts.	• The system is not operating at pressure, pressure testing performed by manufacturers and suppliers of equipment.
Leakage Tests	• Leakage tests will be performed to supplement the pressure tests. • Fully assembled electrolyser for test. • Tests to be performed at maximum operating pressure.	• The system will be tested over the entire range of flow rates. This will induce maximum system pressure with blocked/closed electrodes. • Maximum operating pressure will be atmospheric. • Temperature will be altered to note any variation in operation with temperature.
Airflow test for ventilation	• Where ventilation is used to disperse the product gases, an air flow test should be performed to note whether the gas volume exceeds 1% of product gas.	• A ventilation system mechanism needs to be designed for sufficient dispersion of gases. • Performed by reference of manufacturer's maximum operating gas flow.
Performance tests	• The system will be operating at maximum capacity for 1 h. • Hydrogen and oxygen purity tests.	• Determining the purity will decide the operational characteristics regarding the separation efficiency.

D.7. Marking and Labeling Checklist

Table D7: Marking and Labeling Checklist

Marking and Labelling Checklist		
Sub-heading	*Description*	*Intended Solution*
Hydrogen Generator	• Generator marking should be done as indicated by ISO 22734-1 11.2.	• All applicable system data and information for a quick reference

Marking		guide.
Marking of Components	• All valves, transmitters, motors, pumps and fans shall be identified to match the hydrogen generator drawings. Piping and tubing will be marked to indicate correct direction of flow.	• Signage with the relevant details will be clearly placed around the hydrogen generator test rig. • Classified areas will additionally be marked. • Additional marking for oxygen and hydrogen venting from the system.

APPENDIX E - EMPIRICAL RESULTS FOR THE OPTIMISATION OF THE HYDROX HOLDINGS LTD. AWE ELECTROLYSER TECHNOLOGY

E.1. Concentration Fluctuation and Monitoring

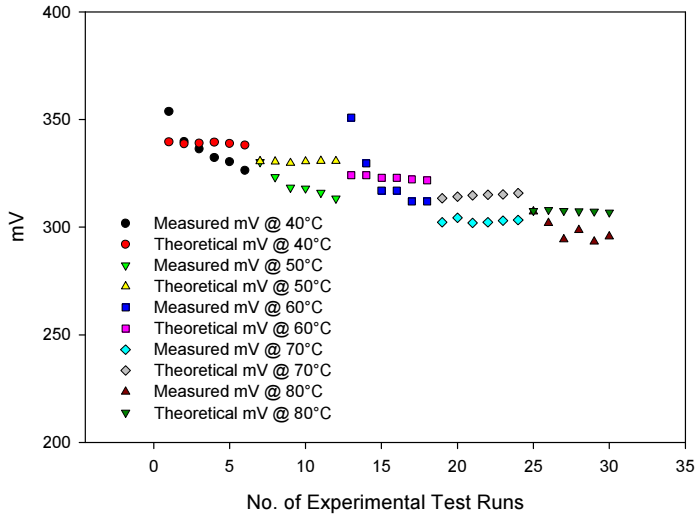

Figure E1: Change in mV for progressing experimental runs for the performance investigation for stainless steel 316 electrodes and 30 wt% potassium hydroxide.

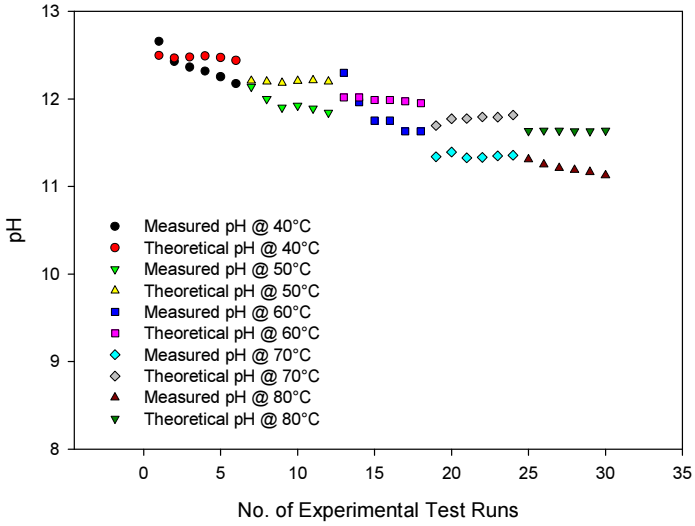

Figure E2: Change in pH for progressing experimental runs for the performance investigation for stainless steel 316 electrodes and 30 wt% potassium hydroxide.

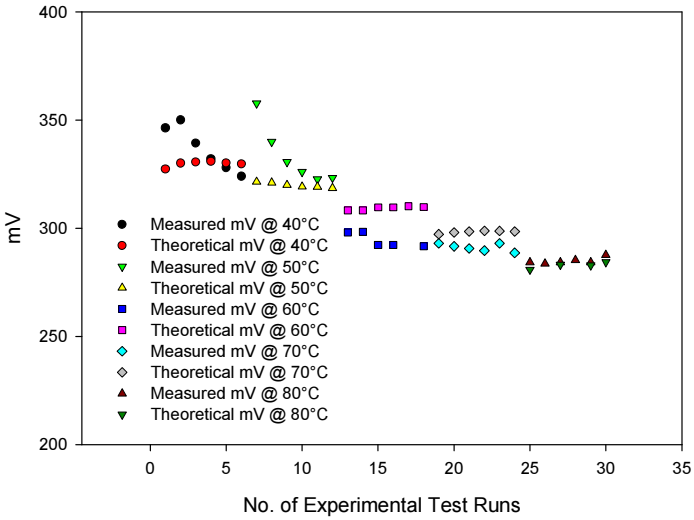

Figure E3: Change in mV for progressing experimental runs for the performance investigation for stainless steel 316 electrodes and 40 wt% potassium. Hydroxide.

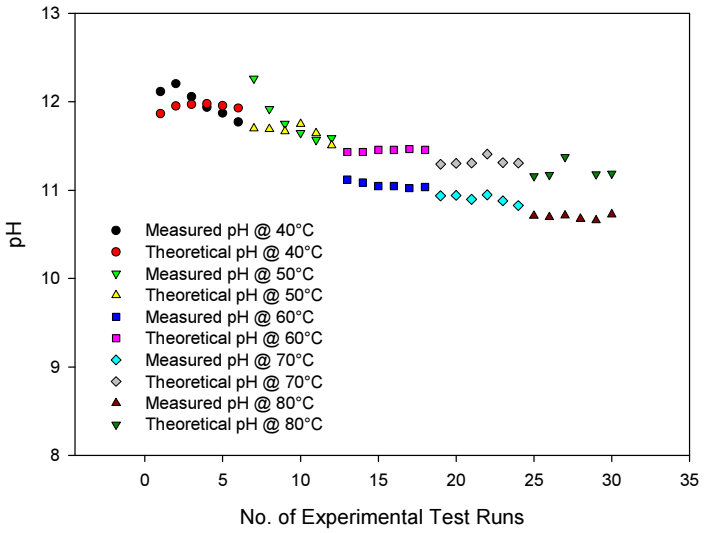

Figure E4: Change in pH for progressing experimental runs for the performance investigation for stainless steel 316 electrodes and 40 wt% potassium hydroxide.

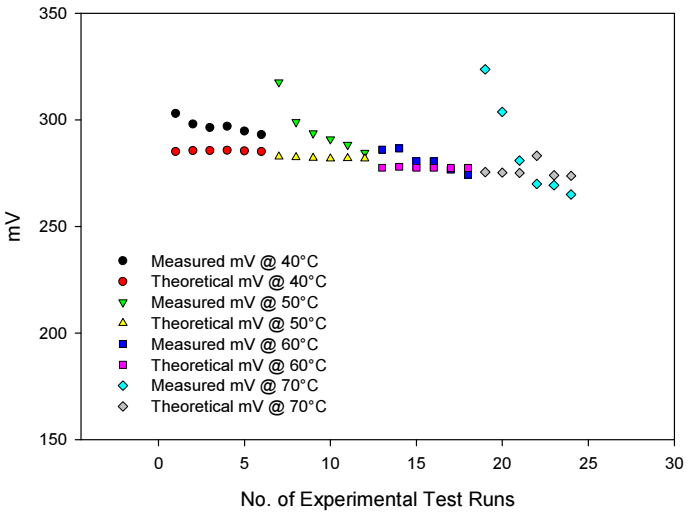

Figure E5: Change in mV for progressing experimental runs for the performance investigation for stainless steel 316 electrodes and 50 wt% potassium hydroxide.

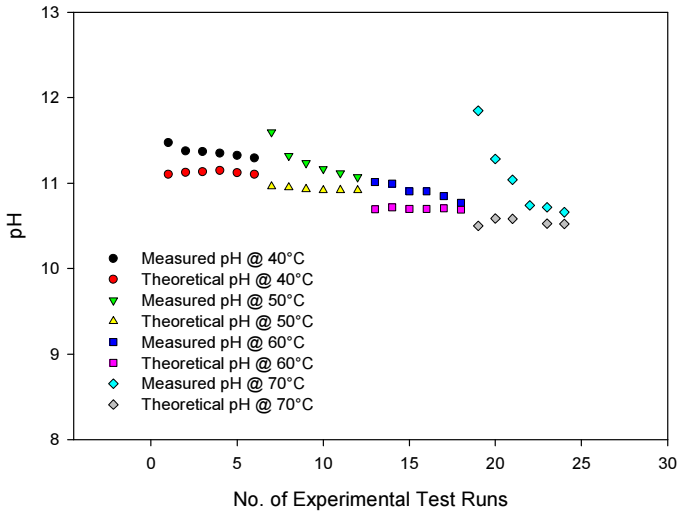

Figure E6: Change in pH for progressing experimental runs for the performance investigation for stainless steel 316 electrodes and 50 wt% potassium hydroxide.

E.2. Concentration as a Function of Flow Velocity and Temperature

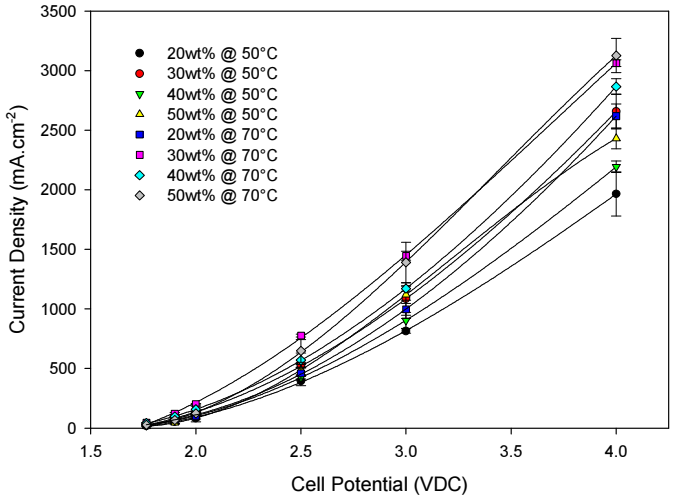

Figure E7: Polarisation curves of test rig as a function of potassium hydroxide (KOH) concentration at a temperature of 50°C and 70°C, an electrode gap of 3.5 mm and a flow velocity of 0.2m.s^{-1} and stainless steel 316 electrodes.

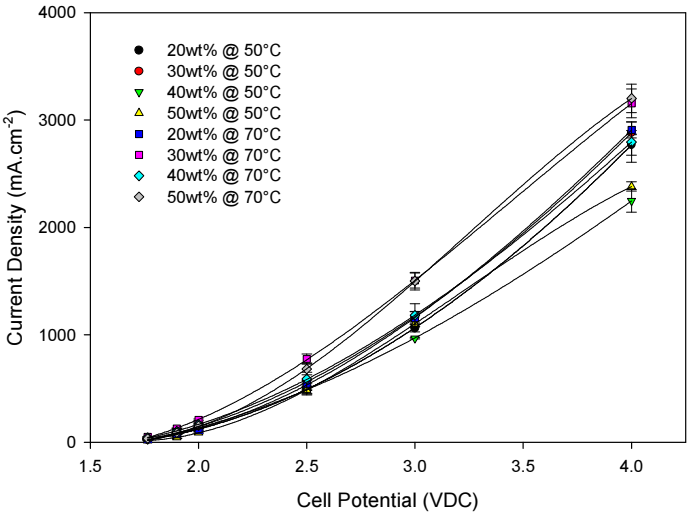

Figure E8: Polarisation curves of test rig as a function of potassium hydroxide (KOH) concentration at a temperature of 50°C and 70°C, an electrode gap of 3.5 mm and a flow velocity of 0.4 m.s^{-1} and stainless steel 316 electrodes.

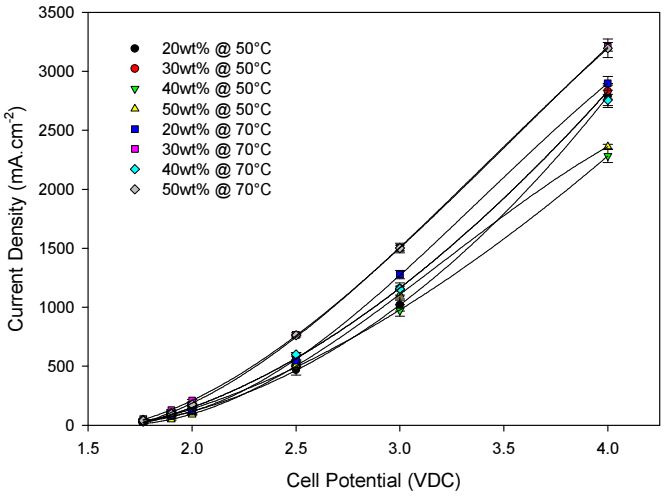

Figure E9: Polarisation curves of test rig as a function of potassium hydroxide (KOH) concentration at a temperature of 50°C and 70°C, an electrode gap of 3.5 mm and a flow velocity of 0.6 m.s^{-1} and stainless steel 316 electrodes.

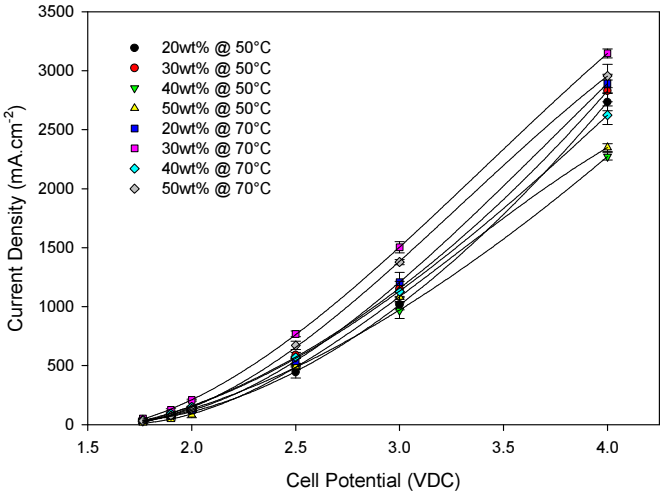

Figure E10: Polarisation curves of test rig as a function of potassium hydroxide (KOH) concentration at a temperature of 50°C and 70°C, an electrode gap of 3.5 mm and a flow velocity of 0.5 m.s^{-1} and stainless steel 316 electrodes.

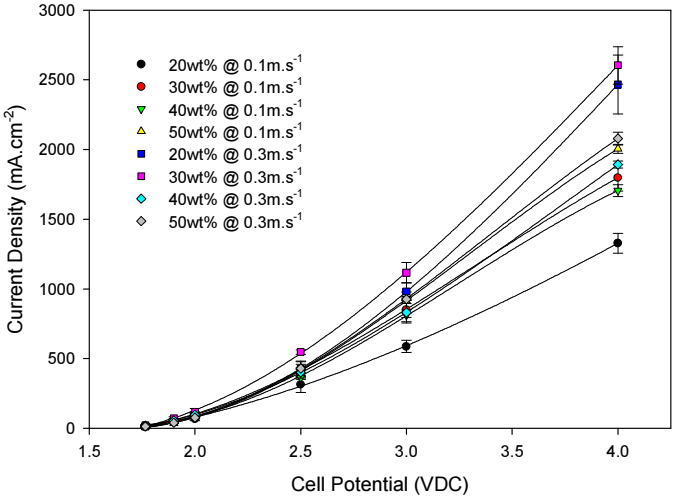

Figure E11: Polarisation curves of test rig as a function of potassium hydroxide (KOH) concentration at a flow velocity of 0.1m.s^{-1} and 0.3m.s^{-1}, an electrode gap of 3.5 mm and a temperature of 60°C and stainless steel 316 electrodes.

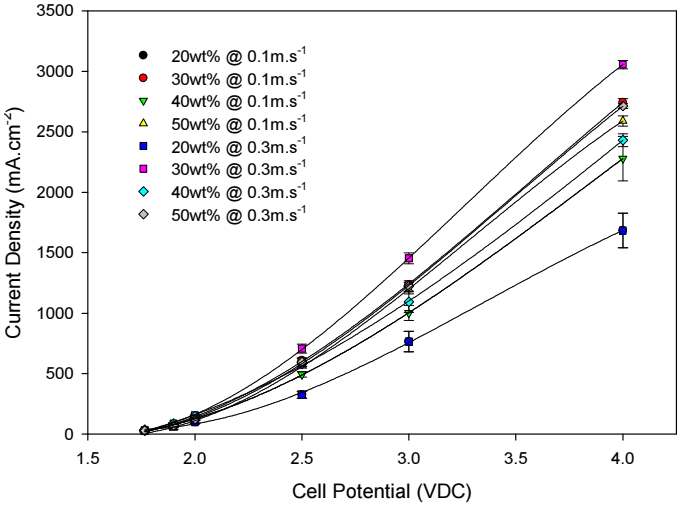

Figure E12: Polarisation curves of test rig as a function of potassium hydroxide (KOH) concentration at a flow velocity of 0.1m.s^{-1} and 0.3m.s^{-1}, an electrode gap of 3.5 mm and a temperature of 40°C and stainless steel 316 electrodes.

E.3. Effect of Increasing Temperature and Flow Velocity on Cell Performance

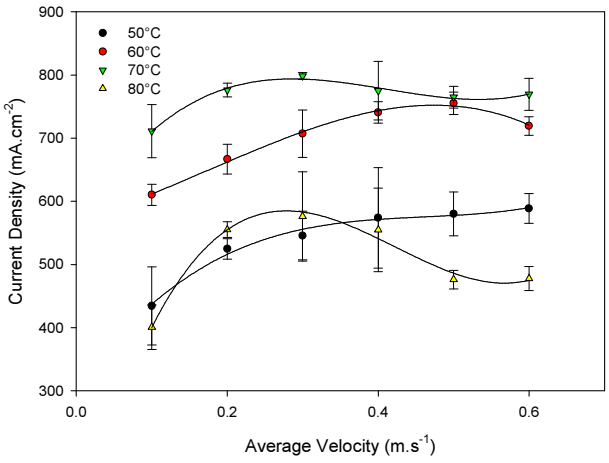

Figure E13: Current Density versus Average Velocity of electrolytic fluid as a function of electrolytic temperature at an electrolytic concentration of 40 wt%, a cell potential of 2.5 VDC and for stainless steel 316 electrodes.

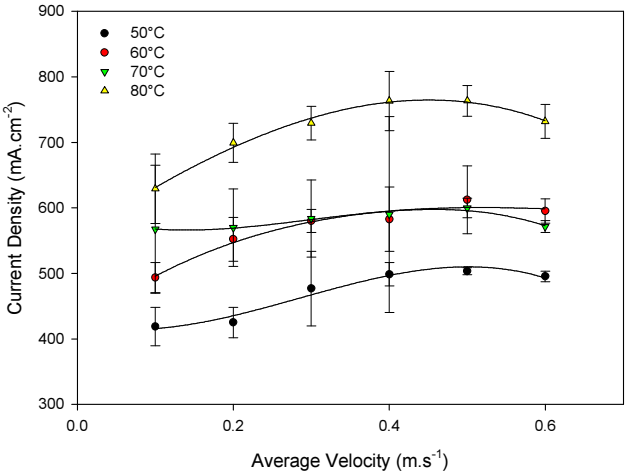

Figure E14: Current Density versus Average Velocity of electrolytic fluid as a function of electrolytic temperature at an electrolytic concentration of 30 wt%, a cell potential of 2.5 VDC and for stainless steel 316 electrodes.

E.4. Optimisation of Electrode Materials to Maximise Cell Performance

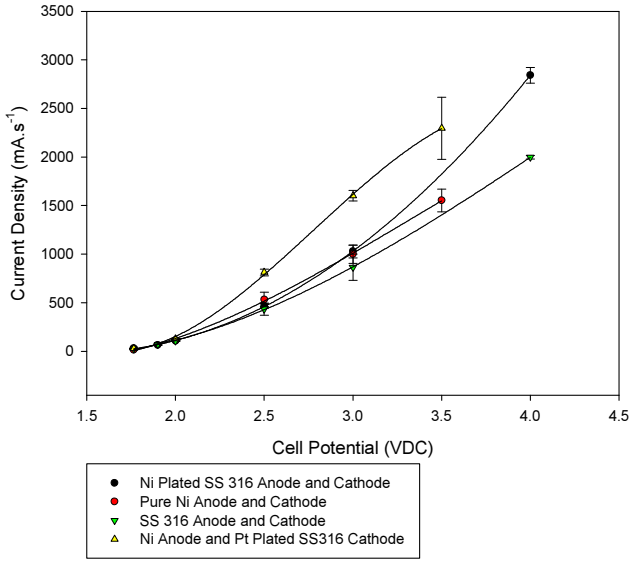

Figure E15: Polarisation curves of test rig as a function of cathodic and anodic material for a temperature of 50 °C, a flow velocity of 0.075 m.s^{-1}, an electrode gap of 3.5 mm and 30 wt% potassium hydroxide (SS: stainless steel).

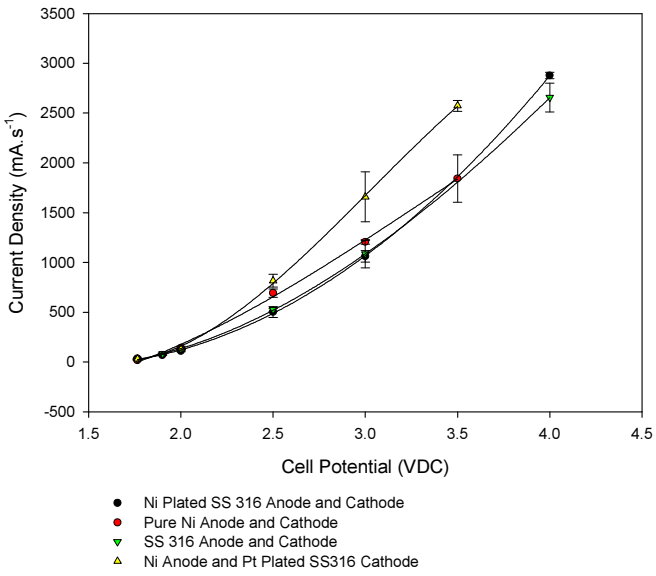

Figure E16: Polarisation curves of test rig as a function of cathodic and anodic material for a temperature of 50 °C, a flow velocity of 0.1 m.s^{-1}, an electrode gap of 3.5 mm and 30 wt% potassium hydroxide (SS: stainless steel).

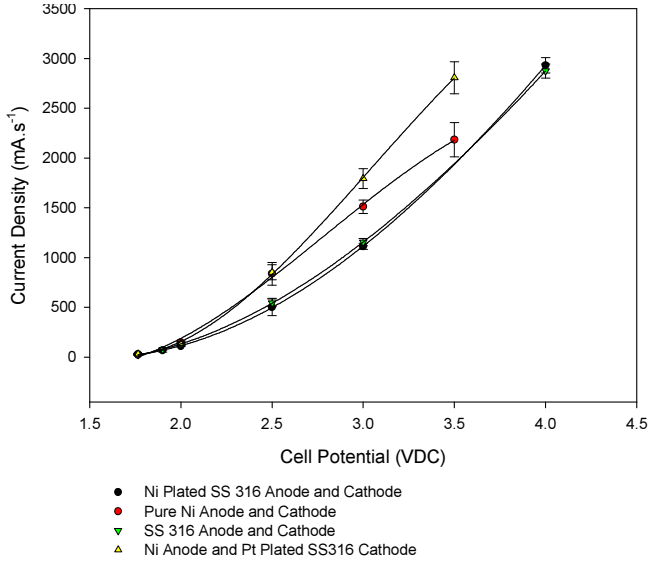

Figure E17: Polarisation curves of test rig as a function of cathodic and anodic material for a temperature of 50 °C, a flow velocity of 0.15 m.s^{-1}, an electrode gap of 3.5 mm and 30 wt% potassium hydroxide (SS: stainless steel).

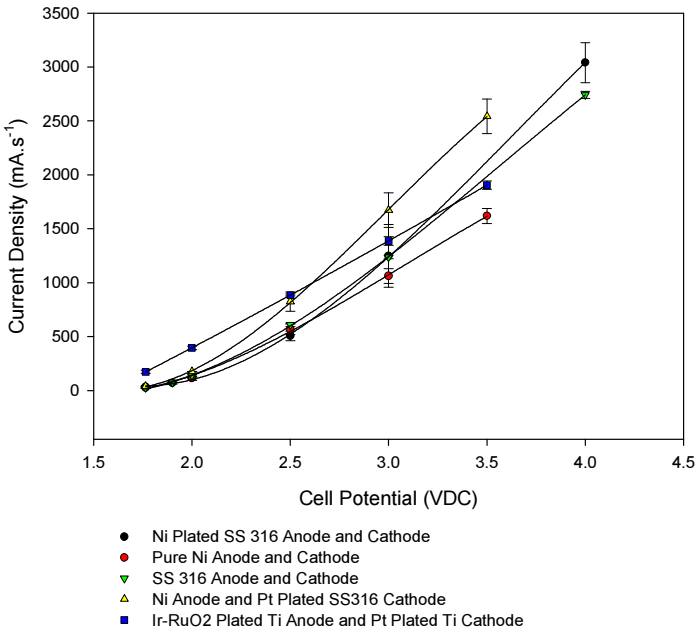

Figure E18: Polarisation curves of test rig as a function of cathodic and anodic material for a temperature of 60 °C, a flow velocity of 0.075 m.s^{-1}, an electrode gap of 3.5 mm and 30 wt% potassium hydroxide (SS: stainless steel).

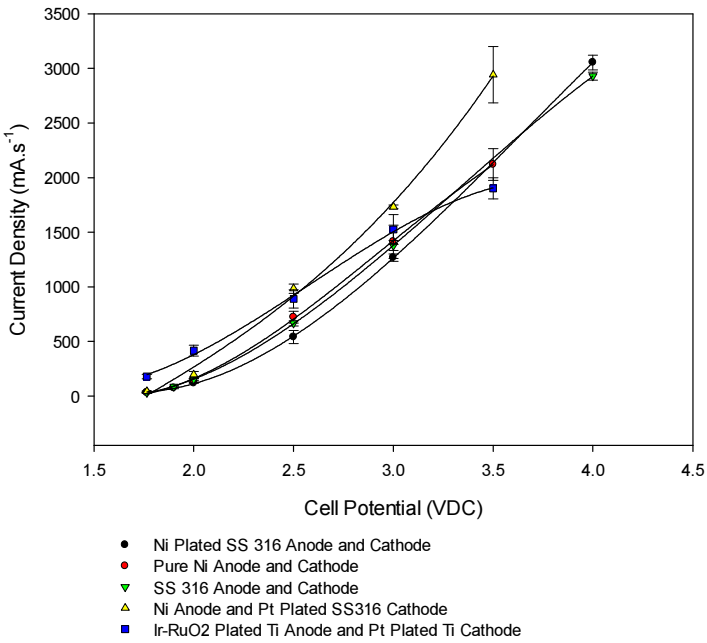

Figure E19: Polarisation curves of test rig as a function of cathodic and anodic material for a temperature of 60 °C, a flow velocity of 0.1 m.s^{-1}, an electrode gap of 3.5 mm and 30 wt% potassium hydroxide (SS: stainless steel).

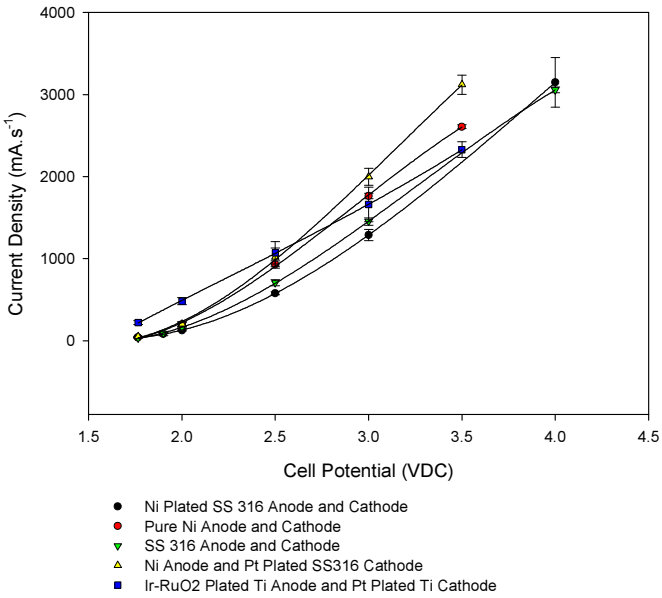

Figure E20: Polarisation curves of test rig as a function of cathodic and anodic material for a temperature of 60 °C, a flow velocity of 0.15 m.s^{-1}, an electrode gap of 3.5 mm and 30 wt% potassium hydroxide (SS: stainless steel).

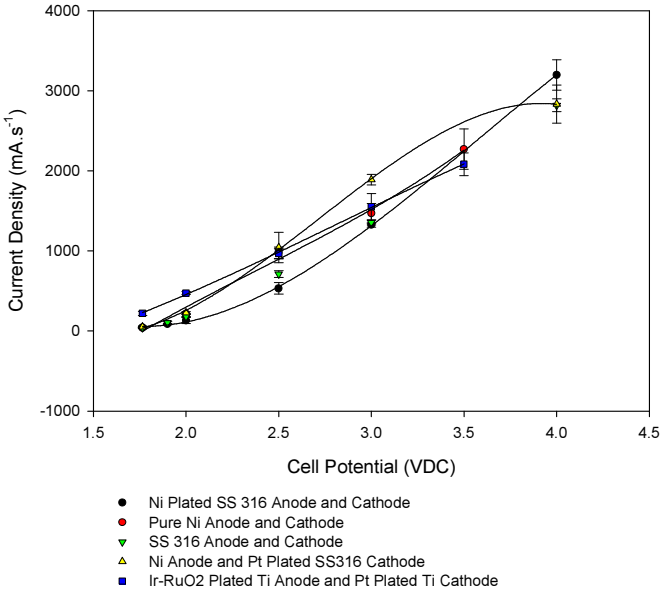

Figure E21: Polarisation curves of test rig as a function of cathodic and anodic material for a temperature of 70 °C, a flow velocity of 0.075 m.s^{-1}, an electrode gap of 3.5 mm and 30 wt% potassium hydroxide (SS: stainless steel).

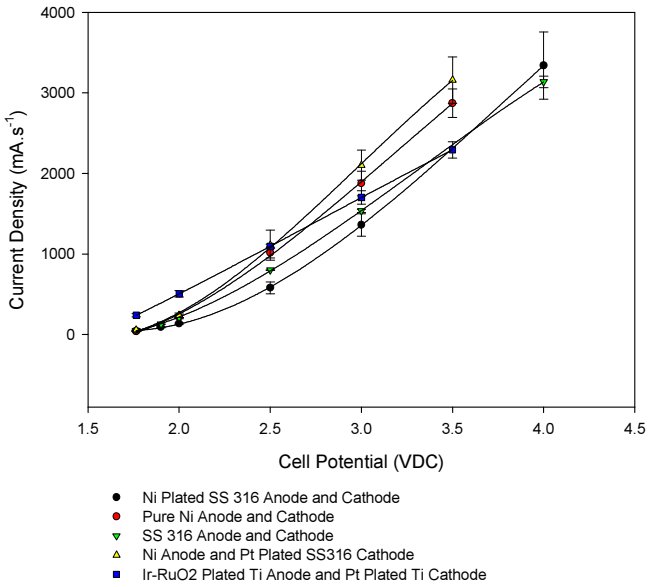

Figure E22: Polarisation curves of test rig as a function of cathodic and anodic material for a temperature of 70 °C, a flow velocity of 0.15 m.s^{-1}, an electrode gap of 3.5 mm and 30 wt% potassium hydroxide (SS: stainless steel).

E.5. Optimisation of the Electrode Gap

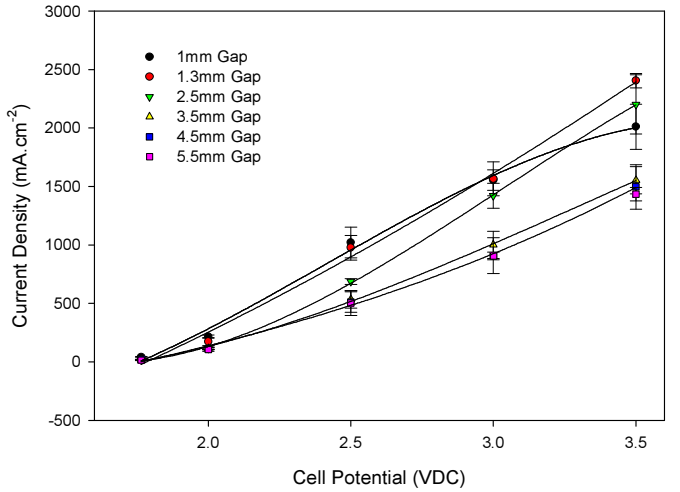

Figure E23: Polarisation curves of a membraneless stack as a function of electrode gap for pure nickel electrodes at a temperature of 50 °C, 30wt% potassium hydroxide and a flow velocity of 0.075 m.s^{-1}.

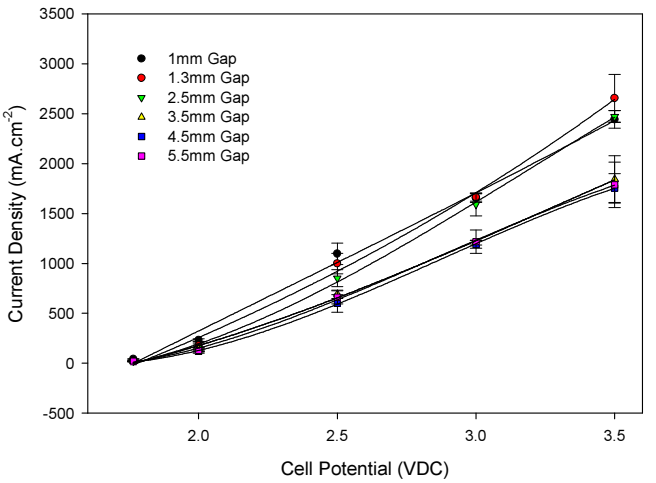

Figure E24: Polarisation curves of a membraneless stack as a function of electrode gap for pure nickel electrodes at a temperature of 50 °C, 30wt% potassium hydroxide and a flow velocity of 0.1 m.s^{-1}.

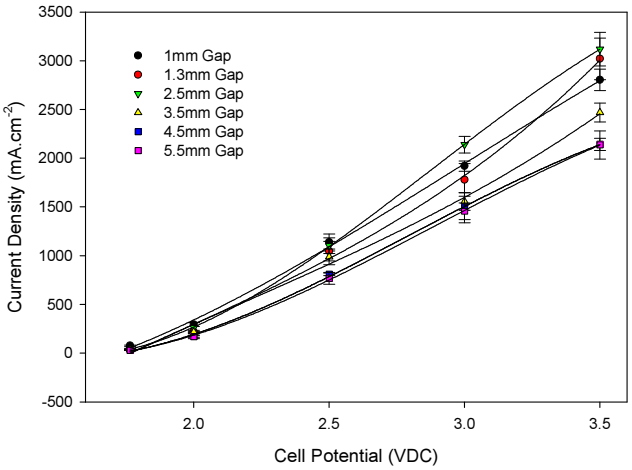

Figure E25: Polarisation curves of a membraneless stack as a function of electrode gap for pure nickel electrodes at a temperature of 70 °C, 30wt% potassium hydroxide and a flow velocity of 0.1 m.s^{-1}.